Numerical and Experimental Characterization of Dissolution and Precipitation Processes in Deep Geothermal Reservoirs

Zur Erlangung des akademischen Grades eines

DOKTORS DER NATURWISSENSCHAFTEN

der Fakultät für

Bauingenieur-, Geo- und Umweltwissenschaften

des Karlsruher Instituts für Technologie (KIT)

genehmigte

DISSERTATION

von

M.Sc. Fabian Nitschke

aus Malsch

Tag der mündlichen Prüfung: 28.07.2017

Referent: Prof. Dr. Thomas Kohl

Korreferent: Prof. Dr. Thomas Neumann

Karlsruhe 2017

Abstract

Geothermal energy has the potential to play a substantial role in the future energy mix. It combines full controllability, the capability to serve baseload demands and suitability for decentralized usage. Particularly important in the transition time towards fossil fuel free energy generation, the quasi-inexhaustible energy source can therefore replace proportions of coal and gas. However, being in an early stage of development the technology still faces rather large challenges. One major challenge on the way of a fast progression is the fluid chemistry. The hot and often highly mineralized geothermal fluids are a harsh chemical environment for pipe strings and surface installations. Resulting in corrosion and scaling formation, both phenomena can severely impair operations. Furthermore, the complex chemical systems also effect exploration, leading to large prospecting risk. The determination of reservoir temperature, which is a key parameter in exploration, from the composition of springs discharge at the surface is still afflicted to large uncertainties. The application of different geothermometers to one sample not uncommonly leads to deviations >>100 K.

The aim of this work is to contribute to a better understanding and quantification of the complex chemical processes associated with hot and highly mineralized geothermal fluids. With scaling formation and geothermometric methods, two autonomous thematic fields, which however base on the same chemical fundamentals, are investigated. One common problem is that fluids sampled at the surface do not reflect the conditions in the reservoir. For a reliable evaluation of scaling potentials as well as for the determination of in-situ temperatures, the knowledge of the original composition in depth is particularly important. In this study, numerical methods and laboratory equilibration experiments were used to improve process understanding and to quantify involved processes. These analysis are presented in the main part of this work in three individual manuscripts.

The first study numerically investigates the thermo-hydraulic-chemical (THC) processes of geothermal single well operations, which led to massive halite scaling formation in a production string. It is shown that the model enables the reproduction of the thermal behavior of the well under production conditions. Due to high salinities (>400 g/kg_W), the application of the Pitzer ion interaction model was required. The parametrization of the model and its verification for the considered chemical system is demonstrated by comparison to solubility data from literature and to results from laboratory experiments. It is demonstrated, that a fully coupled THC model is required to quantify the complex interaction of temperature, flow, permeability and precipitation/dissolution. Doing so, it is possible to reconstruct the chemical composition of the deep brine in terms of scaling relevant constituents and to quantify scaling formation regarding the depth and the precipitated amounts. Furthermore, it is shown that the cost-effective low-risk concept of using existing single wells for geothermal exploitation, has its disadvantages. The model depicts

the immediate increase of the temperature gradient in the production string right at the depth of the beginning counterflow section. For cooling-induced scaling formation, the potential of solid accumulation is largest at this point.

Against the back ground of the urgent need of reliable exploration tools, the second study assesses and improves the performance of multicomponent geothermometry. This is demonstrated in a case study investigating natural fluids from geothermal springs from the geothermal system of the Villarrica area in Southern Chile and fluids derived from laboratory equilibration experiments. Being obviously relative robust against interferences from secondary processes, already initial calculations without corrections lead to comparable well constraint results, with equilibration temperatures for the considered mineral assemblage in the order of <50 K. The anticipated factors most likely causing underestimations of reservoir temperatures, such as dilution of geothermal fluid with surficial water, the pH value and the aluminum concentration, are evaluated and quantified in a sensitivity analysis. According to these results, the calculated temperatures were corrected to obtain realistic in-situ conditions. Doing so, it is shown that well-constraint equilibration temperatures within a range of ≤25 K for the geothermal springs in the Villarrica area and the experimental fluids are obtained.

In the third study, the interfering parameters for SiO_2 and Na-K solute geothermometers are identified and quantified. As for the previously investigated multicomponent method, the geothermometers are applied to the Chilean hot springs and to the same experimental fluids which are derived by equilibrating two reservoir rock analogues from the study area. It is shown, that both applications are obviously effected by reservoir rock composition. Thus, the SiO_2 concentration is controlled by different polymorphs (quartz and chalcedony). Equally, the rock composition is obviously effecting the Na^+/K^+ equilibrium of the fluids. Furthermore, the large effects of dilution and pH value of the fluids on SiO_2 temperatures are demonstrated. Geochemical modeling, chlorofluorocarbon concentration and stable water isotopes measurements of the spring fluids facilitate a correction of data on in-situ conditions and therefore of deduced SiO_2 temperatures. For the selection of the Na-K geothermometers appropriate for the considered fluid, an approach is suggested, to model the stability of Na-K geothermometer governing feldspars (albite and k-feldspar) under in-situ conditions. This supports the allocation of the appropriate geothermometer formulation, which reflects the considered Na^+/K^+ equilibrium best. The obtained SiO_2 and Na-K temperatures fit very well to results from multicomponent geothermometry. The variation between both SiO_2 and Na-K temperatures converge from initially >>100 K to significantly low deviations of ≤10 K.

Kurzfassung

Geothermie hat ein großes Potenzial, um in einem zukünftigen Energiemix eine bedeutende Rolle zu spielen. Sie vereint die Vorteile einer sehr guten Regelbarkeit, bietet alle Voraussetzungen für eine dezentrale Versorgung und ist überdies vollständig grundlastfähig. Dies ist besonders in der Übergangszeit hin zu einer erdölfreien Energiegewinnung wichtig. Hier kann Geothermie sofort Anteile von Kohle und Gas ersetzen. Da sich die Technologie jedoch immernoch in einer frühen Entwicklungsstufe befindet, ist noch eine Vielzahl an Herausforderungen zu bewältigen. Eines der größten Hemnisse ist die Chemie der Fluide. Aufgrund ihrer oft hochmineraliserten Zusammensetzung zusammen mit den sehr hohen Temperaturen, stellen sie ein harsches chemisches Milieu für Rohrstränge und Übertage-Installationen von Kraftwerken darstellen. Die mit der Förderung der Fluide einhergehende Scalingbildung und Korrosion können den Kraftwerksbetrieb stark beeinträchtigen. Darüber hinaus beeinflusst die Komplexität der chemischen Syteme auch die Exploration potentieller Geothermiefelder und trägt maßgeblich zum vergleichsweise hohen Fündigkeitsrisiko bei. Besonders die Geothermometrie, eigentlich eine Standardmethode zur Abschätzung der Reservoirtemperatur aus der chemische Zusammensezung von natürlich austretenden geothermalen Quellen, ist immernoch mit enormen Unsicherheiten behaftet. So führt die Anwendung unterschiedlicher Geothermometer auf eine einzelne Probe nicht selten zu Abweichungen der berechneten Temperaturen in einer Größenordnung von >>100 K.

Mit der Bildung von Scalings und geothermometrischen Explorationsmethoden werden zwei eigenständige Themenbereiche untersucht, die jedoch auf denselben chemischen Grundlagen und Prozessen basieren. Ein gemeinsames Problem beider Themenfelder ist, dass Fluidproben, die typischerweise an der Oberfläche genommen werden, nicht mehr die Bedingungen des Reservoirs widerspiegeln. Um eine belastbare Bewertung des Scalingpotenzials zu erheben und eine Bestimmung der insitu-Temperaturen vorzunehmen, ist es von besonderer Bedeutung, die ursprüngliche Zusammensetzung in der Tiefe zu kennen. In dieser Arbeit werden numerische Verfahren und Laborversuche angewendet, um das Prozessverständnis zu verbessern und die relevanten Prozesse zu quantifizieren. Diese Analysen werden im Hauptteil der Arbeit in drei eigenständigen Untersuchungen dargestellt. Die erste Studie untersucht numerisch die thermo-hydraulisch-chemischen (THC) Prozesse, die in einem Förderstrang eines Einbohrloch-Projekts unter Produktionsbedingungen zu massiver Halit-Scalingbildung führten. Es wird gezeigt, dass das numerische Modell das thermische Verhalten der Bohrung sehr gut abbildet. Aufgrund des hohen Salzgehalts des geförderten Fluids (>400 g/kg$_W$), war die Anwendung des Pitzer Ionen Interaktionsmodells erforderlich. Die Parametrierung des Modells und die Überprüfung ihrer Gültigkeit für das betrachtete chemische System wurden mittels Vergleich der modellierten Löslichkeitsdaten mit

Literaturdaten und mit Resultaten eigener Löslichkeitsexperimente nachgewiesen. Es wird dargestellt, dass ein vollständig gekoppeltes THC Modell benötigt wird, um die komplexe Interaktion von Temperatur, Fluss, Durchlässigkeit und der Präzipitation zu quantifizieren. Dabei ist es möglich, die chemische Zusammensetzung des tiefen Fluids im Hinblick auf die für die Scalings relevanten Bestandteile zu rekonstruieren und die Bildung von Scalings hinsichtlich der Bildungstiefe und der ausgefällten Mengen zu quantifizieren. Darüber hinaus wird gezeigt, dass das kostengünstige, risikoarme Konzept der Verwendung von bestehenden Bohrungen mittels Einbohrloch-Konzept auch deutliche Nachteile hat. Das Modell bildet den unmittelbaren Anstieg des Temperaturgradienten im Produktionsstrang direkt auf der Höhe des beginnenden Gegenstromabschnitts ab. Für eine kühlungsinduzierte Bildung von Scalings ist das Potenzial für ihre Akkumulation in diesem Bereich am größten.

Da ein dringender Bedarf an verlässlichen Tools für die Exploration besteht, wird in der zweiten Studie das Potenzial der Multikomponenten-Geothermometrie bewertet und in einem zweiten Schritt die Methode verfeinert. Das Vorgehen wird in einer Fallstudie gezeigt. Dazu werden natürliche Fluide von heißen Quellen aus dem geothermalen System des Villarrica Vulkans in Südchile und Fluide, aus Laborexperimenten, bei den zwei Reservoirgesteins-Analoge aus dem untersuchnugsgebiet unter insitu-Bedingungen mit Wasser äquilibriert wurden, untersucht. Dabei zeigt sich, dass die Methode vergleichsweise robust gegenüber sekundären Störeinflüssen ist und auch schon ohne Korrekturen Ergebnisse mit nur geringen Schwankungen liefert ($\Delta T < 50$ K). Der Einfluss der Faktoren, die zu einer schematischen Unterschätzung der Reservoirtemperaturen führen, wie die Verdünnung durch oberflächennahes Wasser, der pH-Wert im Reservoir und Schwankungen der Aluminiumkonzentration, werden in einer Sensitivitätsanalyse evaluiert und quantifiziert. Anhand dieser Ergebnisse werden die berechneten Temperaturen korrigiert, um realistische insitu-Bedingungen zu erhalten. So lassen sich für das geothermale System im Untersuchungsgebiet Reservoirtemperaturen errechnen, die zum einen nur eine geringe Schwankungsbreite ($\leq$25 K) zeigen und andererseits sehr gut zu den verfeinerten SiO_2 und Na-K Temperaturen der dritten Studie passen.

In der dritten Untersuchung werden die störenden Parameter für klassische SiO_2 und Na-K Lösungsgeothermometer identifiziert und quantifiziert. Wie im Falle der Arbeit zur Multikomonenten-Methode, wird das Konzept anhand der Quellfluide aus dem chilenischen Untersuchungsgebiet und den Fluiden aus Laborversuchen demonstriert. Dabei wird deutlich, dass beide Geothermometer offensichtlich durch die chemische Zusammensetzung des Reservoirgesteins beeinflusst sind. So hängt das Polymorph, das die SiO_2 Konzentration kontrolliert, offenbar genauso vom Reservoirgestein ab, wie das Na^+/K^+-Gleichgewicht der Fluide. Des Weiteren werden die großen Auswirkungen der Verdünnung und des pH-Werts der Fluide auf die SiO_2 Temperaturen nachgewiesen. Es wird dargestellt, wie mittels

geochemischer Modellierung, Chlorfluorkohlenwasserstoff-Konzentrationsmessungen und der stabilen Wasserisotope eine Korrektur der Daten auf die insitu-Bedingungen möglich ist und wie sich so die SiO_2-Temperaturen korrigieren lassen. Für die Auswahl der geeigneten Na-K Geothermometer, wird ein Ansatz vorgeschlagen, welcher mittels Betrachtung der Gleichgewichtszustände von Albit und K-Feldspat, die Auswahl des passende Na-K Geothermometers für das jeweils betrachtete Fluids unterstützt. Die Abweichung zwischen den so erhaltenen SiO_2 und Na-K Temperaturen konvergieren von zunächst >>100 K zu deutlich niedrigen Abweichungen von ≤10 K. Die Temperaturen passen außerdem sehr gut zu den Ergebnissen der Mehrkomponenten-Geothermometrie. Maximale Abweichungen liegen im Bereich von <20 K.

Table of Contents

1 Introduction

The global climate steadily changes towards warmer temperatures. The annual global mean temperatures already increased by around 0.8 K compared to a commonly considered mean temperature of the time interval from 1951 to 1980 and around 1.3 K compared to pre-industrial times (*Fig. 1.1*).
This global warming is considered to be caused by emissions of greenhouse gases and their accumulation in the atmosphere (Stocker et al., 2013). The IPCC considers above all the combustion of fossil fuels as the major source of anthropogenic CO_2, and therefore as the principal driver of global warming. The consequences comprise extensive glacier melting, droughts, shortage of drinking water and global sea-level rise (Field et al., 2014).
Many studies in the field of global climate system predict a continuation of this trend of increasing earth surface temperature (Bretherton et al., 1990; Crubash and Meehl, 2001). In order to keep climate change and associated consequences on a controllable level, 148 countries recently ratified the Paris Agreement from December 2015, in which the parties decided binding climate targets. Thus, the global warming has to be limited to an increase of smaller than 2 K. It was agreed that CO_2 emission as a major warming driver must be reduced. In 2016, the German government passed the "Climate Action Plan 2050". It represents the guideline towards a nationwide greenhouse gas neutral energy generation until 2050 (BMUB, 2016).

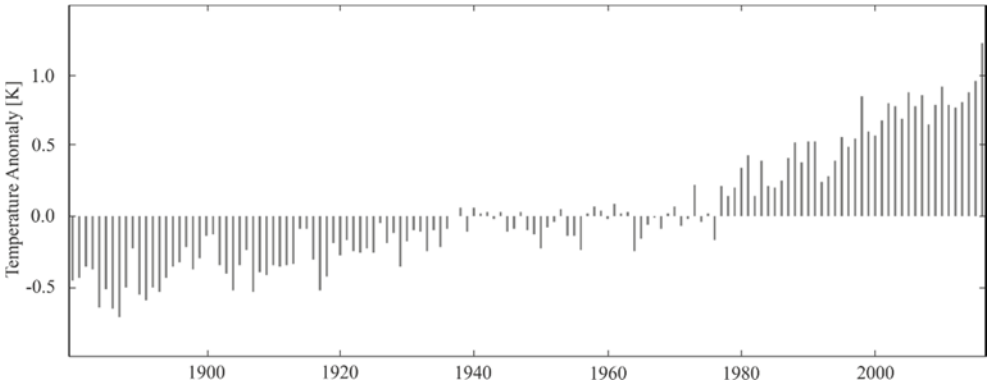

Fig. 1.1: Global annual mean surface temperature anomaly relative to the 1951-1980 interval mean temperature. Data compiled from Hansen et al. (2010) and GISTEMP (2017).

In such a sustainable energy mix relying on renewable resources, geothermal energy can supply a substantial proportion. One major advantage, where geothermal energy stands out from many other renewables, is the ability to supply baseload demands. At the same time geothermal energy is fully controllable and suitable for a decentralized usage.
2015 the worldwide installed capacity of 12,635 MWe produced energy of 73,549 GWh (Bertani, 2015). It is projected to reach 1,400 TWh in 2050 (IEA,

2011). This would be equivalent to ~3.5 % of the world total electricity production. The gap to be filled is still large. Extrapolating the recent development into future, targets would be missed. The development of geothermal energy is still facing major financial impediments, for instance in terms of high investment costs and prospecting risks. Furthermore, also from a scientific and engineering view, the learning curve has to be steepened. Further improvements are required in the handling of the often challenging chemistry of geothermal fluids. Corrosion and scaling formation in the pipe strings and in the surface installations are typical phenomena, which can impair operations substantially.

1.1 Challenges and Chances of Complex Chemistry

The conditions during the genesis of a geothermal fluid are very special in many respects compared to fluids evolved under ambient conditions in our environment at the earth's surface or in shallow groundwater aquifers. Absolute temperatures in geothermal reservoirs are often exceeding twice the values surficial waters are exposed to. Pressures are at least reflecting hydrostatic conditions and, therefore, values range in the order of several hundreds of bar. On the way from recharge areas to the reservoirs, the fluids are in contact and react with a large number of minerals. Under these strongly elevated P-T conditions, fluids have an enormous dissolution capacity. Especially in deep seated reservoirs within basin and graben structures, where the fluids often show long residence times, typically highly mineralized brines prevail. In the Upper Rhine Graben geothermal fluids reach a mineralization of up to 200 g/kg_W (Sanjuan et al., 2016), in the North German Basin fluids have been reported to reach halite saturation, which corresponds to a total salinity of > 400 g/kg_W (Nitschke et al., 2017).

The consequences for the use of geothermal energy are manifold. The highly saline, typically Cl^--dominated fluids represent a harsh and highly corrosive media to metallic construction materials and require the use of resistant and often very expensive alloys. Thus, corrosion is still one of the greatest concerns to operators of geothermal plants (Mundhenk et al., 2013). The high volumes of fluids produced and the associated high temperature and pressure gradients, which are induced by forced flow, favor the formation of scaling. These mineral precipitation occurs in pipe strings and surface installations of many geothermal developments around the world. Gunnarsson and Arnórsson (2003) as well as Brown (2011) consider silica scaling even the principal obstacle for the extraction of energy from high-temperature geothermal fluids.

Beside these engineering and operational problems, often sampling, sample handling in the laboratory and analytics of these fluids are challenging. Most hydrochemical laboratory methods have been developed for the analysis of environmental fluids. For often supersaturated geothermal fluids (under laboratory conditions), new

approaches of solutions stabilization has to be applied. High mineralization of the fluids requires in most cases high dilution for analysis. Therefore, error propagation is becoming an important topic and strategies of trace element determination have to be developed.
Usually, at the surface already cooled and depressurized fluids are sampled. Thus, these samples do not reflect reservoir condition, as the chemical system (P-T conditions) and the fluid composition (e.g. degassing, re-equilibration) have already changed. Therefore complicated and expensive downhole sampling has to be applied, or the in-situ conditions have to be determined using numerical models. This leads to the next challenge, as numeric tools approach their limits of validity and applicability, as thermodynamic data is progressively becoming rare for elevated temperature and salinities
On the other hand, the dissolved load of geothermal fluids as a result of water-rock interaction in depth has also its positive aspects. The composition of a fluid discharging at the surface, is in some way an image of its history and location, where it was formed. Thus, chemical composition of fluids are widely used for exploration purposes. It is possible to draw conclusions on fluid genesis. Thus, it is possible to discriminate old deep-seated fluids, from fossil sea-waters or from fluids having a meteoric origin. The chemical composition entails information whether the reservoir is vapor or fluid dominated, which is especially important for the design of power plants exploiting high-enthalpy resources. Furthermore, questions concerning the sustainability of production of a reservoir like residence times, age and recharge area can be clarified. Moreover, a detailed chemical analysis is basis for the evaluation of the scaling and corrosion potential of a fluid. Certainly the most popular application in geochemical exploration is the application of solute geothermometers. It is a common technique to estimate the temperatures of projected reservoirs mainly from cation ratios of natural discharging hot spring fluids.

1.2 Structure of Thesis

This study aims to contribute to the scientific progress in the field of chemistry of geothermal fluids in order to overcome chemical obstacles impeding a faster development of geothermal energy use. The work investigates two autonomous thematic fields, which both are based on the same water-rock interaction and dissolution/precipitation processes: a) scaling formation as a consequence of geothermal production and b) evaluation and refinement of geothermometric methods. Therefore, the content is sub-divided in two parts. The first part especially focusses the quantification of coupled thermo-hydraulic-chemical processes controlling dissolution and precipitation in a borehole as basis for future scaling potential evaluation and development of production scenarios, which can avoid or reduce scaling. The second part of the work targets to minimize exploration and

prospecting risks by developing numerical and experimental strategies to reconstruct the realistic in-situ conditions. Based on the surface sample compositions a refinement of geothermometer application is then possible and temperatures with reduced uncertainties should be obtained. The result of this research is presented in terms of individual manuscripts, which were published (*chapter 5 and 6*) in or submitted after revision (*chapter 7*) to international journals. One additional peer-reviewed manuscript is attached to the appendix (*app. A*), as major parts of data collection have been conducted before the doctoral studies.
In *chapter 2*, an introduction into the mechanisms of scaling formation is given and fundamentals of solute geothermometry, as well as first insides into the uncertainties of the method are provided. The principles of the used numerical tools for the quantification of the chemical systems and reactive transport processes is described in *chapter 3*. Then, in *chapter 0* insides to the experimental approaches, which were performed for improving process understanding and supporting model parameterization, were given. Thereafter, the manuscripts are presented as outlined below.

Chapter 5
THC Model of Scaling Formation Conditions in the GeneSys Production String

This study investigates the coupled thermo-hydraulic-chemical processes during production leading to scaling formation. As a case study, the 2011 circulation test of the geothermal single-well project GeneSys (Gt1 Groß-Buchholz, Hanover), which failed due to extensive halite scaling formation, is modeled using the fully coupled THC code TOUGHREACT. High brine salinities requires the application of the Pitzer ion interaction model. It is shown that thermal behavior is modeled in very good accordance with on-site wellhead temperature measurements. Also the simulated depth of scaling formation and total scaling volume fit to onsite observations. Determination of reservoir brine composition reveals its large impact on the depth interval where scaling occurs, especially considering the role of $CaCl_2$, which reduces halite solubility considerably and favors scaling formation.

Chapter 6
Parameter Sensitivity Study for Improving Multicomponent Geothermometry

In this work the performance of classical solute geothermometers and the method of multicomponent geothermometry is assessed by applying them to fluids composed from long term batch-type equilibration experiments and to fluids from natural geothermal springs in the Villarrica area, Southern Chile. Strong impact of reservoir rock lithology is highlighted, affecting particularly the classical geothermometers. The more robust multicomponent method is improved by correcting the obtained

equilibration temperatures from secondary processes (dilution, unknown in-situ pH and precipitation affected Al concentrations) by means of sensitivity analysis.

Chapter 7
Refinement of SiO_2 and Na-K Geothermometers

The application of different Na-K and SiO_2 geothermometers, the most widespread used methods, not uncommonly lead to deviations, which reach 200 K for one sample. In this study, the most sensitive interfering factors for these geothermometer applications are identified and quantified. A multi-step approach is proposed, combining experimental and numerical methods together with methods for fluid characterization, to correct the measured data at the spring discharge and to allocate the appropriate geothermometer to every individual fluid type.
A chlorofluorocarbon concentration based mixing model is used to correct SiO_2 concentrations on original in-situ concentrations. A numerical model yield the in-situ pH, which is highly solubility sensitive. Results from long-term laboratory equilibration experiments are evaluated to identify the reservoir type dependent equilibrated SiO_2 polymorph. The Na^+/K^+ ratio of a fluid is obviously not solely temperature dependent, but also effected by reservoir rock composition. By numerically evaluating the stability of albite and orthoclase, it is possible to identify the Na-K geothermometer equation, which reflects the present Na-K equilibrium best. Doing so, well constraint subsurface SiO_2 and Na-K temperatures ($\leq$ 10 K) for the Villarrica geothermal system are obtained.

Appendix A
Bacteria Induced Sulfate-Sulfide Scaling Formation in Soultz-sous-Forêts

Scaling formation in the heat exchanger of the geothermal power plant of Soultz-sous-Forêts, France, substantially affect power production by impairing heat transfer and reducing pipe diameters. For a fundamental process understanding as basis for future inhibition strategies, this study investigates the complex formation mechanisms. Fluids and solids are sampled and analyzed. It is shown, that fluids are oversaturated with respect to barite and celestine. X-Ray diffraction measurements together with scanning electron microscopic observation reveal that the scalings consist of barite-celestine solid solution ($BaSrSO_4$) interlayered with fine beds of galena (PbS). $\delta^{34}S$ measurements indicate bacterial sulfate reduction for the source of reduced sulfur and therefore triggering sulfide scaling. The layered structure of the scalings can be well correlated with the operation state of the plant and the prevailing temperatures. Sulfates form under regular operations, whereas sulfides precipitate during start and shut-off phases.

2 Dissolution and Precipitation Processes in Geothermics

Water-Rock Interaction is a collective term for chemical processes occurring at the interface of solids (minerals) and fluids (aqueous solution), entailing consequences for the chemical (mineralogical) composition of both phases. Chemical systems always tend towards a state of equilibrium (*chapter 3.1*), e.g. by compensating dis-equilibria by dissolving or precipitating solids. The same applies for the interaction of a gas phase with water. A chemical dis-equilibrium of a geothermal fluid can have many causes: conductive temperature changes, depressurization, dilution with low mineralized water, boiling as a consequence of exceeded saturated water vapor pressure, steam heating in volcanic systems or mixing with fluids of incompatible compositions. Thus, any type of fluid (infiltrating meteoric water of low mineralization, sea water or old, highly mineralized fluids) moving along a temperature or pressure gradient, constantly changes its composition as a function of initial salinity, time, temperature- and pressure change. All of these processes disturb the chemical system in a sense that dissolution or precipitation is the result. Being the case in slow natural geothermal systems of rather weak gradients, becoming even more obvious for geothermal projects where deep boreholes, forced fluid flow of big volumes and large heat sinks (heat extraction) interfere the chemical system. In the following sections scaling, a major concern to power plant operators, and the consequences for geochemical exploration are introduced in closer detail.

2.1 Scaling Formation

Geothermal fluids are often considered to be in chemical equilibrium (or near equilibrium state) at depth with respect to the mineral assemblage in the reservoir (Arnórsson, 2000a). That means the fluid is saturated with respect to a number of rock forming minerals under prevailing P-T conditions. The production of a geothermal fluid intrinsically changes these intensive variables governing the chemical system. The large majority of minerals is characterized by a prograde solubility behavior (Brown, 2013). That means they show decreasing solubility with decreasing temperature and pressure. As a consequence, the production of a fluid of near-equilibrium always has a high potential of being supersaturated at surface conditions (or operating conditions of a plant). Mostly due to kinetical barriers, scaling is not occurring at every producing borehole even without inhibiting measures like pressure maintenance or chemical antiscalants. For most minerals, despite being supersaturated, the overall temperature niveaus are too low and the transit times through wellbores and surface installations are too short to precipitate.

Nevertheless, still a large number of geothermal developments are affected by scaling and, thereby, many different types of scaling can be observed.
According to literature reporting from deep fluid productions, there are six different classes of scalings. The most widespread scalings consist of carbonates and silica (Brown, 2013). Carbonates are found as calcite, aragonite, witherite, siderite and malachite (Bjornstad and Stamatakis, 2006; Holl et al., 2003; Stahl et al., 2000). Silica scaling is very common for projects producing from high enthalpy systems. It typically forms precipitates of amorphous SiO_2 (Corsi, 1987).
Furthermore, sulfates are common scalings. Forming a complete solid solution series, barite and celestine represent the most abundant minerals (Nitschke et al., 2014; Schmidt et al., 2000). From other sites also gypsum and anhydrite is reported (Corsi, 1987). Sulfides represent another common scaling class, with galena, copper-, zinc-, iron- and antimony sulfides showing great diversity (Nitschke et al., 2014; Schmidt et al., 2000). Despite halides are highly soluble also halite and sylvite occasionally occur as scaling (Hesshaus et al., 2013; Raymond et al., 2005). Zero-valent metals were often found in association with sulfides. Elemental lead, zinc, copper, iron and vanadium are observed frequently (Lebedev, 1972).
The mechanism for all above named minerals is always the same. Precipitation of those minerals characterized by a prograde solubility (highly sensitive temperature, only minor effects of pressure) occurs as a consequence of cooling. The only exception are the carbonates. The actually favorable retrograde solubility is overcompensate by a very high sensitivity on pressure change. The depressurization of the chemical system during production causes dissolved CO_2 to degas. As a consequence, the pH of the fluid rises and carbonate species are formed until saturation of carbonate mineral is attained (Bjornstad and Stamatakis, 2006) causing precipitation. A third mechanism provoke scaling, accounting for each above named type, is the loss of solvent. By separating steam from geothermal fluids in flash plants, the residual liquid fraction is concentrated (steam loss). In this way, very prompt, a high-degree of supersaturation can occur. Furthermore, scaling formation can also be induced by bacterial activity. Hyper-thermophilic bacteria can alter the chemical system locally. One example are sulfate reducing bacteria, which produce HS^- from SO_4^{2-} as a product of their metabolism. Given the presence of heavy metal cations, the saturation of very low soluble heavy metal sulfides is exceeded rapidly. This type of scaling genesis was proven for instance for the Soultz-sous-Forêts geothermal site in France (in *appendix A*, (Nitschke et al., 2014)).
Scaling causes a number of problems to power plant operation. By impairing the heat transfer between fluid and heat exchanger surfaces, coating of even little thickness affects heat extraction in a plant. Progressing mineral precipitations lead to a decline of diameters of surface installations and can even completely clog pipe strings. For such scenarios of complete pipe obstructions, requiring high precipitation volumes, only a few highly soluble minerals are eligible. It is reported of halite (Hesshaus et al., 2013), calcite (Sánchez-Rivera et al., 2005) and silica (Gunnarsson and

Arnórsson, 2005), which can clog pipes and interrupt production or even lead to the abandonment of projects.
The precipitation of scalings is governed by highly complex coupled thermo-hydraulic-chemical processes. In a case study (*chapter 5*), it is shown how these processes mutually interact leading to massive precipitations and how they can be numerically quantified.

2.2 Solute Geothermometry

Geothermal exploration in general aims to collect data in order to localize resources and evaluate their potentials for exploitation. Methods ideally have to be cost-effective and subject to a minimum of uncertainties. According to equation (*E1.1*) it is, beside of the flow rate, the temperature of the fluid which controls the amount of energy that can be extracted from a reservoir and is therefore a key parameter for the economic evaluation of a future reservoir.

$$E = Q \cdot \rho c_P \cdot \left(T_{prod} - T_{inj}\right) \qquad (E1.1)$$

with flow rate Q, water density ρ, specific heat of water c_P and absolute temperatures of produced fluid T_{prod} and injected fluid T_{inj}.

Due to being cheap and easily applicable, solute geothermometry is a popular and very widespread used tool for estimations of subsurface temperatures. The concept is to measure the chemical composition from a (naturally) discharging geothermal fluid and conclude on the reservoir temperature. The onset of the method was back in the 1960's when Bödvarsson (1960) used the SiO_2 content of different spring fluids as a relative measure for the in-situ temperature. With experimental solubility determination of quartz over a broad temperature range (Morey et al., 1962) and a correlation of silica concentrations and downhole temperatures (Mahon, 1966), quantitative temperature estimation became possible. Recently, typically used silica geothermometer also distinguishing between quartz and chalcedony (Arnórsson, 2000b; Fournier, 1977; Verma, 2000)
Beside of this method, which is based on the solubility of a single mineral phase, especially the ratios of major and trace element cations have been used for geothermometry. The most common application is the (semi-)empirical Na-K geothermometer (Arnórsson, 2000b; Can, 2002; Diaz-Gonzalez et al., 2008; Fournier, 1979; Fournier and Truesdell, 1973; Giggenbach, 1988; Nieva and Nieva, 1987; Verma and Santoyo, 1997), which is considered to reflect temperature dependent Na^+-K^+ substitution of albite and orthoclase (e.g. Can, 2002; Giggenbach, 1988). Extending the Na-K formulation, Fournier and Truesdell (1973) and Kharaka

and Mariner (1989) established the Na-K-Ca geothermometer by additionally considering Ca^{2+} concentrations. Giggenbach (1988) combined the Na-K geothermometer with the also as stand-alone application used K-Mg geothermometer (Fournier, 1991; Michard, 1990). Fournier and Potter (1979) extended it by adding a Mg^{2+} correction. Also the Na-Ca (Tonani, 1980) and the K-Ca (Michard, 1990; Tonani, 1980) ratios are reported to reflect reservoir temperatures. Many formulations have been established entailing the conservative Li^{+} cation. Frequently used ratios are the Na-Li (Fouillac and Michard, 1981; Kharaka and Mariner, 1989; Sanjuan et al., 2014; Verma and Santoyo, 1997) and the Li-Mg geothermometer (Kharaka and Mariner, 1989). Cs-Na and Rb-Na formulations were introduced by Michard (1990).
Each above named geothermometer, except for silica and to some extend also for Na-K applications, are empirically derived by correlating cation ratios to temperature measurements. Ideally, this is done using bottomhole temperatures of wells to really rely on in-situ conditions. Despite the long history of solute geothermometry, their widespread application with associated great existing expertise and progressively made improvements of the methods, geothermometers are still afflicted with large uncertainties.

Table 2.1: Chalcedony and quartz temperatures (Fournier, 1977), Na-K temperatures (Fournier, 1979), K^2-Mg temperatures (Giggenbach, 1988), Na-Li temperatures (Kharaka and Mariner, 1989) and Na-K-Mg temperatures (Nieva and Nieva, 1987) for natural hot springs of the Villarrica geothermal system in Southern Chile. Rearranged table from Nitschke et al. (2016).

Springs	Liquine	Toledo	Menetue	Los Pozones	Conaripe	Liucura	Rinconada
Chalcedony	115 °C	89 °C	99 °C	72 °C	107 °C	73 °C	121 °C
Quartz	141 °C	118 °C	126 °C	102 °C	134 °C	103 °C	147 °C
Na/K	136 °C	138 °C	102 °C	114 °C	134 °C	168 °C	252 °C
K^2-Mg	98 °C	99 °C	56 °C	72 °C	78 °C	63 °C	68 °C
Na-Li	150 °C	184 °C	184 °C	163°C	166°C	93 °C	156 °C
Na-K-Mg	127 °C	115 °C	117 °C	111 °C	147 °C	159 °C	224 °C

In Nitschke et al. (2016) a suite of geothermometers were calculated exemplarily for a selection of hot springs discharging in the Villarrica area in Southern Chile. Despite careful selection with regard to the applicability of geothermometers for the expected conditions, it was demonstrated that there is a high variation of calculated temperatures (*Table 2.1*). The spread of results reaches nearly 200 K for the sample Rinconada comparing the Na-K (252 °C) and the K^2-Mg (68 °C) temperature. Based on these results, a reliable conclusion on realistic in-situ temperatures is not possible. It requires further investigation, concerning the identification of factors which interfere consistent results in order to facilitate a correction of temperatures.

This part of the study introduces into fundamentals of SiO_2 and Na-K geothermometry and gives first insights into the occurrences of large uncertainties of the two most often used applications. Evaluating the Na-K geothermometer, the disadvantage of a (semi-)empirical approach becomes obvious. Together with the unknown or poorly constraint underlying equilibrium reactions, also the interfering factors of the systems remains unknown. And even by knowing some, a quantitative correction is hardly possible. *Fig. 2.1* illustrates the accomplishment of Na-K-temperature interrelation. Plotting the original data and correlations of common Na-K geothermometers (Arnórsson, 1983; Fournier, 1979; Fournier and Truesdell, 1973; Michard, 1990) individually, it seems that the authors mostly worked on data of high quality regarding the scattering and that they found good fits. Especially the Na^+/K^+ data of Arnórsson (1983) and Michard (1990) nicely correlate with temperature. However, the combined plot of the same datasets in *Fig. 2.1e* reveals, that the Na^+/K^+ ratios of all samples scatter significantly in a temperature interval cooler than 150 °C. At warmer temperatures the data is much more consistent, however, unfavorably the gradient becomes progressively smaller. Small measurement errors have large effects on obtained results for temperatures > 200 °C.

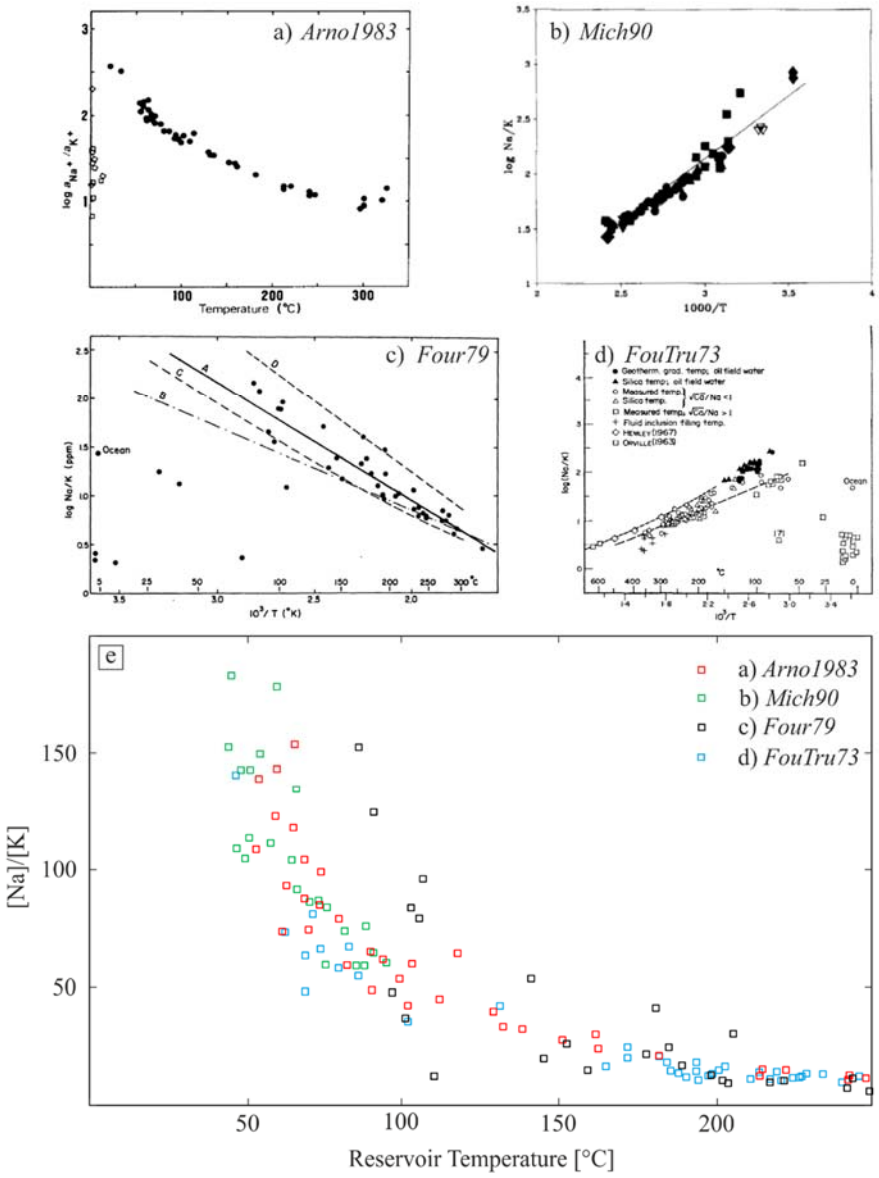

Fig. 2.1: a) to d): Original datasets and correlations of commonly used Na-K geothermometers (Arnórsson, 1983; Fournier, 1979; Fournier and Truesdell, 1973; Michard, 1990) and a plot combining these datasets (e).

Knowing that the above named studies (and many other works which established Na-K geothermometers) correlate fluids from different geothermal systems and geological settings and the large number of different resulting equations, it seems plausible that one of the interfering parameters may be the impact of different geological setting or reservoir mineralogy. These are factors rather less attention is paid to, when selecting the appropriate Na-K geothermometer for the application during exploration.

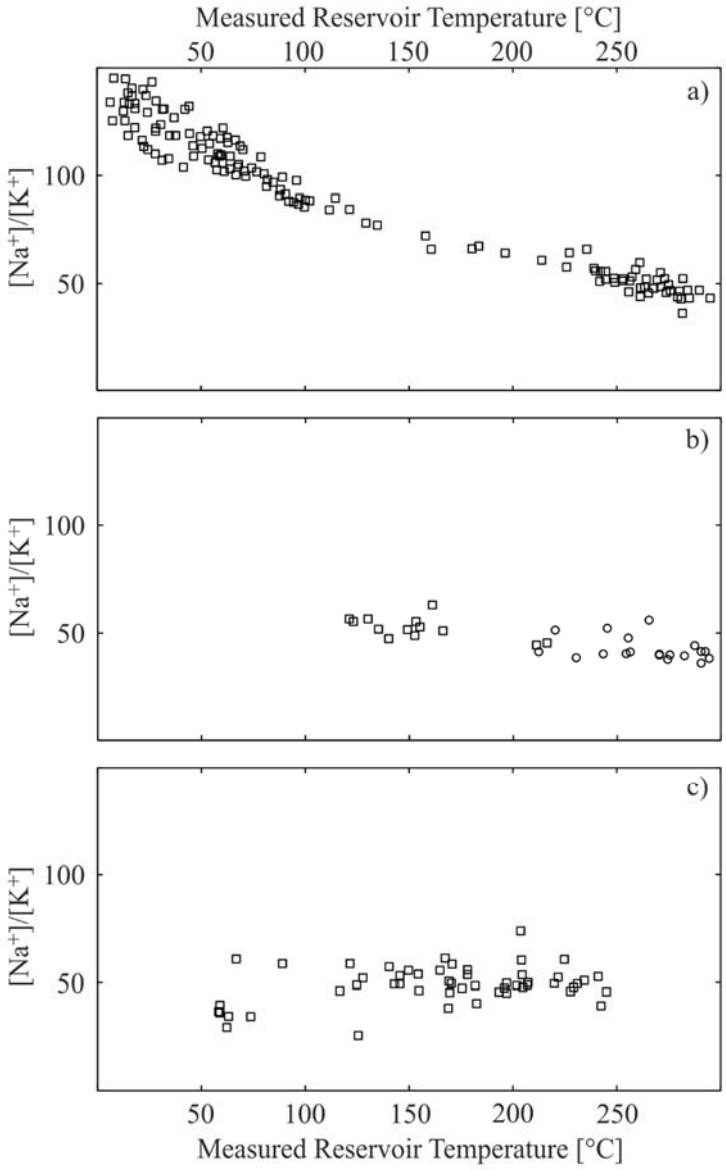

Fig. 2.2: *Compiled data of Na^+/K^+ ratios of geothermal fluids plotted versus measured bottom hole temperatures of wells: a) data for basaltic fluids from Iceland (Arnórsson, 2000b), b) volcanic systems of Rotorua, New Zealand (rhyolithic reservoir), and Olkaria, Kenya (with a broad range of volcanic rocks, most abundantly trachytic) (Karingithi et al., 2010; Mroczek et al., 2003) and c) heterogenic graben setting (gneiss basement, covered by mica schists, phyllites, meta-quartzites, marbles and meta-carbonates of the Buyuk Menderes Graben, Turkey (Filiz et al., 2000; Karakuş and Şimşek, 2013; Simsek, 2003).*

In order to illustrate this effect, *Fig. 2.2a* displays data of Na^+/K^+ ratios of fluids from geothermal wells in Iceland (Arnórsson, 2000b), fluid data from Rotorua geothermal field in New Zealand and the Olkaria field in Kenya (*Fig. 2.2b*) and fluids from Büyük

Menderes Graben in Turkey (*Fig. 2.2c*). In order to exclude perturbation by secondary effects (incorrect temperatures, precipitation, etc.) this dataset compilation only considers well data, ensuring direct temperature measurements and short travel time between reservoir and discharge. Na^+/K^+ ratios of basaltic fluids from Icelandic wells follow an inverse proportional correlation with temperature with very low scattering. For fluids originating also from volcanic systems of Rotorua and Olkaria, which have, however, been in contact with rhyolitic and trachytic reservoir rocks, the gradient of the correlation slope appears to be smaller, whereas no correlation is observed for fluids with heterogeneous origin in the complex setting (gneisses, mica schists, phyllites, meta-quartzites, marbles and meta-carbonates) of the Büyük Menders Graben.

By investigating the interrelation of SiO_2 concentrations and temperatures for the same wells as for the Na^+/K^+ ratios, proportional trends for each system are observed (*Fig. 2.3*). Compared to the results for Na-K temperatures, effects of different geological settings cannot be identified (at least for this dataset). However, some lower outliers exist at temperatures exceeding 200 °C, which are usually attributed to precipitation of amorphous silica (Arnórsson, 2000a), this method seems to be very consistent.

The silica based temperature estimations rely on solubility data of SiO_2 polymorphs and therefore on a profound thermodynamic basis. However, considering only one component of a fluid, this application is particular prone to processes associated with changes of the amount of solvent and to precipitation. Dilution, mixing, boiling and re-equilibration alter SiO_2 concentrations on the way from reservoir to discharge.

For a more precise and site-specific investigation of the impact of reservoir rock composition on both geothermometers, laboratory batch experiments under presumed reservoir conditions, equilibrating reservoir rock analogues, were conducted (*chapter 4.2* and *chapter 6*). In *chapter 7* the impact of further interfering factors like the in-situ pH, the equilibrated SiO_2 polymorph, and dilution and boiling were quantified and results were corrected accordingly, leading to significantly better constraint reservoir temperatures.

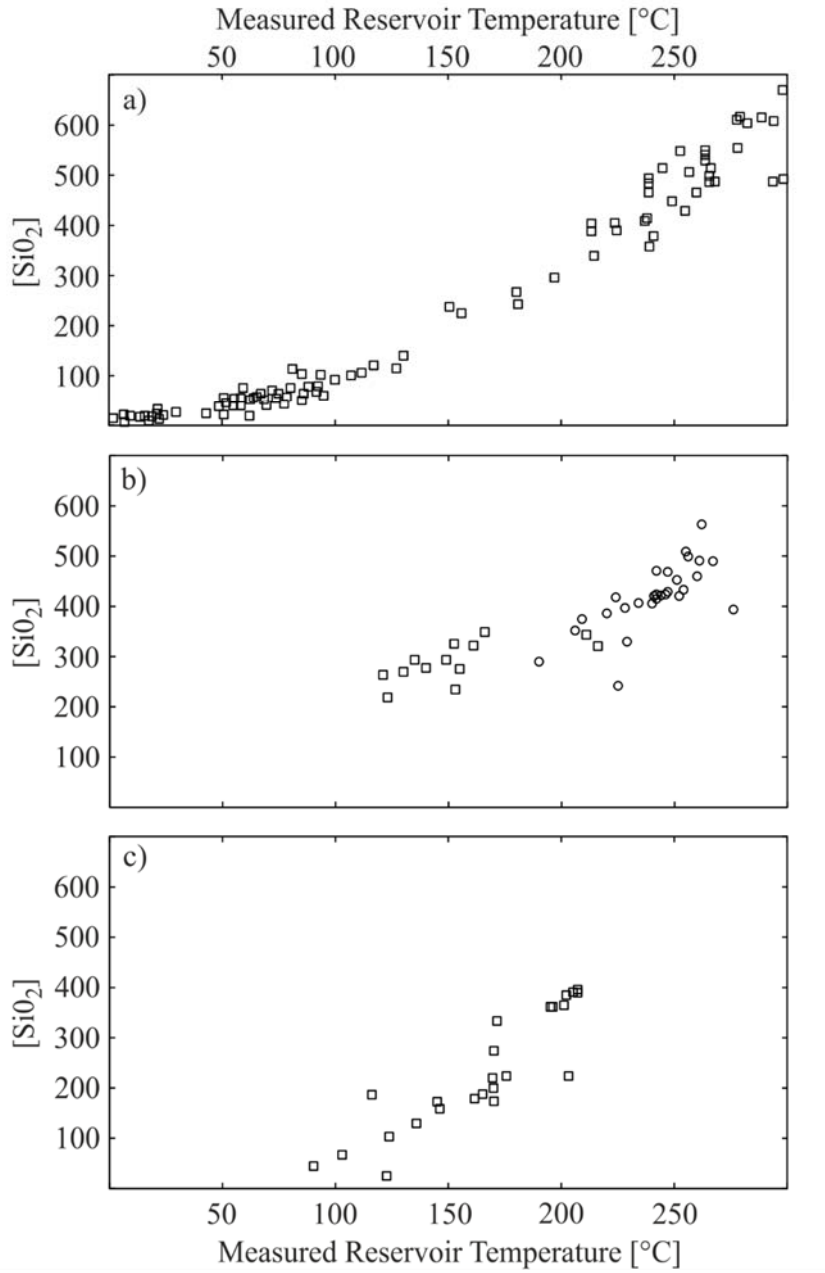

Fig. 2.3: Compiled data of SiO_2 concentrations of geothermal fluids plotted versus measured bottom hole temperatures of wells: a) data for basaltic fluids from Iceland (Arnórsson, 2000b), b) volcanic systems of Rotorua, New Zealand (rhyolithic reservoir), and Olkaria, Kenya (with a broad range of volcanic rocks, most abundantly trachytic) (Karingithi et al., 2010; Mroczek et al., 2003) and c) heterogenic graben setting (gneiss basement, covered by mica schists, phyllites, meta-quartzites, marbles and meta-carbonates of the Buyuk Menderes Graben, Turkey (Filiz et al., 2000; Karakuş and Şimşek, 2013; Simsek, 2003).

3 Numerical Modeling

3.1 Chemical Equilibrium

A chemical system is in equilibrium if all its intensive variables are invariant and the system shows no tendency to change. Showing variations of temperature, pressure and chemical composition from area of infiltration towards the reservoir and finally to the spring discharge, geothermal systems would be a paradigm for a system, which never reaches equilibrium. For this reason, only small spatial sections on a short time scale are considered evaluating water-rock equilibrium. Whenever equilibrium is discussed, the term refers to the local chemical equilibrium within the reservoir.
Chemical equilibrium is considered to be the steady state of a system, when no more overall changes of educts and products can be observed. Even more specifically, in terms of geothermometry it is only the steady state of the fluid, i.e. a partial equilibrium of a single phase of a system, which is of interest.
Chemical equilibrium is defined as the state of a reaction where the function of the Gibbs free energy has its minimum (*Fig. 3.1*) or where the derivative of the function is equal to zero.

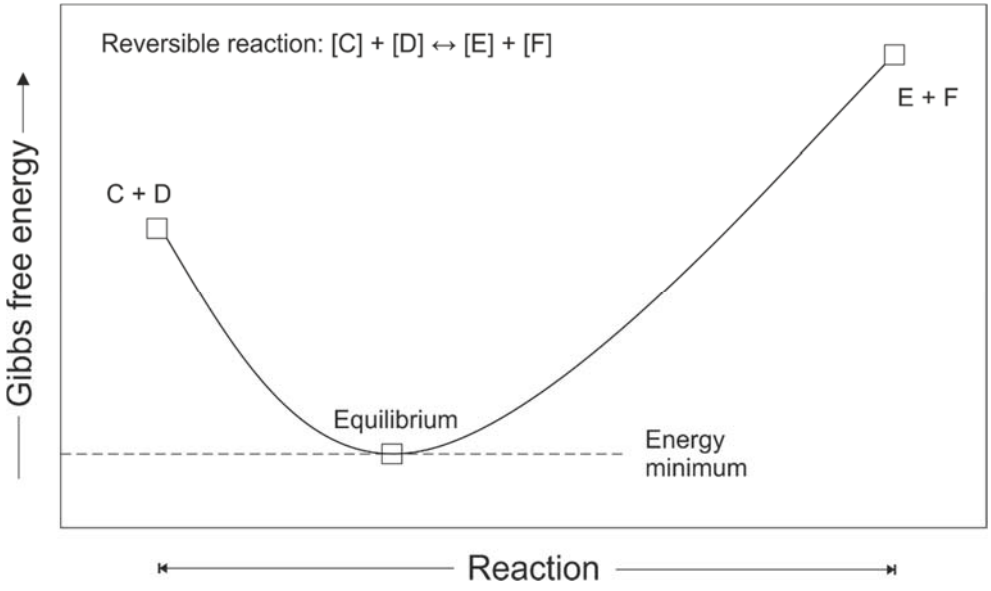

Fig. 3.1: Schematic plot of Gibbs free energy versus progress of reaction. The minimum of the energy function indicates the equilibrium point for the reaction.

The derivative of the Gibbs free energy G of an involved chemical specie C is defined (*E3.1*) to be the chemical potential μ of the species with respect to its amount of substance n.

$$\mu_C \Leftrightarrow \frac{\partial G_C}{\partial n_C} \qquad (E3.1)$$

By defining the reaction coefficients c, d, e and f to represent the amounts of substances n_C, n_D, n_E and n_F, the point of equilibrium for the arbitrary reaction

$$cC + dD \Leftrightarrow eE + fF \qquad (E3.2)$$

with respect to the individual amounts of substances is where the sum of all involved chemical potentials is equal to zero according to *E3.3*.

$$e\mu_E + f\mu_F - c\mu_C - d\mu_D = 0 \qquad (E3.3)$$

The chemical potential of aqueous species is dependent upon temperature T, pressure P and its activity a. It can be calculated from adapting the standard potential of the species (*E3.4*) with R being the gas constant

$$\mu^* = \mu^0 + R \cdot T \cdot \ln(a) \qquad (E3.4)$$

The activity a of the dissolved species accounts for the non-ideal behavior of a real solution. It is linked via the activity coefficient γ quantifying proportionally the deviation from behavior in an infinitely diluted solution (*E3.5*),

$$a = \gamma \cdot n \qquad (E3.5)$$

which then would be $\gamma = 1$. Substitution of the chemical potential of each component *E3.4* into *E3.3* yield the equilibrium criterion for above mentioned exemplary reaction (*E3.2*) in terms of the chemical potentials of its reactants is

$$e\mu_E^0 + f\mu_F^0 - c\mu_C^0 - d\mu_D^0$$
$$= -R \cdot \mathrm{T}(\mathrm{e} \cdot \ln(\mu_E) + f \cdot \ln(\mu_F) - c \cdot \ln(\mu_C) - d \cdot \ln(\mu_D)) \qquad (E3.6)$$

For a convenient calculation the point of equilibrium for a reaction can be given by the equilibrium constant K. It is defined in terms of the standard free energy ΔG^0 of a reaction (and therefore by the Gibbs free energies of all reactants ($\Delta G_{products}$ - ΔG_{educts})) and can be written as (*E3.7*)

$$\ln(K) = -\frac{\Delta G^0}{R \cdot \mathrm{T}} \qquad (E3.7)$$

Thus, the equilibrium criterion (*E3.8*) can be expressed as

$$\ln(K) = \mathrm{e} \cdot \ln(\mu_E) + f \cdot \ln(\mu_F) - c \cdot \ln(\mu_C) - d \cdot \ln(\mu_D) \qquad (E3.8)$$

The transformation of *E3.8* into *E3.9*

$$K_M = \frac{(a_E)^e \cdot (a_F)^f}{(a_C)^c \cdot (a_D)^d} \qquad (E3.9)$$

represents the common mass action equation K_M. This derivation shows that the mass action equation reflects thermodynamic equilibrium for considered P-T-X conditions.
The same applies to the related solubility product K_S. For all minerals considered in this study, we assume pure end-member compositions, entailing the consequences that $a_{xy} = 1$ and $\gamma^* = \gamma^0$ and therefore, with the denominator being equal to 1, the solubility product (*E3.11*) of an arbitrary dissolution reaction (*E3.10*)

$$X_x Y_y \Leftrightarrow xX^{y-} + yY^{x+} \qquad (E3.10)$$

becomes

$$K_S = (a_X)^x \cdot (a_Y)^y \qquad (E3.11)$$

For the evaluation of the equilibrium state of a fluid with respect to a considered mineral phase *m* at given P-T-X conditions the saturation index (*E3.12*) is defined to be

$$SI_m = log\left(\frac{Q_m}{K_s}\right) \qquad (E3.12)$$

with Q being the activity product (*E3.13*) of the dissociated components of the mineral

$$Q_m = \prod_{j=1}^{n_c} a_j^u \qquad (E3.13)$$

where *j* is the amount of components and *u* is the stoichiometric coefficient. The *SI*, therefore, is a measure of the amount which is actually dissolved compared to the dissolved amount at the point of equilibrium. $SI > 0$ indicates an oversaturated fluid, $SI < 0$ reflects undersaturation. The values of *SI*, however, do not reflect the distance

to equilibrium quantitatively, when comparing saturation states of two minerals. As being a function of the size of the formula unit of a mineral, it just allows qualitative comparison.

3.2 Chemical Models

The actual challenge of computing chemical models, in particular for calculating geothermal application with their typically strongly increased mineralized fluids, is the determination of the correct activity coefficients for the dissolved species. The chemical systems, which are considered in this study, show a large bandwidth of total dissolved solids (TDS), but being in any case far away from the idealized consideration of an infinite diluted aqueous solution. Ranging from rather low mineralized geothermal fluids (~ 1000 mg/kg TDS) of the Villarica area (Nitschke et al., 2017a; Nitschke et al., 2016) to saturated NaCl fluids (up to 450 g/kg TDS) produced from the Gt1 Groß-Buchholz borehole in Hanover (Nitschke et al., 2017), the application of the appropriate activity model is of particular significance.

3.2.1 Ion Dissociation Theory

The ion dissociation model basically describes the reversible stoichiometric dissolution of minerals in a solvent and their separation into charged dissolved species (ions). Models based on the dissociation theory (Debye-Hückel-type models), compute the activity of an ion only dependent upon their charge number and size (extended formulations) within a specific solution (ionic strength of the system). Their validity is limited to diluted systems.

A number equations have been established (listed below; compiled from Bethke (2008) and Merkel and Planer-Friedrich (2009)) in order to increase validity of activity coefficient determination over a larger range of ionic strength. All of these formulations stem from the original Debye Hückel model (*E3.14*) and interrelate the activity as a function of the ionic strength *I*, the charge number *z* and parameters for temperature adaption *A, B* (Debye and Hückel, 1923).

$$\log(\gamma) = -A \cdot z^2 \cdot \sqrt{I} \qquad (E3.14)$$

with

$$A = \frac{1.824283 \cdot 10^6 \cdot \sqrt{d}}{(\varepsilon \cdot T)}$$

$$B = \frac{50.2916 \cdot \sqrt{d}}{\sqrt{(\varepsilon \cdot T)}}$$

the temperature adaption for the density *d*

$$d = 1 - \frac{(T_c - 3.9863)^2 \cdot (T_c + 288.9414)}{508929.2 \cdot (T_c + 68.12963)} + 0.011445 \cdot e^{-\frac{374.3}{T_c}} \qquad (E3.15)$$

and the temperature adaption for the permittivity ε

$$\varepsilon = 2727.586 + 0.6224107 \cdot T - 466.9151 \cdot \ln(T) - \frac{502000.87}{T} \qquad (E3.16)$$

Further, commonly used models for the determination of activity coefficients derived from progressively extending the original Debye-Hückel formulation, are listed in ascending order of their validity with respect to the ionic strength of the solution:

Extended Debye-Hückel formulation (Hückel, 1925):

$$\log(\gamma_i) = \frac{-A \cdot z_i^2 \cdot \sqrt{I}}{1 + B \cdot a_i \sqrt{I}} \qquad (E3.17)$$

with parameters a_i and b_i being ion specific factors accounting for the ionic radius of the considered species (e.g. in Parkhurst et al. (1980)).

Davies-equation (Davies, 1962):

$$\log(\gamma_i) = -A \cdot z_i^2 \left(\frac{\sqrt{I}}{1 + \sqrt{I}} - 0.3 \cdot I \right) \qquad (E3.18)$$

Wateq-adapted Extended Debye-Hückel formulation (Hückel, 1925):

$$\log(\gamma_i) = \frac{-A \cdot z_i^2 \cdot \sqrt{I}}{1 + B \cdot a_i \cdot \sqrt{I}} + b_i \cdot I \qquad (E3.19)$$

B-dot equation (Helgeson et al., 1969):

$$\log(\gamma_i) = \frac{-A \cdot z_i^2 \cdot \sqrt{I}}{1 + B \cdot a_i \cdot \sqrt{I}} \dot{B} \cdot I \qquad (E3.20)$$

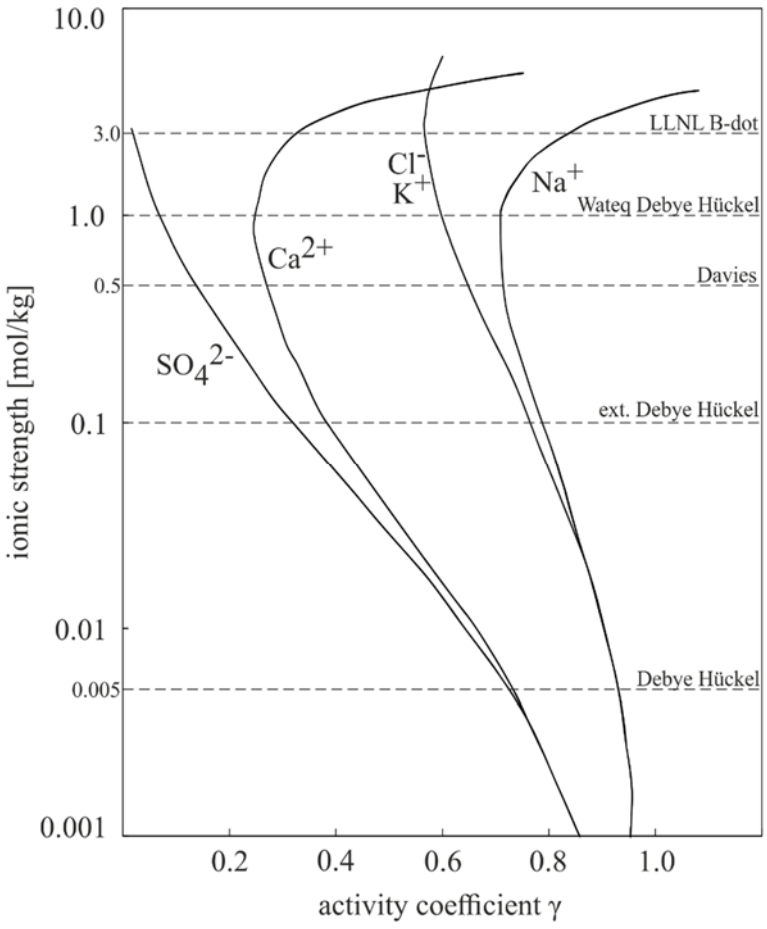

Fig. 3.2: Measured activity coefficients versus the ionic strength of the solution and range of validity of common ion dissociation models. Plot was adapted from Merkel and Planer-Friedrich (2009).

Fig. 3.2 illustrates the differing activity coefficients (measured) of a selection of major ions and the range of validity of the described dissociation models. The activity coefficients calculated with the original Debye-Hückel only account for temperature, charge number and ionic strength. That means that the activity coefficients are equal for all likely charged species at a given temperature. This simplification is valid only to ionic strengths of up to 0.005 mol/kg. For accounting for the different behavior of the ions, the ionic radius was implemented. With this model (Extended Debye-Hückel) validity range of activity coefficient calculation was increased up to an ionic strength of 0.1 mol/kg. Progressive extensions lead to the in recent modeling software very commonly used B-dot equation. By adding a third temperature fitting parameter ($\dot{B}$), it is capable to handle higher mineralized fluids, for NaCl dominated systems even up to 3.0 mol/kg.

3.2.2 Virial Models

Computing concentrated saline systems (or moderately mineralized fluids with a complex composition, the often named reference level is the sea water concentration of ~0.7 mol/kg (Merkel and Planer-Friedrich, 2009)), the ion dissociation theory based models fail and other models has to be used. In such systems, only the application of virial models, often also named the Pitzer models, predict reliable mean activity coefficients as the basis for an accurate quantification of the processes (Bethke, 2008).

In contrast to the dissociation based models, which only account for the ionic strength of a fluid and charge numbers, the Pitzer method considers the concentrations of individual ions and ion specific properties, such as ion size, shape and the affinity to interact with other ions (interaction terms of for each ion-pairs and ion-triples in solution). Furthermore, and particularly important for highly concentrated brines, it also accounts for the activity of the solvent.

The typical form of the Pitzer approach, which various modeling codes uses today, was suggested by Harvie et al. (1984) and is given in a form optimized for numerical modeling by Zhang et al. (2006). It is often referred to as the HMW formulation. This formalism was used for quantifying the chemical system for the THC modeling study (*chapter 5*). The water activity and activities of the dissolved components are calculated according to the following set of equations.

The water activity a_{H2O} is given as

$$\ln\left(a_{H_2O}\right) = -\frac{m_W}{1000}\left(\sum_{i=1}^{N} m_i\right)\phi \qquad (E3.21)$$

where m_i is the molality of the dissolved species i, m_w is molecular weight of water and N is the number of dissolved species. In a slightly simplified form, valid for ionic strengths of up to 10 molal, ternary interaction terms with neutral species involved were neglected. The osmotic coefficient φ is then defined by

$$\sum_{i=1}^{N} m_i\,(\phi - 1) = 2\left(\frac{A^{\phi} I^{\frac{2}{3}}}{1+1.2\sqrt{I}}\right) + \sum_{c=1}^{N_c}\sum_{a=1}^{N_a} m_c m_a \left(B_{ca}^{\phi} + ZC_{ca}\right) \qquad (E3.22)$$

$$+ \sum_c \sum_{c'=c+1} m_c m_{c'} \phi_{cc'}^{\phi} + \sum_a \sum_{a'=a+1} m_a m_{a'} \phi_{aa'}^{\phi}$$

$$+ \sum_{n=1}^{N_n}\sum_{c=1}^{N_c} m_n m_c \lambda_{nc} + \sum_{n=1}^{N_n}\sum_{a=1}^{N_a} m_n m_a \lambda_{na}$$

and the activity coefficients for cations are calculated as

$$\ln(\lambda_M) = Z_M^2 F + \sum_{a=1}^{N_a} m_a (2B_{Ma} + ZC_{Ma}) \qquad (E3.23)$$

$$+2\sum_{c=1}^{N_c} m_c\phi_{Mc} + |Z_M|\sum_{c=1}^{N_c}\sum_{a=1}^{N_a} m_c m_a C_{ca} + 2\sum_{n=1}^{N_n} m_n\lambda_{nM}$$

and analogously the determination of the activity coefficients for the anions

$$\ln(\lambda_X) = Z_X^2 F + \sum_{c=1}^{N_c} m_c(2B_{cX} + ZC_{cX}) \qquad (E3.24)$$

$$+2\sum_{a=1}^{N_a} m_a\phi_{Xa} + |Z_M|\sum_{c=1}^{N_c}\sum_{a=1}^{N_a} m_c m_a C_{ca} + 2\sum_{n=1}^{N_n} m_n\lambda_{nX}$$

with the intermediate parameters F and C_{MX} (containing the actual Pitzer parameters) given by

$$F = -A^{\phi}\left(\frac{\sqrt{I}}{1+1.2\sqrt{I}} + \frac{2}{1.2}ln\left(1+1.2\sqrt{I}\right)\right) \qquad (E3.25)$$

$$+\sum_{c=1}\sum_{c'=c+1} m_c m_{c'}\phi'_{cc'} + \sum_{a=1}\sum_{a'=a+1} m_a m_{a'}\phi'_{aa'}$$

$$+\sum_{c=1}^{N_c}\sum_{a=1}^{N_a} m_c m_a B'_{ca}$$

and

$$C_{MX} = \frac{C_{MX}^{\phi}}{2\sqrt{|z_M z_X|}} \qquad (E3.26)$$

Pitzer parameter B^{ϕ}_{MX}, B_{MX}, B'_{MX}, α_{MX}, C_{MX}, λ_{NC} and λ_{NA} can be computed as follows

$$B_{MX}^{\phi} = \beta_{MX}^{(0)} + \beta_{Mx}^{(1)} e^{-\alpha_{MX}\sqrt{I}} + \beta_{MX}^{(2)} e^{-\alpha'_{MX}\sqrt{I}} \qquad (E3.27)$$

$$B_{MX} = \beta_{MX}^{(0)} + \beta_{Mx}^{(1)} g\left(\alpha_{MX}\sqrt{I}\right) + \beta_{MX}^{(2)} g\left(\alpha'_{MX}\sqrt{I}\right) \qquad (E3.28)$$

with function *g(x)*

$$g(x) = \frac{2(1-(1+x)e^{-x})}{x^2} \qquad (E3.29)$$

where *x* is wether $\alpha_{MX}\sqrt{I}$ or $\alpha'_{MX}\sqrt{I}$

$$B'_{MX} = \beta_{MX}^{(1)}\frac{g'(\alpha_{MX}\sqrt{I})}{I} + \beta_{MX}^{(2)}\frac{g'(\alpha'_{MX}\sqrt{I})}{I} \qquad (E3.30)$$

with function *g'(x)*

$$g'(x) = \frac{-2\left(1-\left(1+x+\frac{x^2}{2}\right)e^{-x}\right)}{x^2} \qquad (E3.31)$$

For 1-1 and 1-2 electrolytes $\alpha_{MX} = 2$ and $\alpha'_{MX} = 12$, for 2-2 electrolytes $\alpha_{MX} = 1.4$ and $\alpha'_{MX} = 12$, for each higher symmetrical and asymmetrical electrolyte $\alpha_{MX} = 2.0$ and $\alpha'_{MX} = 50$.

The like-sign ionic pairs interaction parameter ϕ_{ij}^{ϕ} and ϕ_{ij} have to be adapted to temperature and ionic strength. They were determined using the terms θ_{ij}, ${}^{E}\theta_{ij}(I)$ and $I\,{}^{E}\theta_{ij}(I)$ given in Pitzer (1991).

The sheer number of equations and involved parameters describing the interaction of the dissolved components in a fluid illustrates the requirement of extensive datasets. Particularly in complex systems an adequate parametrization is often lacking or it is not clear if available data appropriately represents the considered fluid. For this reason, the parameterization of a chemical model should always be validated for the specific chemical system.

Therefore, prior to the THC modeling study of the GeneSys project production test (*chapter 5*), solubility experiments were performed (*chapter 4.1*) and data from literature was used to set up a correctly parametrized chemical model (*Table 5.1*).

3.3 Reactive Transport

Between recharge area, reservoir and wellhead or the discharge of a spring, which marks usually the earliest point for observation and sampling, complex thermal, hydraulic and chemical processes occur. For a first approximation, it is often sufficient to consider these processes separately or by only taking into account the mutual influences of the hydraulic and the thermal system. For an integrated system understanding and the quantification of thermal-hydraulic effects on the chemical system, and vice-versa, fully coupled numerical THC models are required.

The study of scaling formation from a saline brine in the production string of the GeneSys geothermal project in Hanover (*chapter 5*), is a great example for the necessity of the application of reactive transport models. It was successfully applied to a) reproduce the thermal and hydraulic conditions in the wellbore during production, b) to conclude on reservoir composition of the brine from surface measurements and c) to reproduce the halite scaling formation.

Coupled THC models (e.g. TOUGHREACT) are usually governed by the following set of equations for the conservation of i) momentum (*E3.32*) and (*E3.37*), ii) mass (*E3.38*) and (*E3.39*), iii) energy (*E3.40*) and iv) solute masses (*E3.41*).

i) Conservation of momentum

a) Darcy's Law

$$q = \phi v_{(f)} = \frac{k}{\mu}\left(\nabla P - \rho_{(f)} g\right) \quad (E3.32)$$

with flowrate q, fluid velocity $v_{(f)}$, pressure gradient ∇P, gravitational force g and the functions for

$$k = k(\phi, P) \quad (E3.33)$$

$$\mu = \mu(T, C_i) \quad (E3.34)$$

$$\rho_{(f)} = \rho_{(f)}(T, C_i, P) \quad (E3.35)$$

with permeability k, fluid viscosity μ, fluid density $\rho_{(f)}$ and the feedback function of precipitation and dissolution on the hydraulic system

$$\frac{\partial \phi_m}{\partial t} = V_{(m)} R_{(m)} \quad (E3.36)$$

with reactive mineral volume fraction ϕ_m, reactive mineral molar volume V_m and reaction rate of the mineral R_m.

b) Cauchy Momentum

$$\frac{\partial v_{(s)}}{\partial t} = \nabla \sigma + f \quad (E3.37)$$

with velocity of solids $v_{(s)}$, body forces f and stress function $\sigma = \sigma(E, \varepsilon)$

ii) Conservation of mass

a) Fluid

$$\frac{\partial (\phi \rho_{(f)})}{\partial t} = -\nabla\left(\rho_{(f)} \phi v_{(f)}\right) \quad (E3.38)$$

b) solids

$$\frac{\partial (1-\phi) \rho_{(s)}}{\partial t} = -\nabla\left(\rho_{(s)} v_{(s)}\right) + \sum_{m=1}^{N_m} \rho_{(m)} V_{(m)} R_{(m)} \quad (E3.39)$$

with density of solids $\rho_{(s)}$, number of reactive minerals N_m and density of reactive minerals ρ_m.

iii) Conservation of energy

$$\left[(1-\phi)\rho_{(s)}c_{p(s)} + \phi\rho_{(f)}c_{p(f)}\right]\frac{\partial T}{\partial t} = \nabla(\kappa_T \nabla T) - \nabla\left(\rho_{(f)}c_{p(f)}\phi v_{(f)}T\right) + \sum_{m=1}^{N_m}\Delta H_m R_m \quad (E3.40)$$

with specific heat of solids $c_{p(s)}$, specific heat of fluids $c_{p(f)}$, heat conductivity κ_T and enthalpy of reaction ΔH.

iv) Conservation of solutes

$$\frac{\partial(\phi C_i)}{\partial t} = \nabla(\phi D_i \nabla C_i) - \nabla\left(\phi v_{(f)} C_i\right) - \sum_{a=1}^{N_a} u_{i,r} R_a - \sum_{m=1}^{N_m} u_m R_m \quad (E3.41)$$

with diffusion coefficient D_i, concentration of dissolved species C_i, numbers of aqueous reactions N_a and reaction rate of aqueous reactions R_a.

The precipitation and dissolution rates for kinetic reaction models are often assigned in terms of assumed mineral specific laws (Bächler and Kohl, 2005) or they are computed as a function of varying parameters (MacQuarrie and Mayer, 2005):

$$R_m = (\phi_m, A_m, D_m, k_m, Si_m, I, C_i) \quad (E3.42)$$

with reactive surface area of the mineral A_m, diffusion coefficient D_m, temperature dependent mineral specific rate constant k_m, ionic strength I, concentration of reaction involved primary species C_i and mineral saturation index Si_m.

The determination of activity coefficients γ_i and the calculation of the saturation index (Si_m) as the parameter governing both, kinetic and equilibrium models, is given in *chapter 3.1* and *chapter 5.3.3*, respectively.

4 Laboratory Studies and Equilibration Experiments

Due to inaccessibility, direct observations and measurements of the chemical processes in geothermal systems, especially in deep reservoirs, are often not possible or only feasible via indirect methods (borehole logging, geophysical methods, studies of analogues etc.). In terms of reservoir chemistry and deep water-rock interaction, laboratory experiments conducted under reservoir conditions (P, T and X) can help leading to a better understanding and quantification of processes. To the same extend they can substantially support modeling approaches. Since models are always simplified images of the reality, they have to be practical, e.g. in terms of data needed and required computational time, but they still have to yield realistic and precise results. Therefore, the set-up of a model has to be done by reasonably abstracting the complex reality and by still retaining required detailedness. In typically very complex chemical environments of geothermal reservoirs, experiments can grant for a balanced abstraction, the calibration of models as well as for a meaningful parameterization. In the following section two examples illustrates the valuable contribution to model parameterization (*chapter 4.1*) and process understanding (*chapter 4.2*).

4.1 Halite Solubility Experiments for Model Parameterization

The here presented laboratory work was conducted to support the parameterization of the model of the GeneSys project production test (*chapter 5*). The chemical composition of the fluid produced from that reservoir (170 °C) sampled at wellhead is reported in Hesshaus et al. (2013). The fluid was characterized as a highly mineralized Na-Ca-Cl brine with a TDS (total dissolved solids) of minimum 452 g/kg_W. With concentrations of the major compounds of 5.3 mol/kg_W Na^+, 7.8 mol/kg_W Cl^- and 0.9 mol/kg_W Ca^{2+} (Nitschke et al., 2017), the limit of validity for the application of ion dissociation derived chemical models is exceeded by far (*chapter 3.2.1*). The application of the Pitzer formalism is necessary. The differences of predicted halite solubilities in the above defined chemical system calculated with both approaches are depicted in (*Fig. 4.2*). The validity of the Pitzer approach for determination of halite solubility in pure H_2O is illustrated by the comparison with experimental data from literature (Li et al., 2005). Solubility data for the presence of the measured amount of $CaCl_2$ is rare. Only two data points for 50 °C and 75 °C were found (Yang et al., 2010; Yang et al., 2011). To increase data, laboratory experiments were performed. Due to limitations concerning laboratory equipment, results could only be generated below 100 °C.

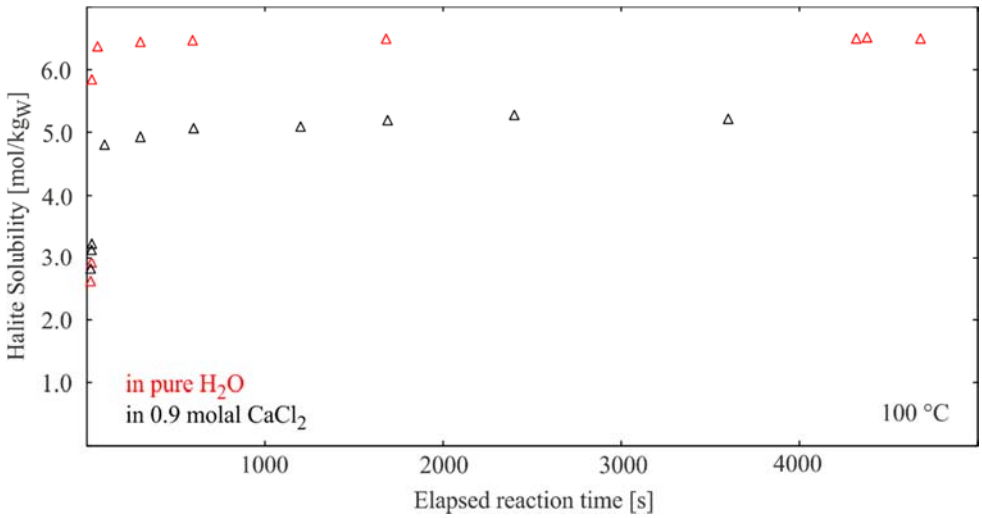

Fig. 4.1: Results from halite solubility experiments in pure H2O and in 0.9 molal $CaCl_2$ solution at 95 °C plotted versus elapsed reaction time.

In order to fill the gaps of literature data, experiments were conducted at 25 °C, 40 °C, 60 °C and 95 °C. A stock solution of 0.9 molal $CaCl_2$ was prepared and heated in an oven on the desired reaction temperature. NaCl was added abundantly. To avoid local equilibrium effects, which would prevent a homogenous solution and to overcome slow diffusion kinetics the experiments were stirred. From this fluid a defined mass (weighing accuracy +/- 0.001 g) was sampled. Prior to sampling, stirring was terminated to ensure particle sedimentation. The solution was completely evaporated at 40 °C to remove the solvent and then at 200 °C for a complete dewatering of possible dihydrates of $CaCl_2$. From the mass of evaporates (NaCl+$CaCl_2$) the mass of $CaCl_2$ (calculated from the initial $CaCl_2$ concentration, the total evaporated water and water from decomposition of dihydrates) was subtracted to obtain the amount of NaCl, which had been dissolved. This procedure was repeated in a time series, which enables the identification of saturation (steady state). *Fig. 4.1* exemplarily shows the observed solubility behavior of NaCl in pure H_2O and in a 0.9 molal $CaCl_2$ solution at 95 °C. It is shown, that dissolution kinetics are very fast. A near saturation state (6.49 mol/kg_W in pure H_2O and 5.17 mol/kg_W in presence of 0.9 molal $CaCl_2$) is reached very fast for both experimental series. After 20 seconds already around 95 % of NaCl (compared to the amounts at the end of the series) is dissolved in pure H_2O. This value is reached after 100 seconds in presence of $CaCl_2$. It is also shown, that the method yields very stable results for the saturation concentrations (*Fig. 4.1*).

Based on the two data points from literature together with the described experimental series, the validity of the parameterization of the Pitzer model was investigated. *Fig. 4.2* illustrates the great consistency of experimental data with predicted halite solubility which was calculated using a combination of the datasets from Greenberg and Møller (1989) for the interaction parameters of the ion combinations Na^+-Cl^-,

Na^+-Ca^{2+} and Ca^{2+}-Na^+-Cl^- and Sterner et al. (1998) for the pair Ca^{2+}-Cl^-. Thus, this parameterization was assigned to the chemical model for the numerical evaluation of the halite salt plug formation in well Gt1 Groß-Buchholz (*chapter 5*). The values of the Pitzer parameters are given in *Table 5.1*.

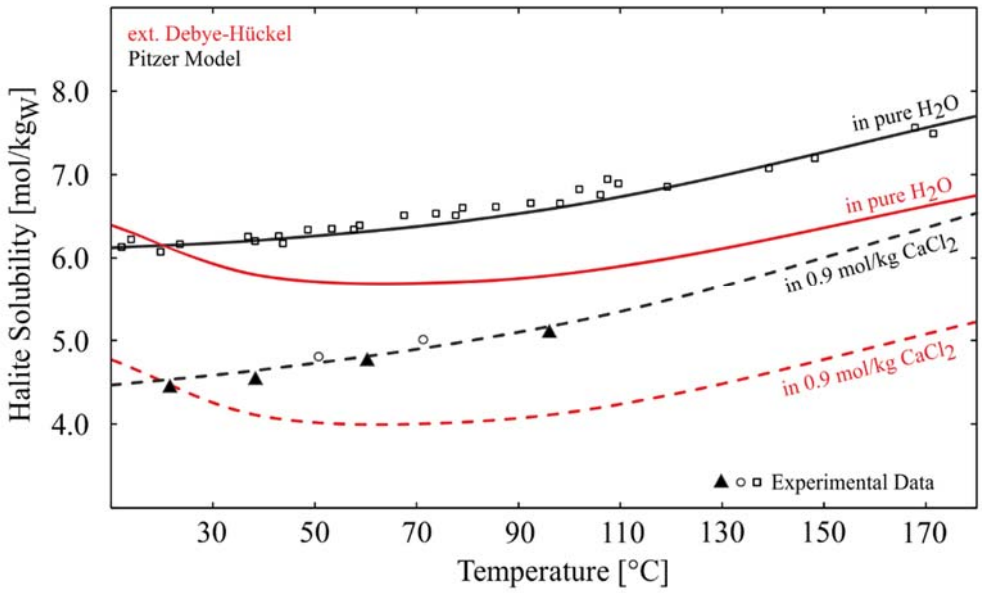

Fig. 4.2: Calculated halite solubility versus temperature: For the binary system NaCl-H_2O (extended Debye-Hückel (red line) and Pitzer model (black line)) and for the ternary system NaCl-$CaCl_2$-H_2O with 0.9 mol/kg $CaCl_2$ (extended Debye-Hückel (dashed red line) and Pitzer model (dashed black lines)). Results of halite solubility experiments (black triangles) indicate very good agreement with modeled solubilities (Pitzer). Literature data is taken from Li et al. (2005) (open squares) and from Yang et al. (2011) and Yang et al. (2010) (open circles).

4.2 Impact of Crystalline Rocks on Fluid Equilibrium

In the framework of a multi-disciplinary exploration campaign of the Villarrica geothermal area in Southern Chile, one main focus was the geochemical investigation of the natural discharging hot spring fluids and the estimation of subsurface temperatures from their composition.

Previous studies found different type of fluids (Sánchez et al., 2013) in the area and explained their differing genesis with the occurrence along different fault zone systems. Held et al. (2016a) found first indications, that differing evolution of the geothermal system may be linked with a prominent lithology change from north to south. In order to investigate to which extend the fluid composition is controlled by the reservoir rock composition, long-term batch-type equilibration experiments were conducted.

The lithology change across the study area is associated with the WNW-ESE striking Andean Transverse Fault-type Mocha-Villarrica Fault Zone. South of this fault granitoids of the North Patagonian Batholith (NPB) outrop, whereas the northern part is dominated by volcanic and volcano-clastic rocks of the Cura-Mallin (CM) formation. For the laboratory experiments two reservoir analogues were selected with the aim to represent both anticipated reservoir types in the study area: a Mesozoic tonalite (NPB) and a Cenozoic porphyric andesite (CM). These rocks are considered to most-likely host the fluids due to their widespread occurrence, large formation thickness and in particular due to their spatial distribution with respect to the spring discharges.

The rock samples were ground with an agate disc mill to a grain size < 63 µm. The very small grain size was chosen to provide the largest surface area possible reducing reaction time towards steady state to a minimum. The procedure of grinding was done extremely carefully. To avoid heat development, which could potentially cause a vitrification of minerals (especially quartz), and therefore it would affect solubility behavior, grinding was interrupted every minute. For obtaining a small, but ideally uniform grain size distribution the powder was at each interruption carefully forced through a sieve, using a soft brush. Avoiding fractionation due to differing material strengths, the procedure was repeated for the residues (larger grain fraction) until the sample material entirely passed the sieve. Being especially important to obtain a comparable reactive surface area for both samples (comparability of results), BET measurements (gas adsorption method) reveal that reactive surface areas of both samples are nearly equal (tonalite: 2.1 m^2/g, andesite: 3.6 m^2/g).

Prior to the water-rock interaction experiments, both rock samples were analyzed in detail. The mineralogical compositions derived from thin-section microscopy and X-ray diffraction is displayed in (*Table 6.1*).

According to estimations in previous works for the most-likely mean reservoir temperature, the reaction temperature for the experiments was chosen to be 140 °C. To keep track of the chemical development of the fluids over time, experiments were sampled and analyzed as a time series after 1, 2, 4, 6, 10, 20, 30, 45, 60, 90, 120, and 180 days. Each time step represents an autonomous experiment. This approach ensures reproducibility of the experiments and concurrently enables the identification of chemical steady state conditions of the fluids.

For each experiment, 40 g of rock powder were transferred to hermetic 150 ml stainless-steel reactors. The remaining volume was completely filled up with pure H_2O to avoid headspace, which would have led to hardly controllable interactions of gas phase, fluids and consecutive effects for pH by CO_2 dissolution, for instance. As a consequence, any dissolved species can then be regarded to originate from rock dissolution. The rock-water ratio was close to 0.3.

Conducting equilibration experiments means that potentially multiple minerals are in equilibrium with the fluid at reaction temperature (140 °C in this case). Every cooling, e.g. for sampling at the end of the experiment, will lead to a state of

supersaturation of the fluid with respect to these minerals (for all minerals of prograde solubility). To increase distance to saturation and therefore to stabilize dissolved species in solution, the fluid of each experiment was diluted immediately (pure H_2O) after opening of the reactor. A small proportion of the samples was previously used to determine the pH. To separate solids from fluids, samples were centrifuged (30 min, 4000 rpm) and filtered using acetate cellulose membranes (pore size < 45 µm).
Fluid composition was measured using inductively coupled plasma mass spectrometry (ICP-MS) for the cations and ion chromatography (IC) for the anions. Silicon concentrations were determined by spectrophotometry.

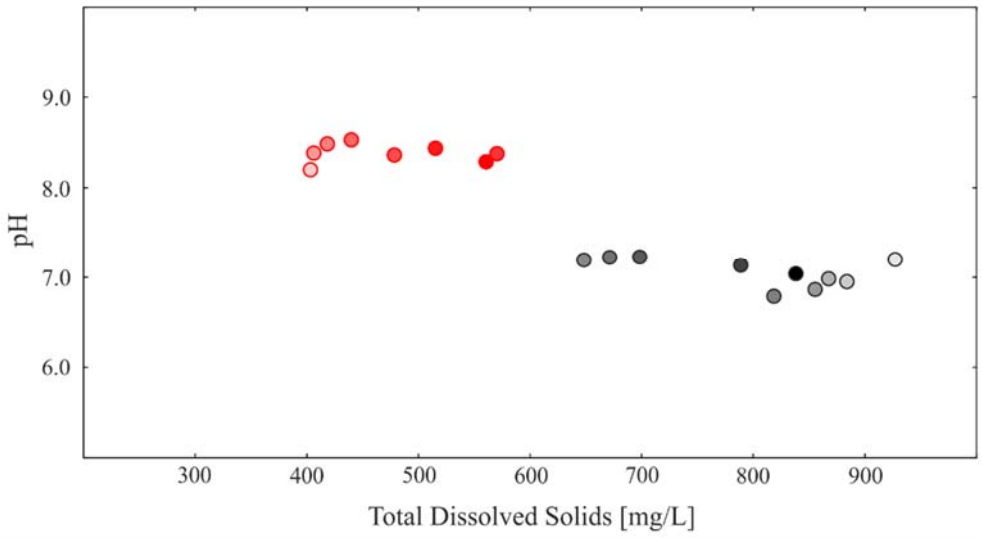

Fig. 4.3: Basic system parameters for both series (andesitic fluids: red circles, tonalitic fluids: black circles (increasing color saturation indicates increasing reaction time)) of the laboratory equilibration experiments. Total dissolved solids (TDS) versus solution pH.

The measured fluid compositions of both experimental series are clearly different. Even basic system parameter vary significantly. The fluids from the andesitic experiment are moderately alkaline (pH 8.2 - 8.5) and have a comparable low mineralization of 400 - 575 mg/L. The fluids from tonalite experiments ranging near neutral conditions (pH 6.7 - 7.2). The TDS is between 670 - 930 mg/L (*Fig. 4.3*).
Since this experimental study was conducted to improve process understanding in view of subsurface temperature estimation, *Fig. 4.4* illustrates the fluid compositions of major fluid constituents, which are of particular interest for geothermometric applications. It is shown, in each displayed ternary system, that the fluids form well separated groups revealing clear differences in their basic chemistry. Chronologically well-ordered trends, obviously representing reaction paths, are

observed in every case. Even though both fluids being Na^+ dominated, the andesite fluid is a Na-Cl type fluid, whereas the tonalite fluid can be classified as Na-SO_4 type. Most striking, both fluids differ also regarding their compounds and ratio of constituents, which are rater considered to reflect temperature differences (therefore they are used for geothermometry) than be effected from mineral composition of the rock. This becomes obvious in the Na-K-(Ca) system, where a differing Na^+/K^+ ratio (with concurrently differing Ca concentrations) is revealed. The same applies to the ternary Na-K-Mg and for SiO_2 concentrations, which are very classical geothermometric applications.

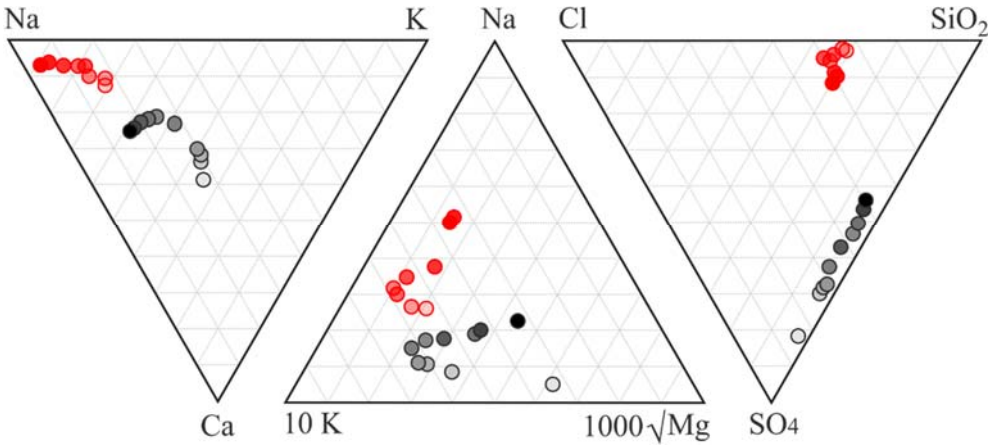

Fig. 4.4: Fluid compositions of experimental series (andesitic fluids: red circles, tonalitic fluids: black circles (increasing color saturation indicates increasing reaction time)), plotted as ternaries (Na-K-Ca (left), Na-K-Mg (center) and Cl-SiO_2-SO_4 (right)) for constituents of special relevance for geothermometer application.

Each of the above described differences will lead to different temperatures when applying classical geothermometers. The design of the experiments allow the conclusion, that these differences are controlled by the composition of the reservoir rocks. This demonstrates the requirement of a more detailed analysis of geothermometry in the study area. The impact of reservoir rock composition on the chemistry of geothermal fluids and other factors interfering an accurate in-situ temperature determination are investigated in *chapter 6* and *chapter 7*.

5 THC Simulation of Halite Scaling in Deep Geothermal Single Well Production

This study has been published in *Geothermics.*

Nitschke, F.; Held, S.; Himmelsbach, T.; Kohl, T. (2017): THC simulation of halite scaling in deep geothermal single well production. *Geothermics 65*, 234-243.

Abstract

Using abandoned wells from oil and gas industry or dry holes, geothermal single well applications enable the prevention of drilling costs and prospecting risks which are crucial inhibitions in geothermal development.
Recently, deep geothermal single wells were numerically investigated for their thermal and hydraulic performance. For the first time, we now include the chemistry of the produced brine in a fully coupled THC model for studies of scaling formation. As a case study, the 2011 circulation test of the GeneSys well Gt1 Groß-Buchholz (Hanover, Germany) was modeled successfully using the fully coupled THC code TOUGHREACT. High salinity requires application of the Pitzer ion interaction model which was verified for this particular chemical system using literature data. Modeled wellhead temperature is in very good accordance with measurements. Also simulated depth of scaling formation and total scaling volume fit to onsite observations. Evaluation of initial reservoir brine composition reveals its large impact on the range of depth where scaling occurs. Furthermore, it is shown that the presence of $CaCl_2$ reduces halite solubility considerably and favors scaling formation. Results show that our modeling concept is capable of quantifying the complex coupled THC processes in single wells.

5.1 Introduction

Geothermal power and heat production are considered to play an important role (Sawin, 2012) for the future energy mix, with an annual worldwide electricity generation of 1’400 TWh and 1’600 TWh of thermal energy production being predicted (Beerepoot, 2011). Although still facing scientific and technical challenges, its highly flexible controllability and capability of meeting baseload demands make geothermal energy assume an outstanding position among the renewables.

Doublet and multi-well configurations are classical approaches to exploiting geothermal energy. They are applied at numerous geothermal fields and in a broad range of different geological settings all over the world. The aim of these concepts is to establish a subsurface heat exchanger. A geothermal fluid is produced and after heat withdrawal, it is reinjected into the reservoir via a second well. Continuous fluid circulation requires a highly permeable reservoir to ensure flow from the injection well to the production well. The reservoir development therefore is a critical factor for the success and profitability of an EGS project. It is necessary to target preexisting structures and to enhance their permeability by hydraulic and chemical stimulation.

Recently, a number of studies investigated a more unconventional approach, where a single borehole is applied for fluid production as well as for reinjection. Commonly, a coaxial borehole heat exchanger is used by circulating a working fluid in a closed loop in the borehole (Franco and Vaccaro, 2013; Kohl et al., 2000; Kohl et al., 2002). Authors also suggested open systems, where the fluid is circulated in the host rock (Jung et al., 2005; Orzol et al., 2005; Wang et al., 2009). Typically, fluid is produced in a coaxial configuration by a deep-reaching inner pipe and reinjection is achieved via the annulus ending at more shallow depth. This concept entails several advantages. As there is no need to target a highly permeable formation or structure, exploration risks are eliminated. The technology also allows for the use of already existing deep boreholes like abandoned oil and gas wells. Hence, no high-risk initial investment is needed for drilling and well completion.

The GeneSys project in Hanover, Germany, was planned to demonstrate the exploitation of geothermal energy from hydraulically tight sediments by operating such a single well (Jung et al., 2005; Orzol et al., 2005; Tischner et al., 2010). A previously performed feasibility study in the nearby well of Horstberg Z1 which has a very similar stratigraphy (Jung et al., 2005) demonstrated the creation of a reservoir in low-permeable sedimentary rock by performing a massive water frac as well as heat production of such one-well systems (Tischner et al., 2010).

The project has been suspended after the failure of the production test of Gt1 Groß-Buchholz, when large amounts of halite scalings precipitated and formed a massive salt plug which clogged the well completely.

Scaling is a common and widespread challenge known from numerous deep geothermal projects. There is a large diversity of minerals forming scaling. Most common groups are carbonates (Bjornstad and Stamatakis, 2006; Stahl et al., 2000), silica (Gunnarsson and Arnórsson, 2003), sulfates (Nitschke et al., 2014; Schröder et al., 2007), and sulfides (Holl et al., 2003; Schmidt et al., 2000). Scalings can substantially affect geothermal exploitation by reducing heat transfer and by physically clogging pipe systems. They have to be removed regularly, resulting in additional operation costs and downtimes of the plant.

In oil and gas industry, also halite scalings occur. Deep high-temperature/high-pressure wells are particularly vulnerable (Frigo et al., 2000; Kleinitz et al., 2003).

Heat withdrawal is considered to be the controlling mechanism for halite scaling formation, as halite solubility is primarily governed by fluid temperature (Guan et al., 2008; Wylde and Slayer, 2010). The usually large quantities of formed halite scalings often result in a complete clogging of the well or surface installations (Crabtree et al., 1999; Guan et al., 2008; Wylde and Slayer, 2010):
The aim of this study is to numerically investigate and quantify the thermo-hydraulic-chemical (THC) processes of geothermal single well operation. Therefore, the production test of well Gt1 Groß-Buchholz which led to the formation of the halite plug and subsequent failure and suspension of the GeneSys project was investigated as a case study. To model the complex interaction of temperature, flow, permeability and precipitation/dissolution, the THC code TOUGHREACT-Pitzer was used. It provides fully coupled simulation of those processes and is suitable for the application in highly saline systems.

5.2 The GeneSys Single Well Project

GeneSys was planned as a pilot project to demonstrate geothermal production of a single well. The plant should cover the heat demand of the BGR (Federal Institute for Geosciences and Natural Resources) buildings in Hanover. The strategy pursued was to produce geothermal fluid from a large-volume frac in the Buntsandstein, which had been created by a massive hydraulic stimulation, using a coaxial pipe configuration. It was intended to establish a cyclic operation state, consisting of alternating injection and production phases, the so-called huff-puff scheme (Tischner et al., 2010). According to the concept, freshwater was to be injected into the fracture via the production string. After heating up, the fluid would have been reproduced via the same string and reinjected through the annulus into the shallower and more permeable Wealden formation. Then, a new cycle would be started with repeated injection of freshwater into the reservoir.
Gt1 Groß-Buchholz was drilled to a depth of 3901 m near the BGR buildings in 2009. Local stratigraphy reflects the horizontal sedimentary sequence of the North German Basin (Orzol et al., 2005). The Triassic units are covered by Jurassic, Cretaceous and Quaternary sediments. A simplified scheme of the geology and the well completion is shown in *Fig. 5.1*.
For coaxial well completion, a 7” casing as inner production string was set extending to bottomhole depth. From the surface down to 1175 m depth, it is enclosed by a 13 3/8” casing. The annulus between both strings acts as the reinjection string. The well reaches into low-permeable layers of the Buntsandstein formation (<1 mDarcy) with a bottomhole temperature of about 170 °C. The injection horizon is the hydraulically conductive Wealden Sandstone (Lower Cretaceous), where the annulus ends. Reservoir development took place in May 2011, when 20 000 m^3 of freshwater were

injected to create a massive frac in the Buntsandstein. The reservoir obtained is assumed to extend over a fracture area of approximately 1 km^2.

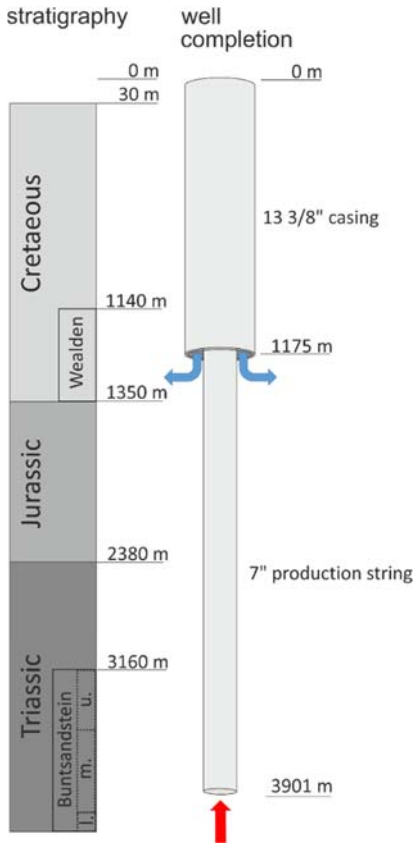

Fig. 5.1: Scheme of well completion and simplified stratigraphy. Arrows indicate fluid flow during production.

After the creation of the reservoir in May 2011, pressure was shut in. The injected fluid remained in the reservoir for 6 months. A production test was performed from Nov. 10 to Nov. 17, 2011 (T111110), producing a total volume of 577 m^3. Due to the high positive differential pressure, generated during injection, the regain of fluid took place by artesian outflow. The production test was carried out in three major cycles which were interrupted by downtimes (*Fig. 5.2*). Once the borehole volume had been produced, salinity of the fluid increased sharply. The Na-Ca-Cl brine had a minimum TDS value of 452 g/kg_w, with 5.3 mol/kg_w Na^+ and 7.8 mol/kg_w Cl^- representing the major chemical components. When injectivity of the Wealden Sandstone decreased significantly during the 3rd cycle, production rate was reduced in a stepwise manner (Fig. 2) to prevent the maximum permissible injection pressure of 188 bar at depth from being exceeded. Finally, with continuously decreasing injectivity, production had to be stopped. The annulus was flushed with freshwater

to remove potential precipitations and increase accessibility to the Wealden formation. After flushing, any attempt to resume production failed. A massive salt plug had formed in the production string. It consisted predominantly of NaCl. Other compounds like KCl, $CaCl_2$, and $(BaSr)SO_4$ were present in trace amounts only. The plug clogged the well completely and extended from 655 m to 1350 m depth. Technical details concerning the Gt1 Groß Buchholz and T111110 were taken from Hesshaus et al. (2013) and from (Tischner et al., 2010).

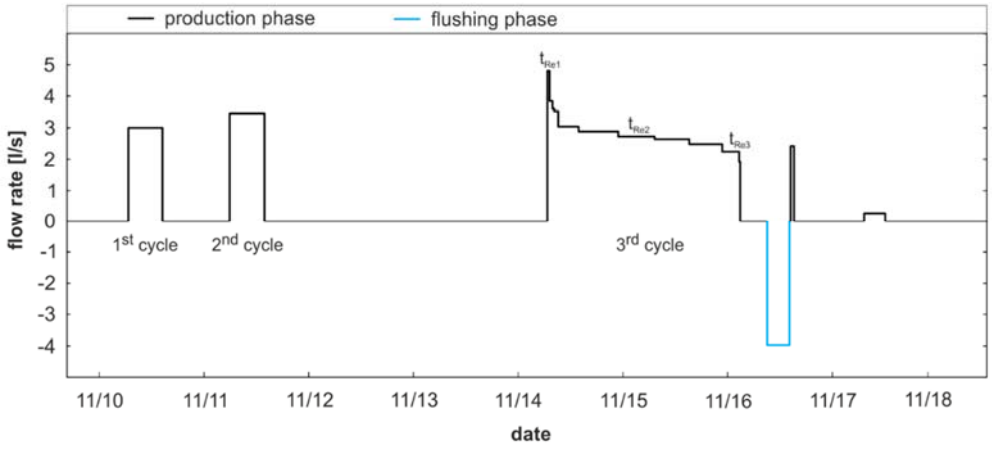

Fig. 5.2: Schematic representation of T111110 with flow rates of the three major production cycles and the flushing phase.

5.3 Numerical THC Modeling

Thermo-hydraulic performance of wells during production and injection has been the subject of numerous studies and was modeled previously (e.g. Francke et al., 2013; Hasan and Kabir, 2012; McGuinness, 2014) . In addition, counterflow in coaxial systems with thermally interacting ascending and descending fluid columns was quantified (Galoppi et al., 2015; Wang et al., 2009). Kohl et al. (2002) numerically investigated the thermal performance of such a single well application in detail. The present study for the first time quantifies the processes of an open system, including the chemistry of the produced formation water and the associated scaling formation. For this purpose, a numerical code capable of calculating fully coupled hydraulic, thermal, and chemical processes is required.

A state-of-the-art simulator for THC modeling is the finite volume code TOUGHREACT (Xu et al., 2012), part of the widely used TOUGH2 (Pruess et al., 2012) code family. Due to high reservoir salinity, application of the extended TOUGHREACT-Pitzer V1.21 version was necessary. It allows for a fully coupled

THC simulation modeling chemically reactive non-isothermal multiphase transport of concentrated aqueous solution (Zhang et al., 2006).

5.3.1 Geometry and Mesh

Mesh generation and element parameterization were made using the graphical interface PetraSim (Thunderhead Engineering). The geometry of the borehole was discretized with a radial symmetric mesh representing a 3-D cylindrical model, with a rotation axis at the center of the coaxial pipe (*Fig. 5.3*). The model extensions of 3900 m (z-direction) and 20 m (x-directions) were selected to reflect reservoir depth and to ensure a sufficient lateral distance of the wellbore to the model boundary. Element sizes (x-direction) were adapted to varying geometrical settings of the model, with a strong refinement at the pipe string elements and the near-wellbore region ($\Delta x_{min} = 10^{-3}$ m), and increased in steps towards the boundaries ($\Delta x_{max} = 6.5$ m).

A sensitivity analysis was performed to determine the impact of vertical discretization on calculated wellhead temperature. Equivalent models with varying Δz-refinements were calculated. It was found that results hardly varied for a number of horizontal layers $nA > 700$ (modeled temperature sensitivity < 0.11 %). Consequently, the model was vertically discretized with 780 layers ($\Delta z = 5$ m), resulting in a total of 13260 elements. Only the two uppermost layers which represent the horizontal deflection from the production string (*Fig. 5.3a*) to the injection string are smaller ($\Delta z = 0.02$ m), to prevent flow velocity from being affected.

Pipe strings, i.e. both the production and the injection string, were discretized by two element columns. The dimensions in x-direction were chosen to obtain equal cross sectional areas perpendicular to the axis of the string columns. Axial flow (only z-permeability assigned), together with coextensive pipe string elements, ensures equal flow velocities through the columns and, hence, uniform mass and heat transfer in both element columns, which is a necessary prerequisite for this model concept. At the deflection of production string and annulus (*Fig. 5.3a*), four cells enable fluid transfer from the ascending to the descending columns. For this reason, both vertical and horizontal permeability was assigned to these cells.

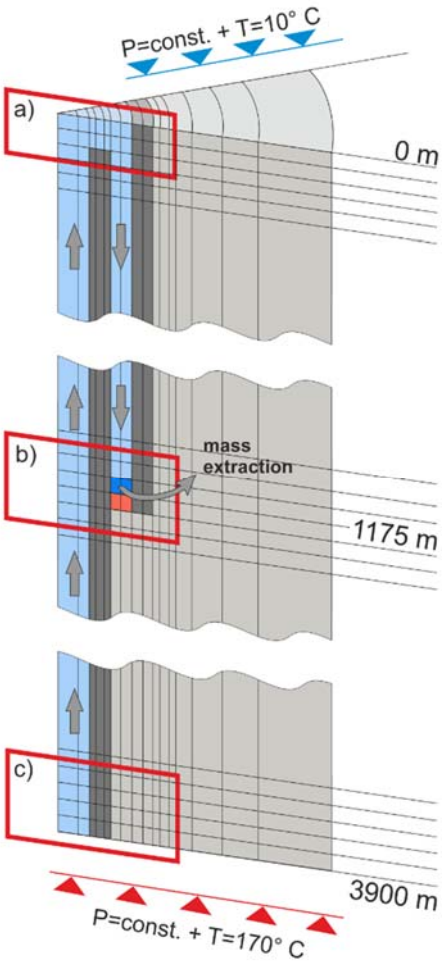

Fig. 5.3: Model concept and boundary conditions. Blue elements represent the production and injection strings, dark gray elements represent pipe walls, light gray elements represent the host rock. In dark blue cells, flow rate for the pipe strings is controlled by time-dependent Neumann-type boundaries (mass extraction). Red cells with zero permeability prevent influx from adjacent rock. Arrows indicate fluid flow during production. a) Wellhead/deflection of production string to annulus, b) end of annulus, c) reservoir.

5.3.2 Hydraulic and Thermal System

The code numerically couples the hydraulics, thermal transport, and chemistry. The calculations were carried out using the standard equations of state module (eos1p). It includes formulations to solve one-phase-multi-component transport by considering vapor pressure lowering due to brine salinity. Fluid flow and heat transfer were calculated by advection and diffusion, including transient change of heat and pressure. The governing equation was given by

$$\frac{\partial M}{\partial t} = -\nabla F + q \qquad (E5.1)$$

where M is mass accumulation, F is mass flux, and q is a source or sink. For the fluid flow, M_f and F_f were calculated from

$$M_f = \phi \cdot S_f \cdot \rho_f \cdot X_f \qquad (E5.2)$$

and

$$F_f = X_f \cdot \rho_f \cdot u \qquad (E5.3)$$

$$\text{with Darcy velocity} \qquad u = -k \frac{k_r}{\mu} \cdot \nabla P \qquad (E5.4)$$

where ϕ is porosity, S_f is fluid saturation, ρ_f is fluid density, X_f is mass fraction, k is permeability, k_r is relative permeability, P is pressure, and μ is viscosity. For heat transfer, M_h and F_h were calculated according to

$$M_h = \left(\phi \cdot S_f \cdot \rho_f \cdot U_f\right) + (1 - \phi) \cdot \rho_s \cdot U_s \qquad (E5.5)$$

and

$$F_h = \left(h_f \cdot \rho_f \cdot u_f\right) - \lambda \cdot \nabla T \qquad (E5.6)$$

where U_f is internal energy of fluid, U_s is internal energy of the solids, ρ_s is density of the solids, h_f is heat, λ is heat conductivity, and T is temperature.
The model is divided into two hydraulically decoupled parts, the highly conductive pipes (k = 10^{-6} m^2) and the impermeable host rock. Flow conditions differ strongly in both parts. In the host rock, flow is controlled by diffusion, whereas advection is dominant in the pipe. The flow regime can be characterized by determining the Reynolds number according to

$$Re = \frac{\rho_f \cdot u \cdot d}{\mu} \qquad (E5.7)$$

where d is the perfused pipe diameter. Calculated Re numbers > 29000 characterize fully turbulent flow in the pipe strings. The application of the thermal and hydraulic laws in TOUGHREACT are uncritical even for these large Re numbers, since flow rate is used as boundary condition and pressure effects are ignored (virtually

irrelevant to halite scaling formation). Also for the thermal field, differences in heat transfer across the pipe wall can be neglected due to the large pipe wall surface in the production string of about 2180 m^2.

Initial and boundary conditions were derived from borehole data and onsite measurements during T111110. Initial and boundary conditions were set to reproduce the natural geothermal gradient of 40 °C/km (Hesshaus et al., 2013). Considering the ambient temperature of 10 °C during T111110, Dirichlet-type boundary conditions of 10 °C and 170 °C were set in the uppermost and lowermost elements, respectively. Using these boundaries, the initial linear temperature gradient was established in a model pre-run. To maintain this temperature distribution in the far field and to ensure constant reservoir temperature (170 °C) throughout the entire simulation, cells at the top and the bottom remain Dirichlet-type in terms of temperature and pressure. An exception is made for the cells representing the lateral flow between production string and annulus in the uppermost layer (*Fig. 5.3a*) to allow for temperature development.

Heat transfer is characterized by fluid flow-driven advection in the pipe strings and thermal diffusion in the pipe walls ($\lambda_i = 25$ W/m·K, $\lambda_{ii} = 50$ W/m·K, $c_p = 477$ J/kg·K) and in the host rock ($\lambda = 50$ W/m·K, $c_p = 477$ J/kg·K). Thermal properties of materials were obtained from model calibration (Tab. 2). The low value of λ_i (25 W/m·K) set for the inner pipe wall separating the production string from the annulus represents an internal small annulus reducing heat conductivity compared to pure steel (50 W/m·K).

Hydraulic conditions in the pipe strings were controlled by Dirichlet-type boundaries at the bottom of the production string ('reservoir cells') to maintain constant reservoir pressure during simulation (*Fig. 5.3c*). Time-dependent Neumann-type boundaries (mass extraction) at the end of the annulus (*Fig. 5.3b*) ensured production flow rates. A suitable load-time function was applied according to flow rates measured throughout T111110 (*Fig. 5.2*).

For the flushing phase (*Fig. 5.2*), when freshwater with a temperature of 5 °C was injected into the annulus, model geometry was changed slightly to hydraulically decouple the annulus from the production string. The cells in the topmost layer of the annulus string were assigned Dirichlet-type (constant pressure, 5 °C).

In the lateral host rock (far field) the simulation was calculated under isobaric conditions, with the hydraulic heads at uppermost and lowermost elements being set to constant values (Dirichlet-type).

In this THC model hydraulic conditions in the pipe strings are closely linked to mineral precipitation. Temperature development affects mineral precipitation directly via change of reaction parameters. For HC coupling, an equivalent poro-perm constitutive law needs to be defined due to the formation of solids. An equivalent string porosity Φ_{st} is initially set to a value of $\Phi_{st} \approx 1$ (*Table 5.2*). There is a variety of poro-perm models linking porosity reduction to permeability decrease. The conventional cubic law (Steefel and Lasaga, 1994) represents a simple form to

estimate changes of permeability within the aperture of parallel planes related to idealized fractures. Bear (1972) and Verma and Pruess (1988) developed formulations to adjust permeability in porous media. Effects of halite precipitations in the production string on the resulting hydraulics are discussed in *chapter 5.5*.

5.3.3 Chemical System

Being near saturation with respect to halite, the chemical system is dominated by a highly saline brine. Halite scales are considered to form virtually instantaneously when the brine reaches saturation during production (Kan and Tomson, 2012; Sandengen, 2006). Therefore, formation of solids was calculated using an equilibrium approach, which appropriately reflects such spontaneous precipitation behavior. To set chemical boundaries, reservoir cells were assigned constant concentrations of NaCl and $CaCl_2$, respectively. All other cells were initially water-saturated (pure H_2O). The brine produced during T111110 has a TDS of at least 462 g/kg_w (Hesshaus et al., 2013), which corresponds to an NaCl equivalent of 7.96 mol/kg_w. It can be classified as an Na^+-(Ca^{2+})-Cl^--type water. Although the brine is strongly NaCl–dominated, it also contains higher amounts of calcium (~ 0.9 mol/kg_w $CaCl_2$). The conventional ion dissociation theory (e.g. extended Debye-Hückel) is limited to diluted waters. For chemical quantifications in such highly saline systems, the Pitzer ion interaction model is commonly used (Harvie et al., 1984; Pitzer, 1973; Pitzer and Mayorga, 1973). Ion interaction in concentrated solution is severely effecting the activity of the involved components. As shown in *Fig. 4.4a*, ion activity coefficients calculated according to Zhang et al. (2006) for Na^+ and Cl^- diverge with increasing ionic strength for both models. This is shown here exemplarily for the reservoir temperature of 170 °C. This holds even more for the ternary system NaCl-$CaCl_2$-H_2O, where unequal activity coefficients for Na^+ and Cl^- reflect their different interactions with the bivalent Ca^{2+}.

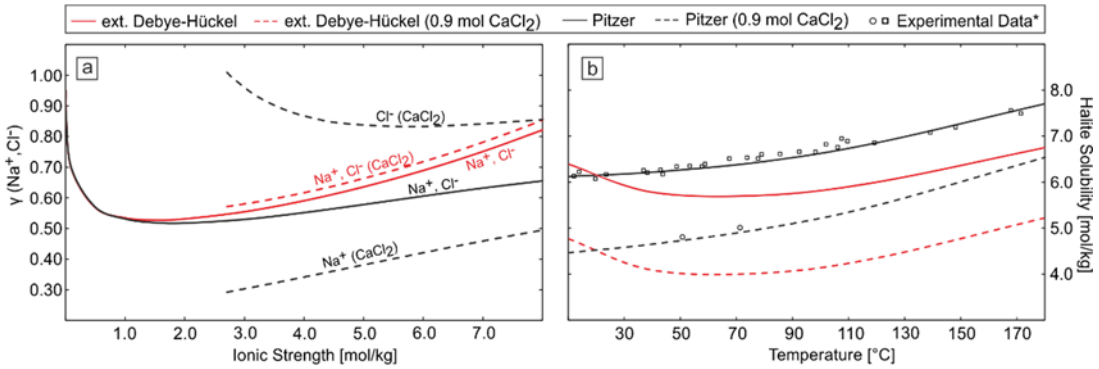

*Fig. 5.4: a) Comparison of calculated ion activity coefficients at 170° C versus ionic strength: For the binary system NaCl-H_2O (extended Debye-Hückel (red line) and Pitzer model (black line)) and for the ternary system NaCl-$CaCl_2$-H_2O with 0.9 mol/kg $CaCl_2$ (extended Debye-Hückel (dashed red line) and Pitzer model (dashed black lines)). b) Calculated halite solubility versus temperature: For the binary system NaCl-H_2O (extended Debye-Hückel (red line) and Pitzer model (black line)) and for the ternary system NaCl-$CaCl_2$-H_2O with 0.9 mol/kg $CaCl_2$ (extended Debye-Hückel (dashed red line) and Pitzer model (dashed black lines)). * Experimental data from Li et al. (2005)(open squares) and from Yang et al. (2011) and Yang et al. (2010) (open circles) indicate good agreement of the numerical model (Pitzer) and laboratory measurements.*

The saturation state of a fluid with respect to a mineral phase is obtained from equation

$$\Omega = K^{-1} \prod_{j=1}^{n_c} c_j^{v} \cdot \gamma_j^{v} \qquad (E5.8)$$

where Ω is the saturation ratio of a mineral phase, K solubility constant, c is concentration of an aqueous species, v is the stoichiometric coefficient of aqueous species, and γ is the activity coefficient derived from Pitzer formalism. The temperature dependence of halite solubility is controlled by adapting K according to Greenberg and Møller (1989) and by thermal fitting of the Pitzer parameters (*Table 5.1*). Differing ion activities influence halite solubility. Lower ion activities result in a generally larger halite solubility for the Pitzer model *Fig. 4.4b*. While solubilities at 25 °C are equal for both models, the discrepancies increase with increasing temperature to deviations of around 20 % at reservoir temperature. Applying the Pitzer parameters from Greenberg and Møller (1989) and from Sterner et al. (1998) displayed in *Table 5.1*, modeled halite solubility perfectly matches laboratory values (compiled by Li et al. (2005)) for the binary system NaCl-H_2O over the complete temperature range considered. However, only few data are available on solubility of halite in the presence of $CaCl_2$ at the considered temperature and $CaCl_2$ concentration, Yang et al. (2011) and Yang et al. (2010) support parameterization for the system NaCl-$CaCl_2$-H_2O.

Table 5.1: Applied Pitzer paramterization and thermal fitting parameters (a_i) for the equation $P(T) = a_1 + a_2\left(\frac{1}{T} - \frac{1}{T_0}\right) + a_3\, ln\left(\frac{T}{T_0}\right) + a_4(T - T_0)$ *given by Wolery et al. (2004), where P(T) are Pitzer parameters, T_0 is the reference temperature of 298.15 °C, and T is the temperature for which the parameter has to be calculated. Parameters were taken from Sterner et al. (1998) and from Greenberg and Møller (1989).*

binary C - A		Na^+ **-** Cl^-	Ca^{2+} **-** Cl^-
α_{MX}		2.0	2.0
α'_{MX}		12.0	12.0
$\beta^{(0)}_{MX}$	a_1	$7.456 \cdot 10^{-2}$	$4.460 \cdot 10^{-1}$
	a_2	$-4.708 \cdot 10^{2}$	$2.207 \cdot 10^{2}$
	a_2	-1.851	$1.606 \cdot 10^{-11}$
	a_4	$1.656 \cdot 10^{-3}$	$2.276 \cdot 10^{-4}$
$\beta^{(1)}_{MX}$	a_1	$2.752 \cdot 10^{-1}$	-1.661
	a_2	$-5.211 \cdot 10^{2}$	$-8.832 \cdot 10^{3}$
	a_2	-2.880	$7.095 \cdot 10^{-11}$
	a_4	$4.715 \cdot 10^{-3}$	$-2.495 \cdot 10^{-2}$
$C^{(\varphi)}_{MX}$	a_1	$1.537 \cdot 10^{-3}$	$-1.727 \cdot 10^{-2}$
	a_2	48.070	-12.990
	a_2	$1.747 \cdot 10^{-1}$	$-3.8717 \cdot 10^{-13}$
	a_4	$-1.563 \cdot 10^{-4}$	$-3.150 \cdot 10^{-5}$
binary C - C		Na^+ **-** Ca^{2+}	
θ	a_1	$5.000 \cdot 10^{-2}$	
	a_2	$1.863 \cdot 10^{-9}$	
	a_2	$7.276 \cdot 10^{-12}$	
	a_4	0	
ternary C - C - A		Ca^{2+} **-** Na^+ **-** Cl^-	
Ψ	a_1	$-3.000 \cdot 10^{-3}$	
	a_2	0	
	a_2	$1.137 \cdot 10^{-13}$	
	a_4	$-6.661 \cdot 10^{-16}$	

5.4 Results

To reproduce the onsite borehole conditions during production and formation of the halite plug, flow rates according to T111110 (*Fig. 5.5*) were applied. The thermal model was calibrated using the available wellhead temperature data from the production test, which had been measured during the 3rd production cycle. As halite formation is predominantly temperature-controlled, this approach is supposed to be appropriate for setting up a valid model.

Table 5.2: Applied hydraulic and thermal material properties.

		pipe string	*pipe wall*	*host rock*
porosity	*[vol.- fraction]*	*0.99*	*0.01*	*0.10*
heat capacity	*[J/[kg·K]*	*2500*	*477*	*1000*
heat conductivity	*[W/[(m·K)]*	*3.5*	*50/25*	*2.5*
material density	*[kg/m³]*	*100*	*7850*	*2600*

As flow in the pipes, temperature development over time, and chemistry (precipitated solids) are coupled processes, calibration was carried out by iteratively fitting the calculated wellhead temperature evolution to the measured data. By using the resulting thermal material parameters shown in *Table 5.2*, the model calculates the thermal behavior of the well in excellent agreement with the measurements (*Fig. 5.5*).

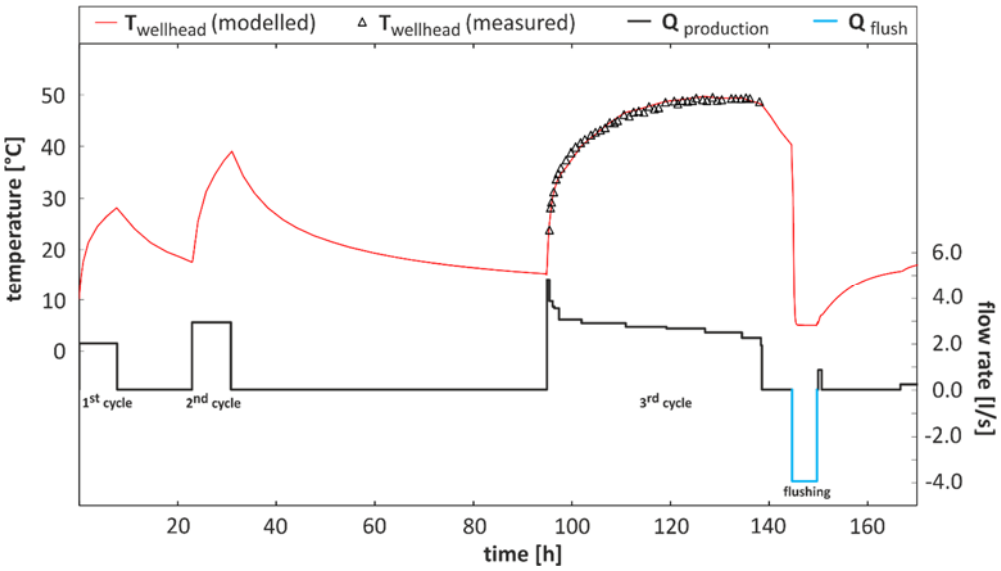

Fig. 5.5: Applied flow rates over the course of T111110 (black curve) and the freshwater flush of the annulus (blue curve) following the 3rd production cycle. The red curve represents the resulting modeled wellhead temperature. The model was calibrated to the onsite wellhead temperature (open squares) measured during the 3rd production cycle.

Fig. 5.6 displays the development of temperature, halite abundance, permeability, and differential pressure per flow rate over the full length of the production string. Initial brine salinity was 6.8 mol/kg_w NaCl. For the relationship of porosity and permeability, the cubic law was applied. It is found that temperatures at the wellhead do not exceed 50 °C (*Fig. 5.6a*). As in all other parts of the well, only moderate positive temperature deviations from the undisturbed linear thermal gradient indicate

rather low overall system warming during production. This is even more the case for the upper part of the string. Here, the descending fluid in the annulus has an intense cooling effect on the production string, which is reflected by an immediately steepening temperature gradient at 1175 m depth. System warming is highest after the 3rd production cycle when largest amounts of fluid (*Fig. 5.5*) have been produced continuously. After flushing the injection string, the well shows lowest temperatures. This is reflected by negative deviations from linear geothermal gradient in the shallowest part.

Modeling of halite abundance is in very good agreement with the observations onsite. The peak of halite abundance coincides excellently with the depth range, where the salt plug has formed in reality. After the 2nd production cycle when well temperatures are still lower, plug formation starts at around 1750 m depth. It moves upwards when temperatures increase (3rd cycle). At the depth of 1175 m, where the annulus ends, a sharply increasing halite abundance (*Fig. 5.6b*) can be noticed, which is caused by the changing temperature gradient (*Fig. 5.6a*) at this point. Predominantly this additional cooling controls the depth of highest halite abundance.

The additional decrease of temperatures during flushing virtually has no impact on halite abundance, as water conditions in the production string are stagnant at this time. That means no supply of saturated fluid takes place, which is likely to form solids. The model reaches peak values of halite abundance of 40 vol.-% at the maximum for the applied initial salinity of 6.8 mol/kg_w NaCl. Hence, it does not reproduce the onsite conditions, where a more massive plug was observed. The halite precipitations, by contrast, are more elongated and reach shallower depths. The total precipitated halite mass is very similar to the mass of 30 t estimated onsite and reported by (Hesshaus et al., 2013).

The precipitation-related decrease of permeability is about one order of magnitude at the end of the simulation (*Fig. 5.6c*). The reduced permeability results in a higher differential pressure to ensure the given flow rates. Differential pressure per flow rate increases by 2.5 bar/kg/s at the maximum for the precipitated volume at the end of the simulation applying the cubic porosity-permeability scheme (*Fig. 5.6d*).

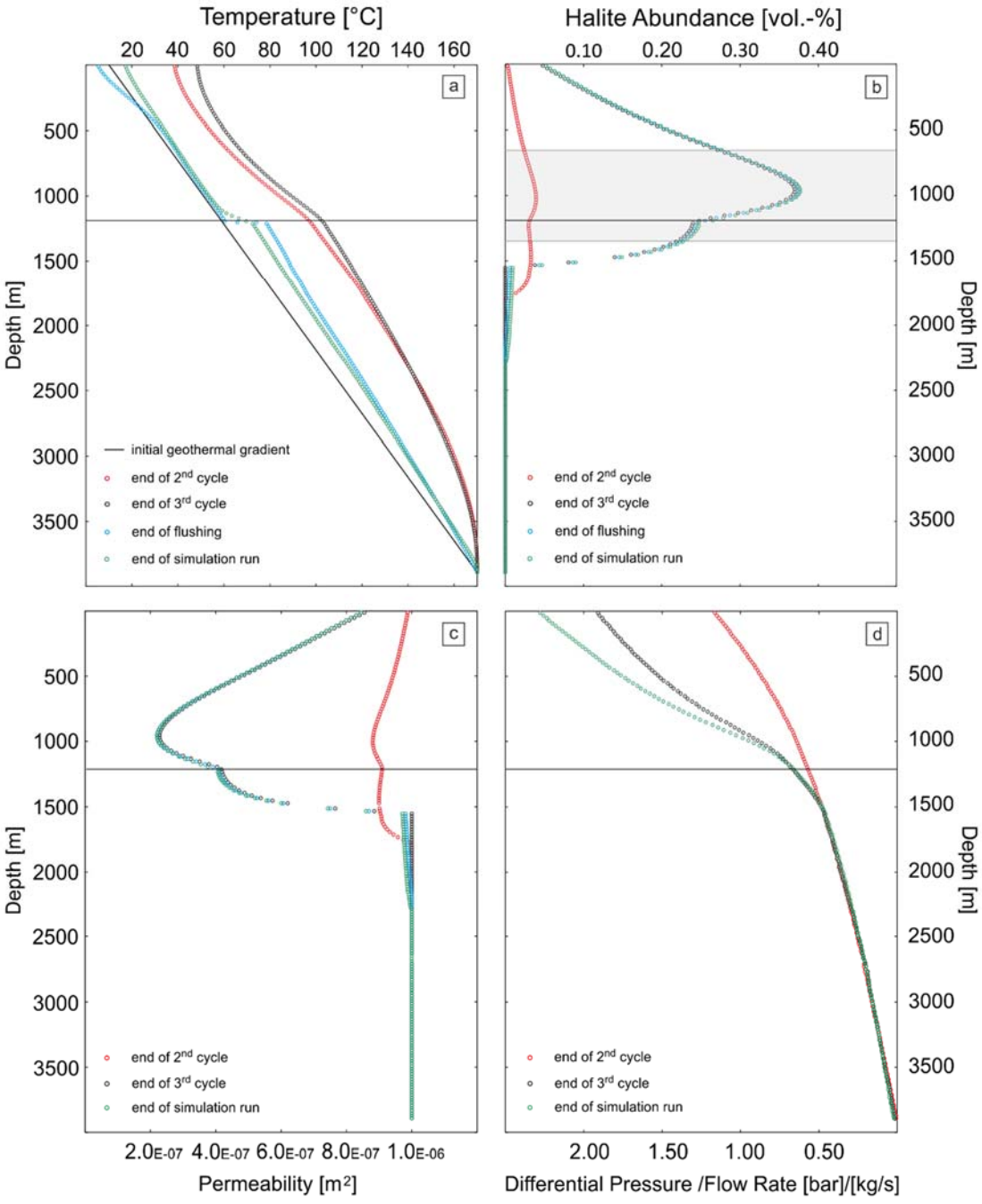

Fig. 5.6: Temperature (Fig. 6a), halite abundance (Fig. 6b), permeability (Fig. 6c), and differential pressure normalized by the flow rate (Fig. 6d) in the production string versus depth for different times. The gray-shaded area represents the depth range, where the halite plug was observed onsite. The horizontal black line at 1175 m depth marks the end of the annulus, where fluid is extracted.

5.5 Discussion

5.5.1 Initial Brine Salinity

Halite precipitation is a direct effect of brine cooling and potentially occurs whenever production takes place in this near-saturation state system. For this reason, wellhead measurements of fluid chemistry rather are estimated minimum values of reservoir brine composition. To investigate real reservoir concentration, the model was calculated as a function of initial brine salinity.

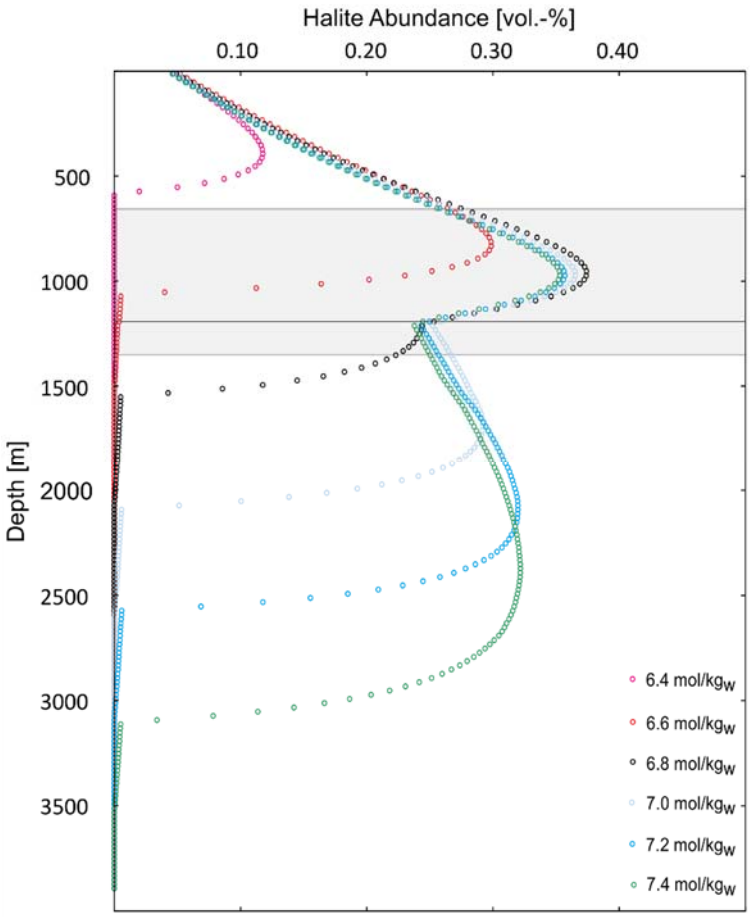

Fig. 5.7: Precipitated halite solids in volume percent in the production string versus depth as a function of initial brine salinity (NaCl). The gray-shaded area represents the depth range, where the halite plug was observed onsite. The horizontal black line at 1175 m depth marks the end of the annulus, where fluid is extracted.

Varying initial salinities were tested, ranging from the near-saturation state at 170 °C (7.4 mol/kg_w NaCl) to less concentrated brines (6.4 mol/kg_w NaCl). Taking the location of the forming halite plug as an indication, an initial (reservoir) brine concentration of 6.8 mol/kg_w NaCl is most likely (*Fig. 5.7*). This applies to the location, where precipitation starts, but also to the location, where halite abundance reaches highest values, even though these do not exceed 40 vol.-%. Lower initial concentrations lead to decreasing abundance and plug locations at shallower depths, whereas brines with increasing NaCl concentrations lead to a start of precipitation at greater depth. The maximum halite abundance per element, however, does not increase when applying higher initial brine salinity. Instead, it is found that the precipitated solid volumes having same values also for higher initial concentrations. In this thermodynamic equilibrium modeling approach the development of halite abundance over depth is controlled by the thermal gradient in the production pipe for a given operation state. The temperature in each element limits the solubility of the brine with respect to halite. Accordingly, the amount of precipitated solids per element is equal to the surplus of dissolved NaCl exceeding the solubility in each element. Therefore, increasing initial brine salinity will only result in precipitations starting at greater depth. With further cooling, however, solid abundance curve just reflects this upper limitation of solubility.

To obtain a more realistic picture of brine chemistry, calcium was added to the chemical calculation. Hesshaus et al. (2013) measured calcium concentrations of up to 0.9 mol/kg_w. The simplified 1:1 Na^+/Cl^- ratio described above also was adapted to the same measuring campaign that reported at least 5.30 mol/kg_w Na^+ and more than 7 mol/kg_w Cl^-. In *Fig. 5.9* halite abundance versus depth is shown for different initial salinities in the ternary system NaCl-$CaCl_2$-H_2O. The effect of Ca^{2+} ions can be seen when plotting halite abundance for an arbitrary low initial concentration of 6.0 mol/kg_w NaCl. For the simple binary system, no halite precipitation can be observed at such low concentration. When adding 0.9 Ca^{2+} mol/kg_w, a significant amount of solids (pure halite) is formed. As the interaction of Ca^{2+} with Na^+ and Cl^-, but also the additional ionic strength of the solution (Yang et al., 2010) considerably reduce NaCl solubility, halite precipitation can be observed at significantly lower initial concentrations. When calculating the model by applying the measured values of 5.30 mol/kg_w Na^+ and 0.90 mol/kg_w Ca^{2+} balanced by 7.04 mol/kg_w Cl^-, these concentrations seems to be slightly too low, as indicated by the misfit of modeled plug location to onsite observations. Best results in terms of plug location were obtained by applying 5.45 mol/kg_w Na^+, 0.90 mol/kg_w Ca^{2+}, and 7.19 mol/kg_w Cl^- to yield charge balance. These values can be considered the most likely reservoir brine composition regarding the major components. Apart from the ion interaction of Ca^{2+} with Na^+ and Cl^-, also the common ion effect of Cl^- changes the precipitation behavior of halite. As the additional Cl^- input from $CaCl_2$ is also part of the solubility equilibrium of halite, it causes precipitation at such low Na^+ concentrations, compared to the binary NaCl-H_2O system.

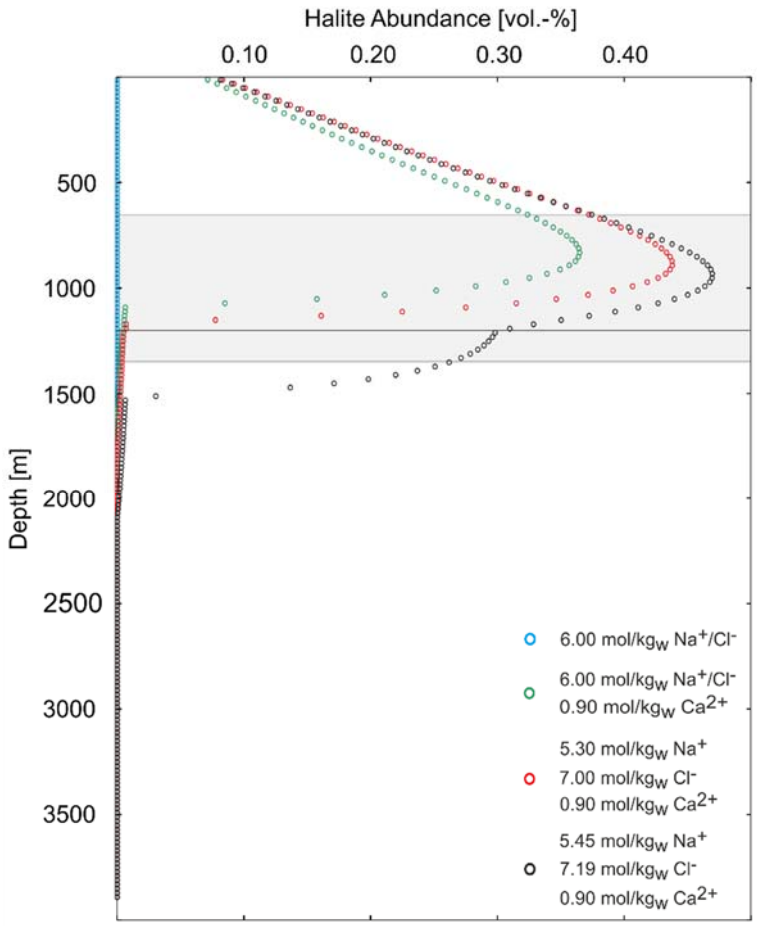

Fig. 5.8: Precipitated halite solids in volume percent in the production string versus depth as a function of initial brine salinity (ternary system NaCl-$CaCl_2$-H_2O). The gray-shaded area represents the depth range, where the halite plug was observed onsite. The horizontal black line at 1175 m depth marks the end of the annulus, where fluid is extracted.

5.5.2 Scaling Formation and the Complete Clogging Phase

The thermo-hydraulic behavior of the system and scaling formation were modeled in good agreement with the observations onsite. Reproduction of a massive halite plug causing a hydraulically tight well, however, remains a challenge. As the model does not reproduce completely clogged conditions, the calculated changes of differential pressure as a consequence of decreasing permeability are rather small (*Fig. 5.6d*). To assess the coupling of porosity and permeability and its application to pipe flow, the calculated hydraulic feedback caused by progressive solid

precipitation was compared to pressure changes in a clogged pipe string. For this purpose, *Fig. 5.9* shows plotted normalized differential pressure as a function of progressing precipitation for the simple Hagen-Poiseuille pipe flow (*E5.9*) compared to conventional porosity-permeability relations (*E5.10 - E5.15*).

Hagen-Poiseuille pipe flow: $\boldsymbol{\Delta P_x = \frac{Q \cdot 8\pi \cdot \nu \cdot l}{((1-x) \cdot A)^2}}$ (*E5.10*)

Darcy flow: $\boldsymbol{\Delta P_x = \frac{Q \cdot \nu \cdot l}{A \cdot K'}}$ (*E5.11*)

Cubic law: $K' = K_0 \cdot \left(\frac{\phi_0 - x}{\phi_0}\right)^3$ (Steefel and Lasaga, 1994) (*E5.12*)

Carman-Kozeny relation: $K' = K_0 \cdot \left(\frac{(1-\phi_0)^2}{(1-(\phi_0 - x))^2}\right) \cdot \left(\frac{\phi - x}{\phi_0}\right)^3$ (Bear, 1972) (*E5.13*)

Verma-Pruess relation: $K' = K_0 \cdot \left(\frac{(\phi_0 - x) - \phi_c}{(\phi_0 - \phi_c)}\right)^n$ (Verma and Pruess, 1988) (*E5.14*)

Davis-Davis relation: $K' = K_0 \cdot exp^{c \cdot \left(\frac{\phi_0 - x}{1 - \phi_0}\right)}$ (Davies and Davies, 1999) (*E5.15*)

with

$\boldsymbol{\Delta P_x}$	differential pressure as a function of the precipitated volume fraction [Pa]
$\boldsymbol{Q}$	flow rate [m^3/s]
$\boldsymbol{A}$	cross section area [m^2]
$\boldsymbol{\phi, \phi_0, \phi_c}$	porosity, initial and critical porosity [volume fraction]
$\boldsymbol{K'}$, $\boldsymbol{K_0}$	permeability, initial permeability [m^2]
$\boldsymbol{\nu}$	dynamic water viscosity [Pa·s]
$\boldsymbol{n}$, $\boldsymbol{c}$	empirical parameter

According to the Hagen-Poiseuille model, an increase of pipe diameter initially would cause a very small change of differential pressure. Flow resistivity will strongly increase at very small pipe diameters only, after larger amounts of solids have formed. Using different porosity-permeability coupling schemes for porous media, the cubic law applied in this study matches the hydraulic feedback of a clogged pipe most closely (Hagen-Poiseuille).

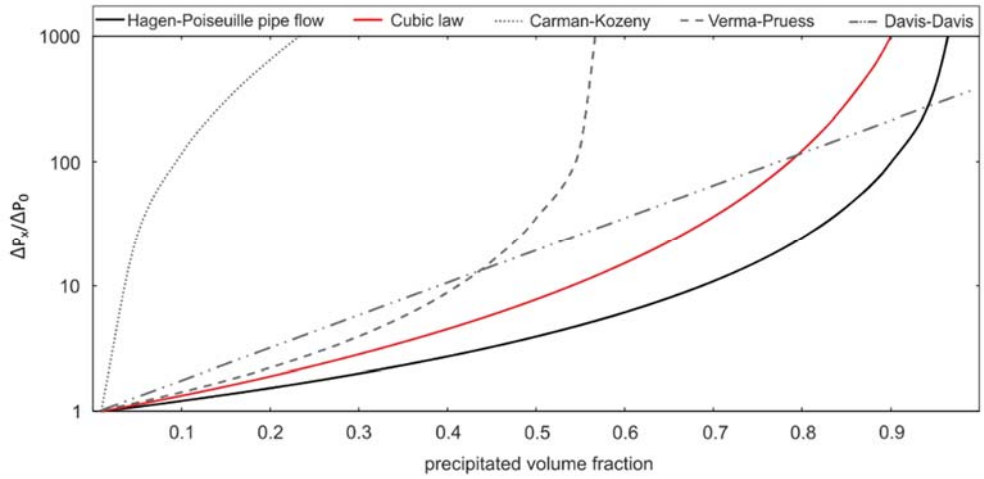

Fig. 5.9: Development of normalized differential pressure versus progressing solid precipitation as hydraulic feedback for common porosity-permeability relations (Darcy flow) and for simplified pipe flow (Hagen-Poiseuille).

But for values of halite abundance reaching merely 50 vol.-%, both the Hagen-Poiseuille pipe flow model and the Darcy-related cubic law coupling do not reach tight conditions. It is rather the applied chemical model which causes a strongly elongated salt plug which would not clog the pipe under the particular conditions of T111110. Modeling the reactive transport of a saturated brine on the basis of thermodynamic equilibrium, the amount of precipitated solid per kilogram fluid inherently only depends on the temperature difference from the preceding model element. That means the modeled elongated low-density plug is a plausible result of temperature-dependent halite solubility, given temperature gradient in the production pipe, and the total mass of fluid produced during T111110. This may also reflect the precipitation process onsite. However, precipitated solids in the model will remain at the place where they have formed. Particles in open water columns of a pipe string are dragged along at high flow rates or they sink down when they exceed a certain grain size or under stagnant conditions. Both processes would lead to a more concentrated halite accumulation and a more massive plug that is potentially able to clog the pipe.

5.6 Conclusion

The approach of establishing geothermal single well applications in abandoned boreholes is a low-risk concept compared to conventional doublet systems. The better affordable investment could pave the way to a more general use in the future.

However, single well applications according to the concept of Gt1 Groß-Buchholz will be characterized by a rather strong cooling of the produced brine by the descending fluid in the counterflow section. Our model shows the resulting sudden increase in the temperature gradient of the production string right at the depth of the ending annulus. For cooling-induced scaling formation, the potential of solid accumulation is largest at this point.

In the presented study we demonstrated that our numerical approach is capable of simulating complex coupled THC processes during production in single well systems. The highly saline chemical system was successfully quantified by applying the Pitzer ion interaction model, which was parameterized and validated on the basis of halite solubility data for the onsite reservoir conditions (ternary NaCl-$CaCl_2$-H2O system). For the simulated thermo-hydraulic conditions, a suitable chemical model can also reproduce the phase of scaling formation numerically and yields plausible results. The observed complete clogging of the pipe needs additional adaptations of the chemico-physical model and requires further investigations. The depths of scaling accumulation in the model and onsite are in very good agreement and correspond exactly to the critical counterflow section as well as the total precipitated volume of solids.

Acknowledgements

The Authors wish to thank the BGR (Federal Institute for Geoscience and Natural Resources) for providing production test data and for granting the publication. Many thanks are owed to Yodha Nusiaputra (KIT) for a great number of enlightening discussions. Finally, we like to thank the EnBW Energie Baden-Württemberg for supporting geothermal research at the KIT.

6 Assessment of Performance and Parameter Sensitivity of Multicomponent Geothermometry applied to a Medium Enthalpy Geothermal System

A revised version of this study was submitted to *Geothermal Energy*.

Nitschke, F.; Held, S.; Villalon, I.; Neumann, T.; Kohl, T. (rev. subm.): Assessment of Performance and Parameter Sensitivity of Multicomponent Geothermometry applied to a Medium Enthalpy Geothermal System. *Geothermal Energy.*

Abstract

The determination of reservoir temperatures represents a major task when exploring geothermal systems. Since the uncertainties of classical solute geothermometry are still preventing reliable reservoir temperature estimations, we assess the performance of classical geothermometers and multicomponent geothermometry by applying them to fluids composed from long term batch-type equilibration experiments and to fluids from natural geothermal springs in the Villarrica area, Southern Chile. The experiments, weathering two reservoir rock analogues from the Villarrica area, highlight a strong impact of reservoir rock composition on the fluid chemistry and consequently on calculated in-situ temperatures. Especially temperatures calculated from classical solute geothermometry are strongly affected. Multicomponent geothermometry is obviously more robust and independent from rock composition leading to significantly smaller temperature spreads. In a sensitivity analysis, the dilution of geothermal fluid with surficial water, the pH and the aluminum concentration are anticipated to be the factors causing underestimations of reservoir temperatures. We quantify these parameters and correct the results to obtain realistic in-situ conditions. Thus, enabling the application of the method also on basis of standard fluid analysis, our approach represents an easy-to-use modification of the original multicomponent geothermometry leading to very plausible subsurface temperatures with significantly low scattering.

6.1 Introduction

The estimation of reservoir temperatures is a major goal in geothermal exploration. The in-situ temperature is a key parameter for the assessment of geothermal potentials and the economic efficiency of prospected reservoirs. Deducing these temperatures from the chemical composition of geothermal fluids emerging at the earth´s surface is a commonly used and relatively cost-effective method. Over more than five decades a large number of solute geothermometers have been established and constantly improved (e.g. Fournier and Rowe (1966), Giggenbach (1988), Can (2002), Sanjuan et al. (2014)). Many of these interrelations, linking the concentration of one constituent or the ratios of cations (SiO_2, Na-K, K-Mg, Na-K-Ca) to the in-situ temperature, are based on rather well known water-rock interaction processes (silica solubility, cation exchange in the feldspar system and equilibria of micas). Furthermore, empirical geothermometers using the ratios of Na-Li and Mg-Li (Fouillac and Michard, 1981; Kharaka and Mariner, 1989; Sanjuan et al., 2014) has been established, additionally accounting for fluid salinity, chloride concentration and the geology of the reservoir. However, solute geothermometry still is afflicted with great uncertainties often leading to a broad range and often inconsistent calculated reservoir temperatures (Santoyo and Díaz-González, 2010; Verma and Santoyo, 1997), in particular exploring geothermal systems, where only few information (geology, borehole data etc.) is available. Even in studies in which the individual geothermometers has been carefully selected regarding their applicability and validity for the expected conditions, the resulting temperatures show variations of often more than 100 K for the same sample (e.g. Pepin et al. 2015, Aquilina et al. 2002, Mutlu 1998, D'Amore et al. 1994).

Recently, a number of geochemical surveys have evaluated the in-situ temperatures of the geothermal system in the Villarrica area in Southern Chile, where many natural geothermal springs discharge in direct vicinity of the active Villarrica volcano. The estimations of subsurface temperatures resulted in widely differing and even inconsistent data. Sánchez et al. (2013) roughly determined temperatures of 100 °C - 180 °C from cation ratio geothermometers, with the warmest temperatures close to the volcanoes. Whereas, estimations based on the temperature dependent oxygen isotope fractionation in the system SO_4^{2-}-H_2O (Held et al., 2015), temperatures ranging from 80 °C - 130 °C, are significantly lower. Although, in a previous work from these authors (Nitschke et al., 2016), the warmer temperatures of the first study (in the North) as well as the cooler of the latter (in the South) were partly confirmed, the results were accompanied with large uncertainties for the individual springs of up to 130 K. Temperature estimations with uncertainties of that level are unsatisfactory for reliable exploration.

Many factors interfering precise and consistent results have been identified and discussed in literature. For calculating reservoir conditions based on the solubility of only one mineral phase (e.g. SiO_2 geothermometers), the amount of solvent has to

remain constant from reservoir to the discharge. Therefore, dilution with superficial water and boiling due to pressure relief are often considered to have greatest impact. For cation ratio geothermometers, which are not affected by changes of the amount of solvent, other processes like immaturity (not yet attained water-rock equililibrium) of fluids, fast re-equilibration kinetics and precipitation during ascent prevent from obtaining true in-situ temperatures. The role of the reservoir lithology, as a major interfering factor becomes obvious, when for example comparing studies from e.g. Giggenbach (1988), Arnórsson (2000), Fournier (1979) and Fournier und Truesdell (1973), indicating rather large discrepancies of the Na/K ratios of fluids from equilibrated geothermal systems of different lithologies for a given system. The same applies to other cation ratios (Na-K-Ca, K-Mg, Na-Li, etc.), commonly used for geothermometry.Also the authors of this study have previously found strong indications for the significant effect of different reservoir lithologies on the hydrochemical composition of the fluids affecting the calculation of reservoir temperatures (Meller et al., 2016; Nitschke et al., 2015; Nitschke et al., 2016). In this work, laboratory experiments are conducted to investigate the site-specific impact of rock composition on the equilibrated fluids in detail and to deduce implications for classical solute geothermometer applications. Furthermore, the numerical multicomponent geothermometry method as proposed originally by Reed and Spycher (1984) is assessed, evaluating if its statistical nature can overcome dependence upon reservoir rock composition. In order to facilitate the application of multicomponent geothermometry on basis of a standard fluid analysis, we suggest an easy-to-use modification of the original method.

6.2 Methods and Results

The detailed geological setting of the study area is documented in previous works of Held et al. (2016b) and Sánchez et al. (2013). They found a prominent change of lithology associated with the virtually E-W striking Mocha-Villarrica-Fault Zone. South of that fault plutonic rocks of the North Patagonian Batholith (NPB) prevail, while to the north mainly volcanic and volcano-clastic rocks of the Cura-Mallin (CM) formation outcrop. Depending upon this local lithology change, strontium isotope measurements (Held et al., 2015) reveal spatially differing geothermal fluids, with a plutonic signature south of the volcanic chain and a volcanic signature in the north of the study area. Accordingly, for the experimental approach, two reservoir rock analogues were selected, representing the two different geological units: a Mesozoic tonalite (NPB) and a Cenozoic porphyric andesite (CM) for long term batch reaction experiments.

Usually, reservoir rocks and their compositions are poorly known during exploration of a geothermal system and effects of different mineralogical compositions on geothermometers are difficult to handle. By calculating the equilibration temperature

of a large number of (reservoir) rock forming minerals, multicomponent geothermometry provides a more statistical approach of determining in-situ temperatures. Therefore this method is more unbiased from reservoir rock composition. To test this hypothesis, we apply the method on natural emerging geothermal fluids from the Villarrica area and on the fluids derived from laboratory experiments to compare the results to temperatures calculated with classical solute geothermometers.

6.2.1 Laboratory Water-Rock Equilibration Experiments

A tonalite and the andesite were chosen for the experiments as they were presumed to be the most likely reservoir rocks for the natural geothermal fluids due to their spatial distribution in the study area. Prior to the water-rock interaction experiments, the mineral compositions of both rock samples were analyzed in detail. The quantification of the mineral assemblages [vol.-%], derived from thin-section microscopy and X-ray diffraction (Siemens D500) are given in *Table 6.1*. The absence of K-feldspar in the tonalite and the differing SiO_2 polymorphs (only chalcedony in the andesite and only quartz in the tonalite) are of particular importance in terms of geothermometry.

Table 6.1: Volumetric mineral composition of reservoir rock analogues used for laboratory experiments.

	Tonalite [vol.-%]	***Andesite [vol.-%]***
Quartz	*50*	*-*
Chalcedony	*-*	*5*
K-feldspar	*-*	*5*
Plagioclase	*25*	*40*
Pyroxene	*-*	*30*
Serizite	*10*	*-*
Muscovite	*< 5*	*-*
Chlorite	*< 5*	*< 5*
Biotite	*10*	*-*
Clay minerals	*-*	*10*
Magnetite	*-*	*10*

The experimental setting described below was designed according to the findings from several test runs leading to a progressive refinement of the laboratory procedure due to an increasing expertise. In order to reduce reaction time towards equilibrium to a minimum, the reactive surface was enlarged by grinding the rock samples with an agate disc mill to a grain size < 63 µm. After that treatment, the surface area of both samples is in the same order of magnitude (tonalite: 2.1 m^2/g, andesite: 3.6 m^2/g) as revealed by BET measurements. Then, 40 g of rock powder was transferred to a hermetic stainless-steel batch reactor. Avoiding any head space, the

vessel (150 ml) was then completely filled up with pure H_2O. The rock-water ratio was ~0.3. The reaction temperature was chosen to be 140 °C, which is the anticipated mean reservoir temperature in the study area. To control the development of fluid composition over time and to enable the identification of steady state conditions, the experiments were sampled and analyzed in a time series after 1, 2, 4, 6, 10, 20, 30, 45, 60, 90, 120, and 180 days (*Fig. 6.1*). Each time step represents an autonomous experiment and therefore ensures the reproducibility of results. After termination of the experiments, fluids were centrifuged and filtered (cellulose acetate membrane, pore size <0.45 µm). In order to stabilize the solution (preventing supersaturated phases from precipitation), an immediate dilution of the cooled sample with pure H_2O is of particular importance. The fluid composition was measured using inductively coupled plasma mass spectrometry (Thermo Fisher, X-Series2) for the cations and ion chromatography (Dionex, ICS-1000) for the anions. Silicon concentrations were determined by spectrophotometry (Perkin Elmar Lambda 2S).

The chemical evolutions of the major constituents over time are depicted in *Fig. 6.1* and in a tabular form in the appendix. Measured aqueous constituents are assumed to be present as a result of water-rock interaction. Due to the fact, that only low mass transfer occur for both experiments, the minerals being educt and product of fluid-solid reactions were not determined (resulting changes of solids were below the detection limit of XRD (< 5 mass-%) and SEM-EDX (very thin alteration products). Therefore, conclusions made in terms of geothermometric applications, are based on changes of water chemistry only. Comparing both experiments, significant differences in fluid compositions become obvious. Towards the end of the reaction time, the fluid in contact with tonalite has a TDS of about 700 mg/L, whereas the TDS of the fluid from the andesite experiment is about 500 mg/L. The tonalite fluid can be classified as a Na-SO_4 fluid of near neutral pH (6.7), while the andesite fluid is a Na-Cl fluid with a higher pH of 8.5. Sodium concentrations are very similar (5-6 mmol/L) for both experiments at the end of the reaction time, with a nearly continuous, but diminishing increase over time. The tonalite fluid is found to have high concentrations of potassium and calcium at early stages, but decreasing over the duration of the experiment. The andesite fluid is showing relatively constant concentrations for both cations, but remaining on a significantly lower level compared to the tonalite fluid. Aqueous SiO_2 concentrations of both fluids reach a steady state already in relatively early stages of the experiments (after 4 days for the tonalite fluid, after 45 days for the andesite fluid). However, they differ strongly from each other. Being hardly explainable, although, we observe that the andesite fluid saturates with respect to quartz, whereas the chalcedony saturation of the tonalite fluid, leads to significantly higher SiO_2 concentrations.

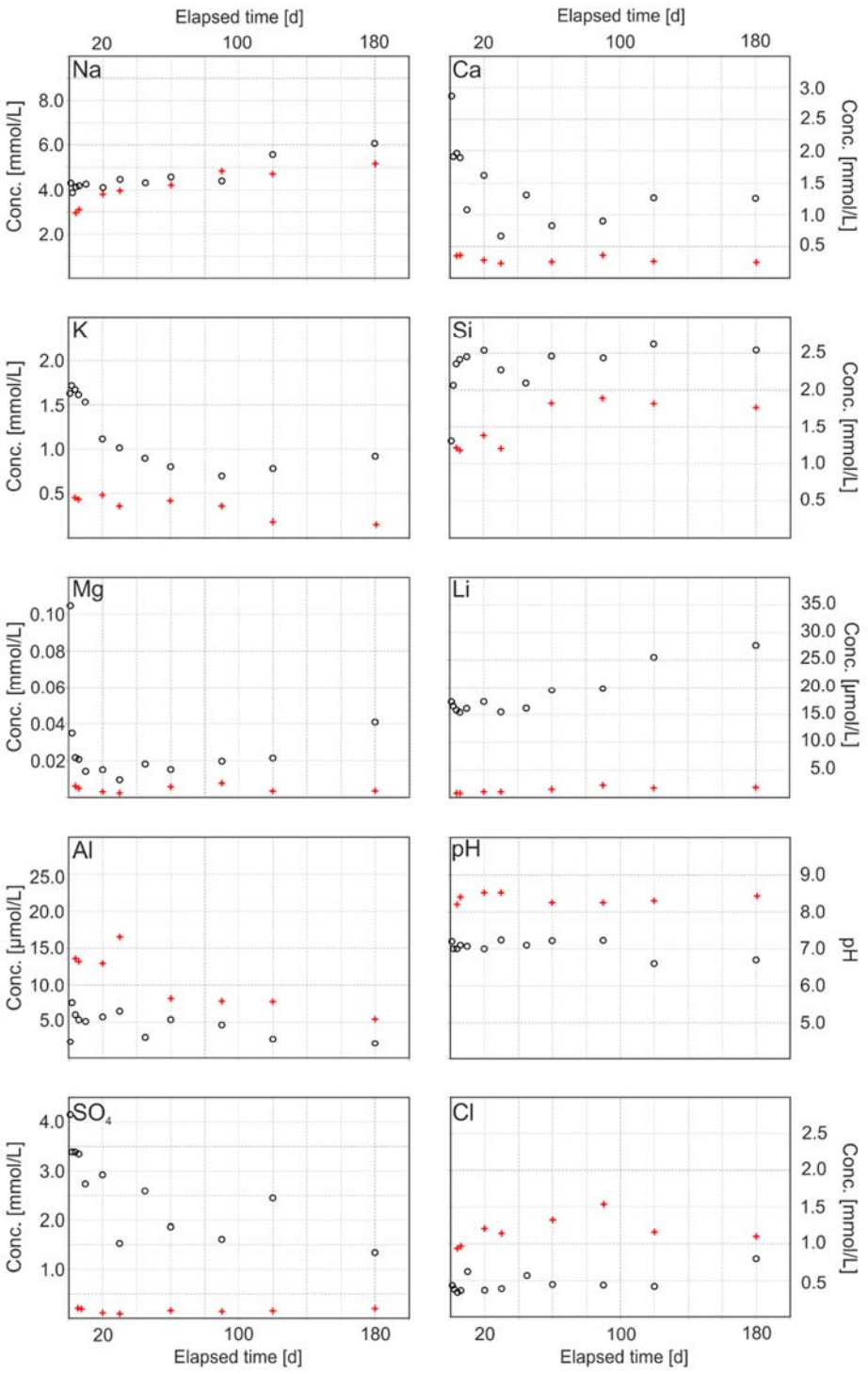

Fig. 6.1: Temporal development of concentrations of major constituents (Na, K, Ca, Mg, Li, Si, Al, SO_4, Cl and pH) of the laboratory equilibration experiments plotted versus elapsed reaction time (tonalite experiments: black circles, andesite experiments: red crosses).

Applying these results to geothermometry, the consequences for SiO_2 geothermometers are becoming obvious (*Fig. 6.2*), resulting in over- or underestimations of about 20 K (for the given reaction temperature of 140 °C). But also for further geothermometers, the reservoir rock composition affects temperature estimations. The application of Na-K geothermometer equations lead to even significantly higher discrepancies (*Fig. 6.2*).

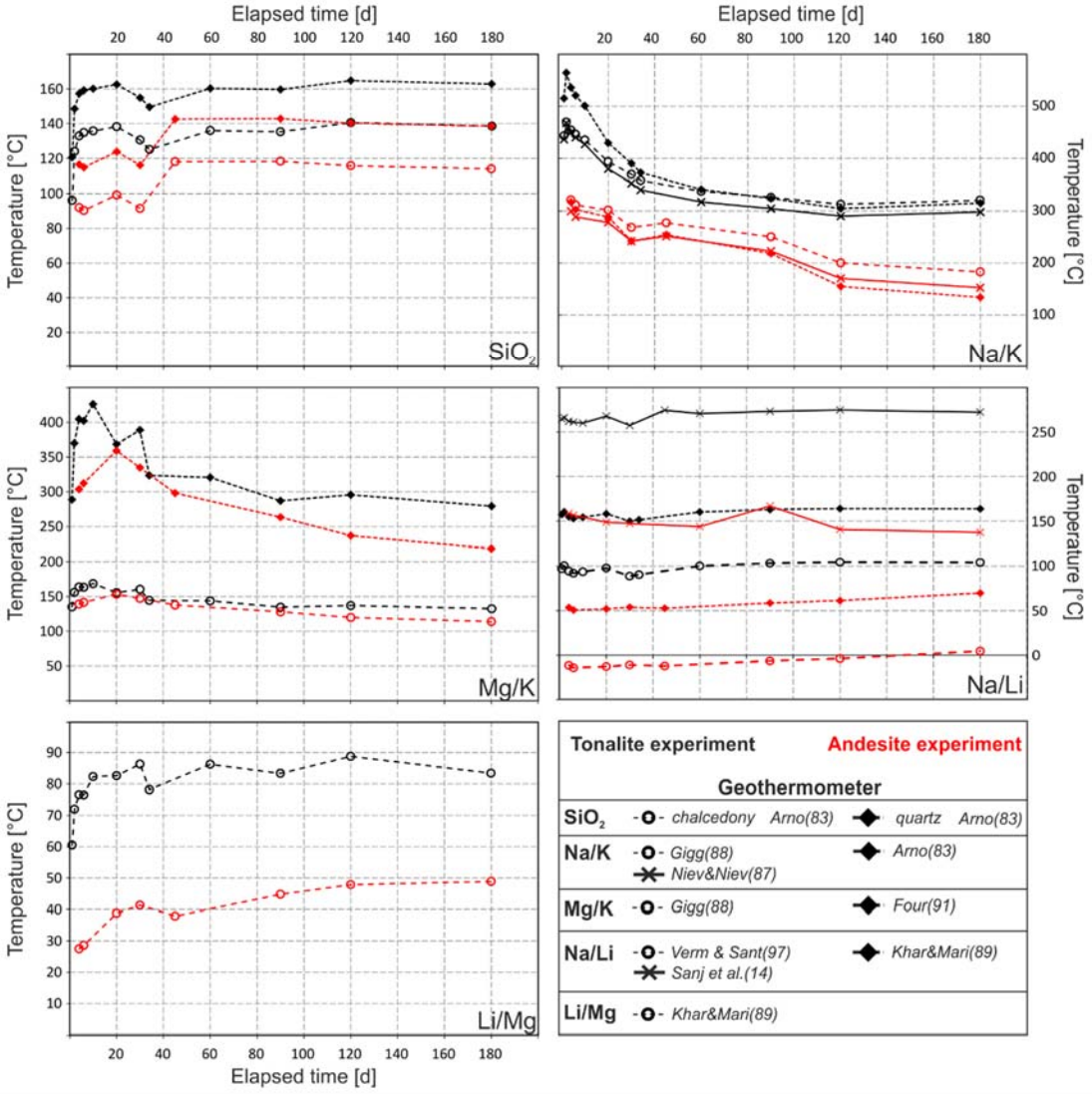

Fig. 6.2: Calculated solute geothermometer temperatures for the experimental fluids plotted versus elapsed reaction time (tonalite experiments: black symbols, andesite experiments: red symbols). Temperatures were calculated from Arnórsson (1983), Fournier (1991), Giggenbach (1988), Kharaka and Mariner (1989), Nieva and Nieva (1987), Sanjuan et al. (2014) and Verma and Santoyo (1997).

Formulations of Arnórsson (1983) or Fournier and Truesdell (1973) work very well for the andesite fluids approaching the reaction temperature of 140 °C towards the end of the experiments, whereas the temperature of the tonalite fluids is strongly overestimated with temperatures of > 300 °C. This failure may be explained by the absence of K-feldspar in the tonalite and therefore the Na^+/K^+ equilibrium in this case is controlled by other potassium phases (e.g. muscovite), leading to a relative potassium enrichment, which results in that significant temperature overestimation.
The Mg-K geothermometer of Giggenbach (1988) estimates reaction temperatures for both experiments quite well. Especially for the tonalite fluids, the calculated temperature (137 °C) reflects the reaction conditions in nearly perfect agreement. For the andesite fluids calculated temperatures approach reaction temperature over the course of the experiments, but decrease to slightly underestimated temperatures towards the end (120 °C). Na-Li based temperature determination (Kharaka and Mariner, 1989; Sanjuan et al., 2014; Verma and Santoyo, 1997) is obviously rather less appropriate, giving a broad range of apparently erratic results depending upon experiment and applied formulation. The method leads to dramatic underestimated temperatures (Verma and Santoyo, 1997) but also really well fitting results (Sanjuan et al., 2014) for the andesite experiment. Calculated temperatures for the tonalite fluids range from underestimations (Verma and Santoyo, 1997) to high overestimations (Sanjuan et al., 2014). The Li-Mg geothermometer (Kharaka and Mariner, 1989) underestimates the reaction temperature for both experiments to a great extent.
As the steady state of the fluids is a crucial point for further analysis, the chemical water-rock equilibrium is assessed considering the concentrations of K^+, Ca^{2+} and Mg^{2+} (*Fig. 6.3*). The method was originally proposed by Giggenbach and Goguel (1989). In contrast to many other methods for the evaluation of water-rock equilibrium, which plot fluid data versus theoretical concentrations derived from solving geothermometer equations (Giggenbach, 1988; Tassi et al., 2010), this approach is (beside of the K-Mg geothermometer) taking account for the equilibrium of K-feldspar, K-mica, chlorite, calcite and silica (Hedenquist, 1991). It is shown that the experimental fluids plot far away from the state of initial crustal rock dissolution, but very close to the full equilibrium curve.

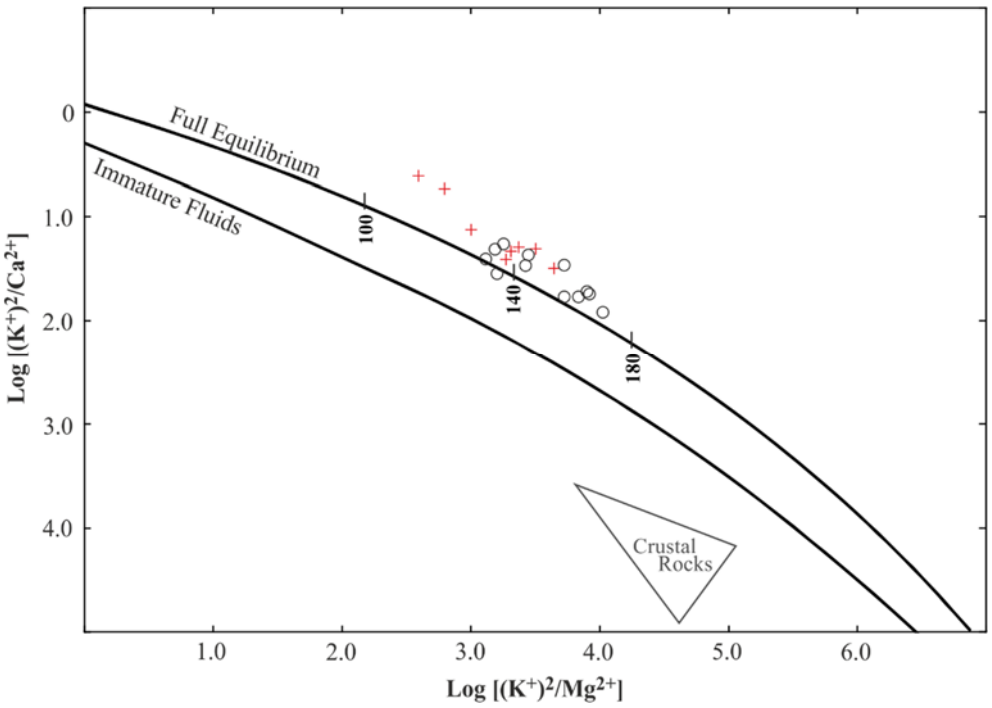

Fig. 6.3: Plot of K^+/Mg^{2+} versus K^+/Ca^{2+} ratios according to Giggenbach and Goguel (1989) of the experimental fluids (tonalite experiments: black circles, andesite experiments: red crosses), illustrating the near equilibrium state of the fluids.

If the application of one geothermometer is successful, inaccurate or failing cannot be explained in every case (e.g. like for the Na-K geothermometer). As laboratory procedures are identical for both experiments (sample preparation for solids and fluids and the setup of experiments), we conclude that the differences of fluid compositions comparing both experimental series in this specific case can only be due to the differences in rock composition. These discrepancies lead to different steady states of fluid compositions, which is consequently resulting in differences of calculated temperatures. Even if one of the geothermometers would yield a correct estimation of the reservoir temperature, there is no indication for the selection of that appropriate one when exploring a geothermal site.

6.2.2 Multicomponent Geothermometry

The determination of in-situ temperatures by multicomponent geothermometry, is based on the calculation of the saturation indices (SI = log(Q/K)) for a suite of possible (reservoir) rock minerals in a conceivable temperature interval. Based on a complete fluid analysis, an equilibrium temperature (temperature for which SI = 0) for each considered mineral phase is obtained. In contrast to classical solute geothermometry, the results represent a temperature distribution in which the fluid

has been equilibrated with the host rock minerals. This enables the calculation of a mean in-situ temperature from the bandwidth of obtained equilibration temperatures and gives insight on the uncertainty of this estimation (maximum spread of temperatures). From that point of view, multicomponent geothermometry can be considered as a statistical approach to predict reservoir temperatures and therefore it might be more applicable for the evaluation of systems with unknown mineralogy, which is often the case especially in early stages of geothermal exploration campaigns.

This study applies an approach similar to the original method suggested by Reed and Spycher (1984) and revisited by Spycher et al. (2014), Peiffer et al. (2014) and Palmer et al. (2014). Equilibration temperatures are calculated for feldspars (K-feldspars and albite), SiO_2 polymorphs (quartz or chalcedony), phyllosilicates (muscovite, paragonite, biotites, kaolinite), zeolites and epidotes based on concentrations of major constituents Na, K, Ca, Si, Al, Fe, Cl, alkalinity and sulfate. Magnesium phases are excluded intentionally, since dilution of geothermal fluids with superficial, Mg-rich waters will significantly bias reservoir temperature estimations, by overestimating equilibration temperatures for magnesium minerals. The determination of the critical parameters, such as in-situ pH and aluminum concentration is done differently than in the above named studies. Contrasting the methods of Spycher et al. (2014) and Palmer et al. (2014), we determine in-situ pH as a sum parameter via a sensitivity analysis (*section 6.3.2*), thus accounting for measurement errors as well as for degassing and speciation driven processes, which potentially effect the pH. The same applies for aluminum concentrations (*section 6.3.3*). Differing from the FixAl method proposed by Pang and Reed (1998), the here presented approach determines the aluminum concentration by minimization of the equilibrium misfit for all considered alumino-phases not by forced equilibrium of one single mineral. Numerical calculations were conducted using PhreeqC version 3.1.4 (Parkhurst and Appelo, 2013) and thermodynamic data of Delany and Lundeen (1991)**.**

According to this, in-situ temperatures were calculated for the wells Caranco (Car), Chihuio (Chi), Liquine (Liq), Liucura (Liu), Los Pozones (Poz), Menetue (Men), Palguin (Pal), Panqui (Pan), Rincon (Rin), Rinconada (RinCo), San Luis (SL) and Trancura (Tra), all located in the vicinity of the Villarrica volcano (*Fig. 6.4*). In a first run, the SiO_2 polymorph was determined, to calculate the appropriate silica equilibration temperature. For further analysis (pH- and aluminum sensitivity and for the final temperature determination) the polymorph, which yield the better fitting temperatures (smaller deviation to mean temperatures from total mineral assemblage) was applied. Chalcedony was applied to the three southernmost springs (Car, Chi and Liq) and to the the tonalite experiment. In-situ temperatures for all other samples were calculated for quartz. The fluid compositions were determined analogously to measurements of experimental fluids (*section 6.2.1*). The detailed chemical compositions (major constituents) are depicted in the appendix.

Fig. 6.4 provides a comparison of temperatures derived from multicomponent geothermometry (preliminary temperatures without correction of dilution, pH and aluminum concentration) to results calculated by a suite (n = 23) of classical solute geothermometers (SiO_2, Na-K, Na-K-Ca, K-Mg, Li-Mg and Na-Li geothermometers according to the equations given by Arnórsson (1983), Can (2002), Diaz-Gonzalez et al. (2008) Fouillac and Michard (1981), Fournier (1977), Fournier (1979), Fournier and Potter (1982), Fournier and Truesdell (1973), Giggenbach (1988), Kharaka and Mariner (1989), Michard (1990), Nieva and Nieva (1987), Tonani (1980), and Verma and Santoyo (1997)). The results were depicted as boxplots, plotting the mean (median value) equilibration temperature, the lower and upper quartiles (comprising 50 % of all temperatures) and the lower and upper extremes. The ranges of temperatures for the springs in the Villarrica area and for the fluids derived from the experiments calculated by multicomponent geothermometry is significantly smaller compared to the very large spread obtained from classical solute geothermometers. Despite special attention was paid to the applicability of each solute geothermometer, it is shown that classical geothermometers generally lead to a broad spread of temperatures of in some cases >>100 K. The spread of temperatures derived from multicomponent geothermometry is much smaller.

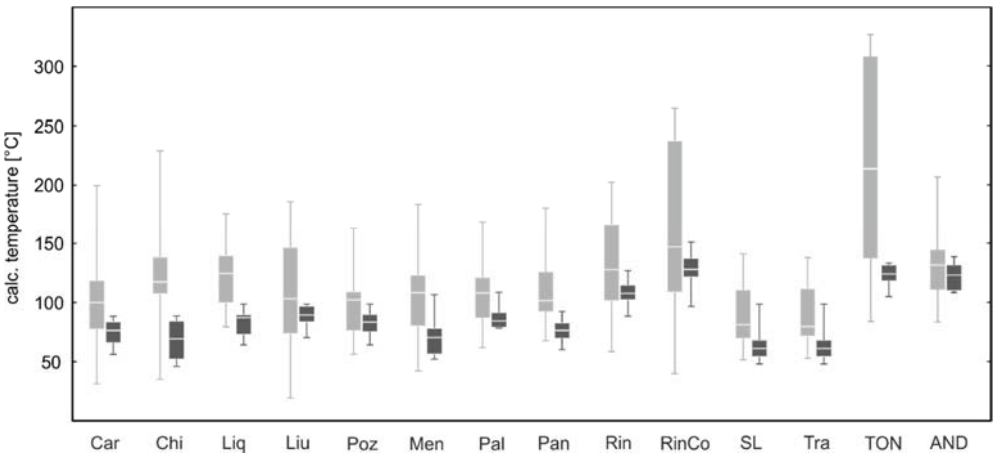

Fig. 6.4: Distribution of temperatures calculated for the Villarrica springs and the laboratory batch experiments (TON: tonalite experiment (180 days), AND: andesite experiment (180 days)) using classical solute geothermometers (light colors) compared to temperature distributions derived from multicomponent geothermometry (dark colors). Classical solute geothermometer temperatures (SiO_2, Na-K, Na-K-Ca, K-Mg, Li-Mg and Na-Li) were calculated using formulations of Arnórsson (1983), Can (2002), Diaz-Gonzalez et al. (2008), Fouillac and Michard (1981), Fournier (1977), Fournier (1979), Fournier and Potter (1982), Fournier and Truesdell (1973), Giggenbach (1988), Kharaka and Mariner (1989), Michard (1990), Nieva and Nieva (1987), Tonani (1980), and Verma and Santoyo (1997).

At the same time, the calculated mean (median) temperatures are significantly lower. Although deviation of calculated temperatures for the experimental fluids is quite

small (124 °C for the andesite experiment and 133 °C for the tonalite experiments), estimations for some springs lead to implausible low values, ranging below the discharge temperature (e.g. discharge temperature/calc. temperature for Car = 82/77 °C or Chi = 85/69 °C). At least in those cases temperatures are interfered by processes which were obviously not taken into account in this preliminary calculation. Generally, calculated temperatures appear to underestimate in-situ temperatures, as in any case being significantly cooler compared to classical geothermometer temperatures. The identification and quantification of the critical parameters being most sensitive for the system and necessary corrections calculated realistic reservoir temperatures are presented in the following section.

6.3 Discussion

For the systematical underestimation of calculated temperatures discerned in *section 6.2.2*, a number of processes or parameters are worth considering. Anticipated processes are the dilution with superficial water during ascent of fluids, the deviation of measured pH from in-situ pH (due to degassing and as a function of temperature), as well as the uncertainties of aluminum concentrations (due to precipitations, sampling, sample storage and measurement errors). To quantify the impact of each parameters and to obtain realistic in-situ conditions is a major task. Therefore we conduct a sensitivity analysis on each of the mentioned parameter. In terms of the pH and the aluminum concentration, the best-fit results of this analysis (minimization of total temperature spread and densification of clustering of the majority of temperatures) are assumed to represent the most-likely in-situ conditions, which are then basis for the final temperature estimation.

6.3.1 Dilution with superficial water

On the basis of chlorofluorocarbon measurements (CFC-11, CFC-12 and CFC-113), which yield the degree of dilution of the fluids from the geothermal springs (Held et al., 2016a), the deep reservoir fluid composition is reconstructed. To obtain the original composition, a simple binary mixing model of the discharged fluid and the composition of the Lake Villarrica (representing the superficial water) according to *E6.1* is applied.

$$C_{r,i,j} = \frac{C_{m,i}+(x_j \cdot C_{s,i})}{1-x_j} \qquad (E6.1)$$

with concentration C and dilution fraction x for the reservoir fluid r, the chemical components i and the springs j.

To evaluate the impact of dilution (mixing) on calculated reservoir temperatures, equilibration temperatures for the sample compositions and the adjusted original reservoir fluid compositions are plotted versus their degree of dilution (*Fig. 6.5*). It is shown that the expected impact of dilution on reservoir temperature calculation is hardly notable. The spread of calculated temperatures shows no trend with the degree of dilution. The deviation of mean equilibration temperatures of the original reservoir fluid compared to the sample composition is very low, reaching maximum ~15 K for sample Liu, which is the most highly diluted sample (1:1). At least in the presented case, where relatively low mineralized geothermal fluids occur (concentrations of most constituents of geothermal fluids and surficial waters range in the same order of magnitude), multicomponent geothermometry appears to be quiet robust against dilution. Applying this to highly mineralized fluids, the system may be more sensitive and hence temperature estimation uncertainty may increase.

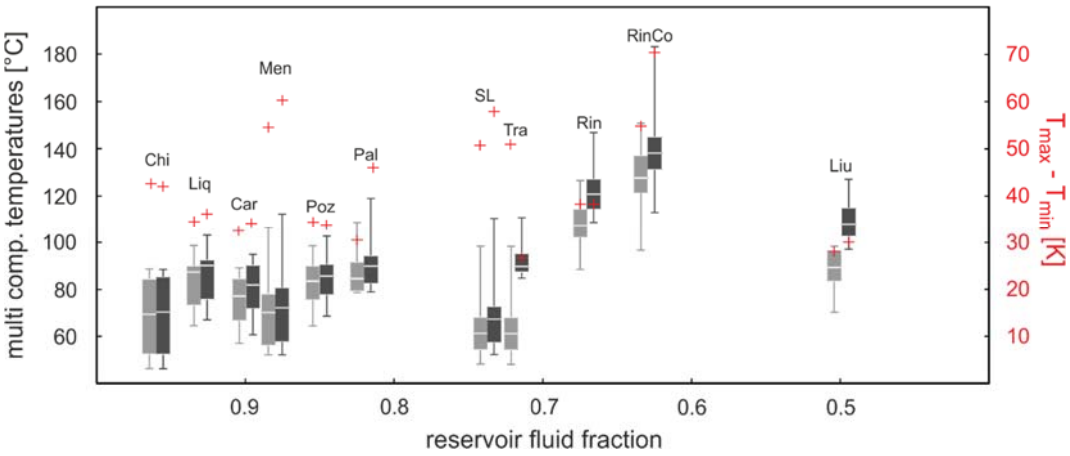

Fig. 6.5: Distribution of temperatures for the Villarrica springs calculated by multicomponent geothermometry for original sample compositions (light grey) and for dilution corrected concentrations (dark grey) plotted versus degree of dilution. The spread of temperature (T_{max}-T_{min}) is indicated by red symbols.

6.3.2 In-situ pH value

Among the reservoir rock forming minerals, (alumino-)silicates are of major importance. The solubility of silicates is beside of its temperature dependence also controlled by the pH of the solution. As a consequence of degassing of geothermal fluids (depressurization during ascent) and the cooling of the fluid, measured pH can

strongly differ from in-situ values affecting calculated multicomponent geothermometer temperatures. Due to an increasing solubility of silicates with increasing alkalinity, the application of an excessive elevated pH will lead to an underestimation of temperatures (*Fig. 6.6* and *Fig. 6.7*). Therefore the pH is a crucial and critical system parameter to the same extent. In order to correct the measured pH to in-situ conditions, numerical approaches have been established (e.g. Reed and Spycher (1984)), which require an extensive high-precision fluid analysis with respect to pH-controlling species and parameters (CO_2, H_2S, organics, redox condition, etc.). However, the majority of geochemical surveys and exploration campaigns usually only perform standard fluid sampling and analysis implying limitations in this regard. To enable the application also for standard fluid analysis, the determination of in-situ pH and the subsequent correction of equilibration temperatures is done based on a numerical sensitivity analysis. In a first step, fluids derived from the laboratory experiments, where the reaction temperature is controlled and degassing can be excluded, were investigated (*Fig. 6.6*). It is shown that calculated temperatures reflect experimental conditions in a quite good agreement, being only slightly too low for both experiments for the measured pH values. Mean temperature for tonalite experiment at pH 6.7 is 133 °C, and 124 °C for the andesite experiment at pH 8.5. A decrease of pH reduces the equilibration temperature spread and slightly increases the calculated in-situ temperature (Fig. 6). Considering the least temperature spread as the indication for the most likely in-situ pH, calculated mean temperature for the andesite experiment can be corrected to 130 °C at pH 7.5. The measured near neutral pH of the tonalite experiment obviously already reflects conditions, which are close to reaction condition.

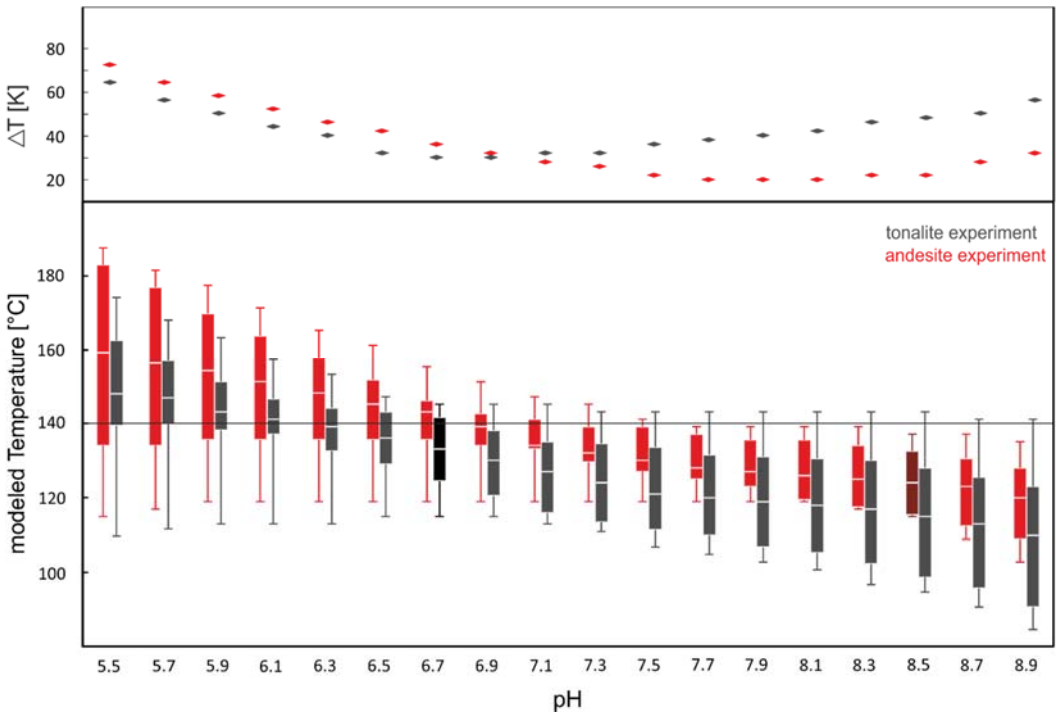

Fig. 6.6: Distribution of calculated temperatures for the laboratory experiments using multicomponent geothermometry together with the according temperature spreads (ΔT) plotted versus solution pH. Measured pH is indicated in black (tonalite experiment) and dark red (andesite experiment).

Variation of calculated equilibration temperatures as a function of pH can also be documented for the spring fluids (*Fig. 6.7*). Applying the measured pH, the obtained temperatures appear to be too low (partly below discharge temperature, e.g. Car and Chi). Especially for samples with high measured pH (e.g. Car and Liq), which potentially reflects extensive degassing, a large temperature spread is obtained. Applying lower pH values results in an increase of modeled temperatures and a decrease of temperature spread. The minimum of the equilibration temperature spread (and secondly the clustering of the majority of calculated temperatures) was taken to determine the most likely in-situ pH, which then can be used to deduce the reservoir temperature. For samples with a measured slightly acidic pH (e.g. RinCo), modeled in-situ pH will trend also towards neutral conditions resulting in a decrease of modeled mean temperature.

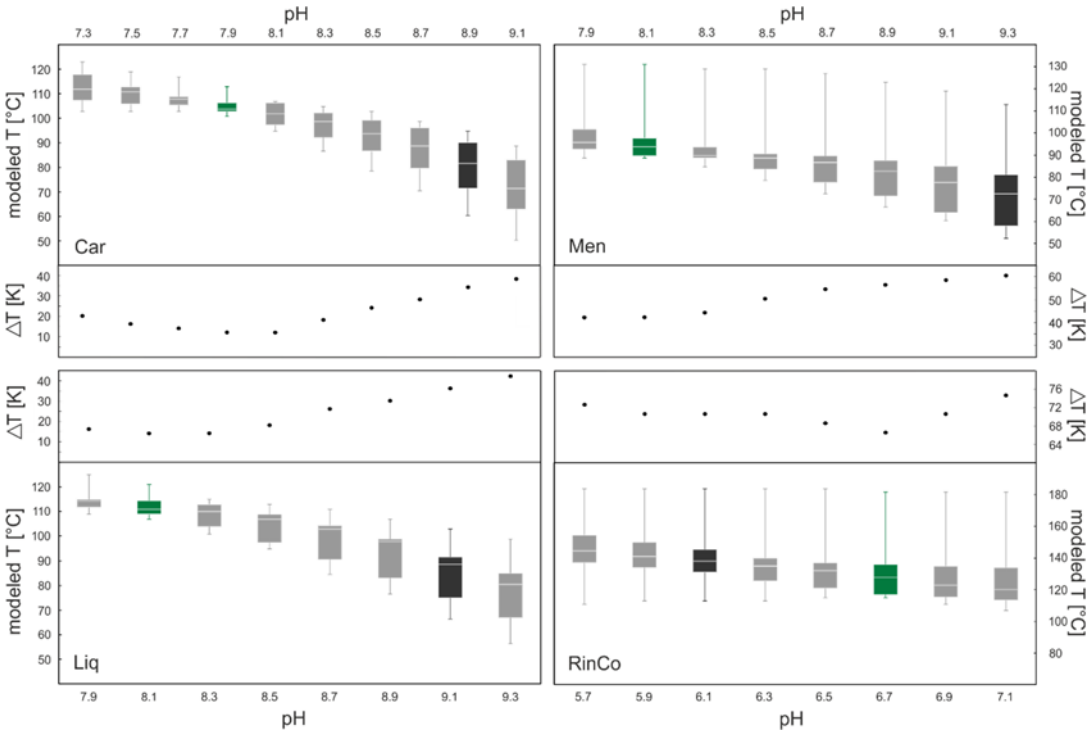

Fig. 6.7: Distribution of temperatures for selected geothermal springs of Villarrica area (Car, Men, Liq, RinCo) calculated by multicomponent geothermometry together with the according maximum temperature spreads (ΔT) plotted versus solution pH. Measured pH is indicated in dark grey, most likely pH in green.

6.3.3 Aluminum Concentration

Besides the pH, also the aluminum concentration is a critical parameter effecting temperature calculations significantly. Being component of most fluid composition controlling minerals (alumino-silicates), correct aluminum concentrations are necessary to calculate reliable equilibration temperatures for those minerals. Unfavorably, the determination of dissolved aluminum in geothermal fluids is often interfered by secondary processes during ascent of fluids (precipitation), sampling and sample handling (e.g. coagulant for silica gel formation and incorporation) in the laboratory (Brown, 2013).

Table 6.2: Aluminum concentrations of Villarrica springs measured by ICP-MS in comparison to results of previous studies.

Aluminum	this study [mmol/L]	Sanchez et al. (2013) [mmol/L]	Perez (1999) [mmol/L]
Car	0.004	n/a	n/a
Chi	0.001	0.073	n/a
Liq	0.005	0.040	0.004
Liu	0.002	n/a	0.011
Poz	0.001	n/a	bdl
Men	0.002	n/a	0.030
Pal	0.003	0.075	0.004
Pan	0.001	n/a	n/a
Rin	0.003	0.026	n/a
RinCo	0.001	n/a	bdl
SL	0.001	0.013	bdl
Tra	0.004	n/a	bdl

These issues are evident, when comparing aluminum concentrations of spring fluids in the study area measured in this study to results from previous works (*Table 6.2*). Results differ partly up to a factor of 20, which will increase the saturation indices by ~1.3.

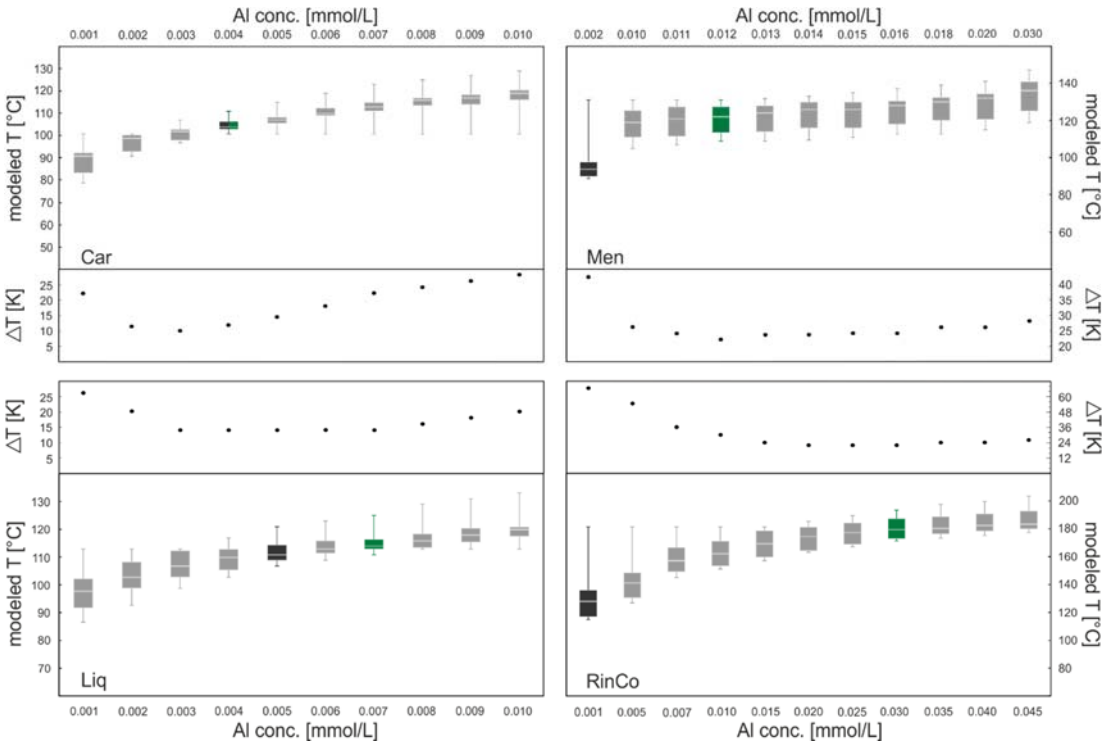

Fig. 6.8: Distribution of temperatures for selected Villarrica springs (Car, Men, Liq, RinCo) calculated by multicomponent geothermometry together with the according temperature spreads (ΔT) are plotted versus aluminum concentration. Measured aluminum concentrations are indicated in dark grey, most likely aluminum concentration in green.

Thus, aluminum concentrations (input parameter) were varied within the bandwidth of reported measured aluminum concentrations in the study area (*Table 6.2*). The pH values were set according to the findings from pH sensitivity analysis.

As anticipated, calculated mean equilibration temperatures increase with higher aluminum concentration (*Fig. 6.8*). Yet, the spread of temperatures is decreasing significantly until a minimum is reached. Also the majority of equilibration temperatures cluster in a smaller range. The best-fit in-situ aluminum concentration is determined analogously to the in-situ pH determination (least temperature spread). It can be shown that for the sample Car (*Fig. 6.8*) and the experimental fluids, measured aluminum concentrations already represent that best-fit aluminum concentrations, i.e. these fluids are in the state closest to equilibrium. The calculated temperatures for the majority of the spring fluids increase in the range of 10 - 35 K. Sample RinCo obviously, had been in a state of largest distance to equilibrium, resulting in 51 K warmer temperature estimation as a result of aluminum correction. Therefore we suggest that, the consecutive correction of pH and aluminum concentration will lead to more realistic in-situ temperatures. Equilibration temperatures which were determined in this way are displayed in *Table 6.3*. The multicomponent geothermometer approach, including the application of pH and aluminum concentration adjustments, seems to yield plausible temperature estimates, as the initially rather low temperatures indicated by aluminum containing minerals increases and converge towards the initially significantly higher SiO_2-phases temperatures. This is true for the natural geothermal fluids as well as for the already very accurate initial estimations of the laboratory experiments carried out at 140 °C.

Table 6.3: Mean in-situ temperatures for Villarrica springs and laboratory experiments calculated by a suite of classical solute geothermometers, multicomponent geothermometry and pH/aluminum-corrected multicomponent geothermometry

	classical solute geothermometers		multicomponent geothermometer		corr. multicomponent geothermometer	
spring	mean T [°C]	ΔT [K]	mean T [°C]	ΔT [K]	mean T [°C]	ΔT [K]
Caranco	100	(-69/+99)	77	(-20/+12)	102	(-5/+5)
Chihuio	117	(-82/+112)	69	(-23/+19)	108	(-10/+6)
Liquine	124	(-45/+51)	87	(-23/+11)	112	(-4/+8)
Liucura	103	(-84/+83)	89	(-19/+9)	117	(-10/+12)
Los Pozones	102	(-46/+61)	84	(-19/+15)	100	(-11/+7)
Menetue	108	(-66/+75)	71	(-18/+35)	119	(-11/+12)
Palguin	108	(-46/+61)	85	(-6/+24)	113	(-12/+9)
Panqui	101	(-34/+79)	77	(-17/+16)	96	(-13/+5)
Rincon	128	(-69/+75)	108	(-20/+19)	138	(-11/+13)
Rinconada	147	(-40/+118)	128	(-32/+23)	179	(-8/+14)
San Luis	81	(-30/+60)	61	(-13/+37)	117	(-17/+7)
Trancura	80	(-27/+59)	61	(-13/+37)	108	(-14/+10)
Andesite exp.	134	(-52/+83)	123	(-8/+16)	128	(-9/+10)
Tonalite exp.	212	(-129/+123)	135	(-19/+10)	135	(-19/+10)

6.4 Conclusion

In many cases, the application of different classical solute geothermometer equations leads to a wide range of calculated temperatures. An important factor interfering consistent calculation are differences in reservoir rock composition and their impact on fluid chemistry. Long-term batch equilibration experiments in this study clearly show that reservoir rock composition has a major impact on temperatures calculated by classical solute geothermometry, with variations of >200 K. In order to overcome the strong dependence upon rock composition, we assess the statistical multicomponent geothermometer approach. Since the original method demands high quality fluid sampling and analysis, we suggest a modification which can be used also on the basis of standard fluid analysis. Compared to classical solute geothermometry, the resulting calculated equilibration temperatures have a significantly smaller scattering for fluids of plutonic and volcanic origin in the investigated area. It is shown that the pH value and the aluminum concentration are extremely sensitive parameters for the calculation of equilibration temperatures on basis of multicomponent geothermometers. Thus, as measured values for both parameters can differ significantly from in-situ conditions, we suggest to apply a correction for the pH and the aluminum concentration prior to temperature determination. In doing so, multicomponent geothermometry lead to more realistic mean temperature estimation with significantly low variances of mostly <<30 K for the natural samples as well as for the experimental fluids. The well-fitting calculations of reaction temperatures for both experiments, reveal a higher independence from reservoir rock composition compared to classical solute

geothermometers. This could make multicomponent geothermometry an ideal complementary approach to classical solute geothermometer methods evaluating subsurface temperatures particularly in unknown lithologies. The general applicability to a wide range of reservoir rocks has to be proven in the next step. In terms of classical solute geothermometry, we conclude that the impact of reservoir rock composition is of outstanding importance and has to be taken into account in future applications.

Acknowledgements

The study is part of a collaborative research project of Karlsruhe Institute of Technology (KIT) and the Andean Geothermal Center of Excellence (CEGA, Fondap-Conicyt 15090013). The authors appreciate the support of the BMBF-CONICYT International Scientific Collaborative Research Program (FKZ 01DN14033/ PCCI130025). Additional support under the topic “Geothermal Energy Systems” of the Helmholtz portfolio project “Geoenergy” and by EnBW Energie Baden-Württemberg AG is gratefully acknowledged.

7 Geochemical Characterization of the Villarrica Geothermal System, Southern Chile, Part II: Site-specific Re-evaluation of SiO_2 and Na-K Solute Geothermometers

This study is ready for submission to *Geothermics.*

Nitschke, F.; Held, S.; Neumann, T. and Kohl, T.

Abstract

Solute geothermometry often leads to a broad range and often inconsistent calculated reservoir temperatures, in particular when exploring geothermal systems, where only limited information (geology, borehole data etc.) is available. The application of different Na-K and SiO_2 geothermometer, the most widely used methods, not uncommonly lead to deviations of results by up to 200 K for one sample.

In this study, the most effective interfering factors for these geothermometer applications are identified. A multi-step approach is proposed, combining experimental and numerical methods with specific fluid characterization to quantify these factors and to transfer these findings to the natural system enabling the correction of temperatures to realistic in-situ values.

Taking into account dilution with surface water, a chlorofluorocarbon concentration based mixing model was set up to correct measured SiO_2 concentrations to original in-situ concentrations. A numerical model was used to determine the in-situ pH, which is highly sensitive to silica solubility. Results from long-term laboratory equilibration experiments were evaluated to identify the reservoir type dependent equilibrated SiO_2 polymorph.

In the case of the Na-K geothermometer, it is shown that the Na^+/K^+ concentration ratio in fluids is obviously not unequivocally controlled by temperature but is also dependent upon reservoir rock composition. Thus, different reservoir lithologies lead to different equilibration states in terms of Na^+/K^+. This is obviously one reason for the existence of the large number of different Na-K geothermometers. By modelling the stability of the Na^+/K^+ ratio governing feldspars, albite and orthoclase, we suggest a method that reveals the Na^+/K^+ equilibration state for each fluid supporting the allocation of the appropriate geothermometer equation.

The improvement procedure is demonstrated in a case study evaluating fluid data of geothermal springs from the Villarrica geothermal system, Southern Chile. It is

shown that initially highly scattered results strongly converge after corrections, leading to a substantial improvement in in-situ temperature estimations with small deviations of ≤10 K between SiO_2 and Na-K geothermometers. Also absolute temperature calculated for each spring in the study area, ranging from 84 – 184 °C agree well (within $\Delta T < 20$ K) with results of multicomponent geothermometry temperatures reported in a previous work.

7.1 Introduction

The determination of reservoir temperatures is of outstanding importance for geothermal exploration as subsurface temperature is a key parameter for the assessment of the economic potential of a future reservoir. Deducing subsurface temperatures from the fluid composition of natural emerging geothermal springs by using solute geothermometers, has been a common practice for decades. Already in the late 1960ies methods were established using the silica concentration as a measure of the equilibration temperature of a fluid (Bödvarsson, 1960; Fournier and Rowe, 1966). Later empirical and semi-empirical approaches, like the Na-K, for which later also thermodynamic calibration approaches have been presented (Arnórsson, 2000b; Giggenbach, 1988) and the Na-K-Ca geothermometers came up, linking cation ratios to in-situ temperatures (Ellis, 1970; Fournier and Truesdell, 1973). In order to improve the reliability of temperature estimations, the development of new interrelations of fluid composition and temperature as well as the revision of existing geothermometers and their thermodynamic calibration are subject of ongoing research until today (e.g. Arnórsson (2000b), Pérez-Zárate et al. (2015), Verma (2015), Sanjuan et al. (2014)). However, uncertainties in solute geothermometry are still very large (Santoyo and Díaz-González, 2010; Verma and Santoyo, 1997). Applying different geothermometers to a single fluid sample, the scattering of resulting temperatures is often >>100 K (Aquilina et al., 2002; Mutlu, 1998; Nitschke et al., 2016; Pepin et al., 2015). Facing such large uncertainties reliable reservoir temperature estimations are hardly possible.

The geothermal system of the Villarrica area in Southern Chile has been investigated in a number of recent surveys using different geothermometry methods. The studies yield widely differing estimations for the in-situ temperatures (*Table 7.1*). In this regard, the only valid conclusion, is that the subsurface temperatures are apparently rather cool for a geothermal system situated close to an active volcano. Reservoir temperatures >200 °C are indicated only in a few exceptional cases but mostly in a significantly cooler range (100 - 180 °C). Of particular note are the very large discrepancies of up to 200 K for some samples obtained from the calculations of a suite of classical, commonly applied solute geothermometers (Nitschke et al., 2017a).

Table 7.1: Reservoir temperature estimations from previous works on the Villarrica geothermal system based on classical solute geothermometers (Nitschke et al., 2017a; Sánchez et al., 2013), oxygen isotope fractionation (Held et al., 2015) and multicomponent geothermometry (Nitschke et al., 2017b)

	Sanchez et al 2013	***Nitschke et al. 2017a***	***Held et al. this issue***	***Nitschke et al. rev. sub.***
geothermometer	classical solute	classical solute	oxygen isotope	multicomponent
springs	[°C]	[°C]	[°C]	[°C]
Carranco (Car)	-	31 - 200	84 - 88	102 (-5/+5)
Chihuio (Chi)	100 - 150	35 - 229	91 - 94	108 (-10/+6)
Liquine (Liq)	100 - 150	79 - 176	83 - 87	112 (-4/+8)
Liucura (Liu)	-	20 - 186	99 - 101	117 (-10/+12)
Los Pozones (Poz)	-	56 - 163	123	100 (-11/+7)
Menetue (Men)	-	42 - 184	110 - 112	119 (-11/+12)
Palguin (Pal)	140 - 180	62 - 169	110 - 112	113 (-12/+9)
Panqui (Pan)	-	68 - 180	138 - 139	96 (-13/+5)
Rincon (Rin)	140 - 180	59 - 203	116 - 117	138 (-11/+13)
Rinconada	-	40 - 265	98 - 101	179 (-8/+14)
San Luis (SL)	100 - 150	52 - 141	126	117 (-17/+7)
Trancura (Tra)	-	53 - 138	125	108 (-14/+10)

In order to reduce this range of uncertainties, it is obviously still a state-of-the-art procedure to calculate a large number of geothermometers (Powell and Cumming, 2010) and then just "select the most appropriate temperature" (Harvey et al., 2016). However, exploring a geothermal system, reliable indications for a reasonable selection or rejection of individual temperatures are typically rare or lacking at all.
Nevertheless, with shallow dilution (mixing), re-equilibration during ascent, immaturity (degree of dis-equilibrium), steam loss due to subsurface boiling (Arnórsson, 2000b; Giggenbach, 1988; Pérez-Zárate et al., 2015) and effects from different reservoir rock compositions (Meller et al., 2016; Nitschke et al., 2017b), parameters interfering with the results of calculations of well constrained subsurface temperatures are widely known. However, the handling of these parameters in the literature usually remains descriptive and their impact on calculated temperatures is only qualitatively discussed.
In this study, we suggest an approach to identify the most sensitive parameters and quantify their effect on in-situ temperature calculations of classical solute geothermometers and to correct results in order to obtain realistic in-situ conditions. Reflecting ongoing research, this work focusses on SiO_2 and Na-K geothermometers, which are, due to their widespread use, certainly the most important applications among the solute geothermometers. The proposed refining approach is demonstrated by applying it to data of natural fluids from hot springs from Villarrica geothermal system in Southern Chile (Held et al., 2017) and to fluids obtained from batch-type equilibration experiments of reservoir rock analogues from that area (Nitschke et al., 2017b). For the convenience of the reader, theses fluid compositions (main constituents) are again presented in this study (*annex*). Being

thoroughly investigated and well characterized previously, this study area was selected due to the occurrence of a large number of hot springs and the availability of particularly good data from a number of recently conducted geological and chemical surveys. A detailed description of the study area, its geology and the geothermal system in particular, is given in Part I by Held et al. (this issue). They specifically focus on the quantification of dilution, by establishing a chlorofluorocarbon concentration based mixing model, which is used in this study to determine realistic reservoir fluid composition. Additional background information is taken from strontium isotope measurements enabling the identification of the reservoir rock for each spring. Data of stable water isotopes (Held et al., 2017) is used for the quantification of boiling related loss of solvent.

7.2 SiO_2 Geothermometry

The basic concept of standard SiO_2 geothermometry is the temperature-only control of SiO_2 solubility. For natural systems this is a strongly simplified first-order approximation. Effectively, the measured SiO_2 concentrations of fluids, are not only a function of the reservoir temperature but also of a number of other processes interfering with the temperature signal from the deep reservoir: 1) Changes in the amount of solvent as a consequence of mixing and boiling processes are considered to cause the greatest interference to SiO_2 geothermometers (Arnórsson, 2000b). 2) Due to the more defective crystalline structure of chalcedony, its solubility is significantly higher than that of quartz (Gislason et al., 1993), which leads to different equilibration temperatures calculated for the two most commonly applied polymorphs in geothermometry (*Fig. 7.1*). 3) The pH of a fluid is a key parameter controlling SiO_2 solubility and very sensitive for the obtained SiO_2 temperature (e.g. Arnórsson et al., 1982). A correction of SiO_2 solubility was proposed by Arnórsson (2000a) for fluids with a pH value in excess of pH 9. Since the original pH at depth can significantly differ from the pH of the cooled fluid at discharge, it is also necessary to determine the in-situ pH.

To illustrate the sensitivity of the SiO_2 polymorph and the pH on SiO_2 geothermometry, we set up a geochemical equilibrium model. Theoretical equilibration temperatures for quartz and chalcedony are modeled by equilibrium dissolution of the polymorphs for the pH bandwidth measured at discharges in the study area (pH 6.1 - 9.3). Reaction temperature is increased stepwise. Geochemical modeling in this study is conducted using PhreeqC version 3.1.4 (Parkhurst and Appelo, 2013) and thermodynamic data of Delany and Lundeen (1991).

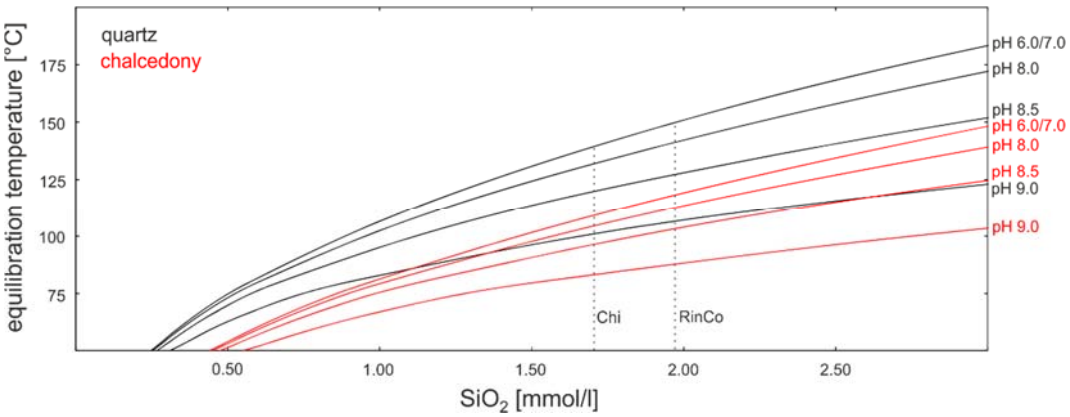

Fig. 7.1: Modeled equilibration temperatures for quartz (black lines) and chalcedony (red lines) versus measured SiO_2 concentrations for the pH range observed in the study area.

The results clearly reveal an impact of pH on calculated equilibration temperature already at pH >8.0. In combination with the impact regarding the relevant polymorphs, large deviations in resulting SiO_2 temperature estimations are possible. As an example, for the SiO_2 concentrations determined for sample Chi this deviation could be up to 59 K and for RinCo 63 K (*Fig. 7.1*). This spread of temperatures demonstrates the necessity of a precise in-situ pH determination as well as for the specification of the equilibrated SiO_2 polymorph. In the following sections, a stepwise methodology is suggested, to numerically determine the in-situ pH, to identify the equilibrated polymorph and to correct the data for effects of mixing and boiling.

7.2.1 In-situ pH determination

The pH values for the spring fluids at discharge conditions vary strongly across the study area (*annex*), being slightly acidic (RinCo) to moderately alkaline for the majority of hot springs (e.g. Men, Car, Liq, Chi). However, for geothermometry the dissolution conditions at depth are of interest. The measured pH at discharge, however, can significantly deviate from the in-situ pH being a function of temperature dependent speciation. Therefore it has to be corrected with respect to reservoir conditions. Since the reservoir temperature is intrinsically unknown in geothermometry applications, we apply an approach similar to the speciation method proposed by Arnórsson et al. (1982). By computing the speciation numerically using PHREEQC, both mutually influencing parameters are determined iteratively. Based on complete fluid analysis (Held et al., 2017), the model accounts for the most sensitive temperature dependent reactions altering the pH:

1) autoprotolysis of water

$$H_2O \Leftrightarrow H^+ + OH^- \quad (E7.1)$$

2) speciation of carbon

$$H_2CO_3 \Leftrightarrow H^+ + HCO_3^- \Leftrightarrow 2H^+ + CO_3^{2-} \quad (E7.2)$$

3) speciation of SiO_2

$$H_4SiO_4 \Leftrightarrow H^+ + H_3SiO_4^- \Leftrightarrow 2H^+ + H_2SiO_4^{2-} \quad (E7.3)$$

4) speciation of sulfur

e.g. $$H_2SO_4 \Leftrightarrow H^+ + HSO_4^- \Leftrightarrow 2H^+ + SO_4^{2-} \quad (E7.4)$$

5) speciation of metals

e.g. $$3H_2O + Fe^{2+} \Leftrightarrow 3H^+ + Fe(OH)_3^- \quad (E7.5)$$

Starting from measured discharge temperature and pH, the reaction temperature is increased stepwise with a concurrently gliding pH until saturation (SI = 0) for the desired SiO_2 polymorph is attained. Doing so, a SiO_2 equilibration temperature is obtained, which is valid for the prevailing in-situ pH. Computed in-situ pH values are presented in *Fig. 7.7*.

7.2.2 Equilibrated polymorph

The SiO_2 concentration of a fluid at given temperature is additionally controlled by the equilibrated polymorph. Until now, a clear indication whether a fluid is saturated with respect to quartz or to chalcedony is lacking or it is assumed to be dependent upon reservoir temperature level or the type of minerals precipitated during ascent (Arnórsson, 1983, 2000a). Consequently, in most cases it is unclear whether to apply the quartz or the chalcedony geothermometer, as these processes defy a direct observation. However, the application of the appropriate polymorph is of high importance. Quartz and chalcedony temperatures (Arnórsson, 1983; Fournier, 1977; Verma and Santoyo, 1997) differ by at least 30 K.

Long-term laboratory experiments has been conducted equilibrating two representative reservoir rock analogues from the study area under assumed reservoir conditions. The thorough description of these experiments is presented in Nitschke et al. (2017b). For the convenience of the reader the most important details are recapitulated in the following. A tonalite (50 % quartz, 25 % plagioclase, 10 % serizite, 10 % biotite, <5 % muscovite, <5 % chlorite) belonging to the North Patagonian Batholith and an andesite (40 % plagioclase, 30 % pyroxene, 10 % clay minerals, 10 % magnetite, 5 % chalcedony, 5 % K-feldspar, <5 % chlorite) of the Cura-Mallín formation were selected according to the findings of Held et al. (this issue). The rock samples were ground (<63 µm) and equilibrated in a time series (1, 2, 4, 6, 10, 20, 30, 45, 60, 90, 120, and 180 days) with pure H_2O at 140 °C in hermetic vessels. Every time step represents an autonomous experiment ensuring reproducibility of results. The analysis of the experimental fluids are displayed in

the *annex*. Despite equal reaction conditions, the experimental series clearly reveal two different SiO_2 concentration levels. The concentrations of these fluids exactly match the modeled equilibrium (SI = 0) with respect to quartz (fluids from andesite experiments) and chalcedony (fluids from tonalite experiments), respectively at 140 °C for these fluids (*Fig. 7.2*), including a pH correction for in-situ conditions (analogous to the procedure in *section 7.2.1*). We concluded that in this case, the specific rock composition controls the type of equilibrated polymorph.

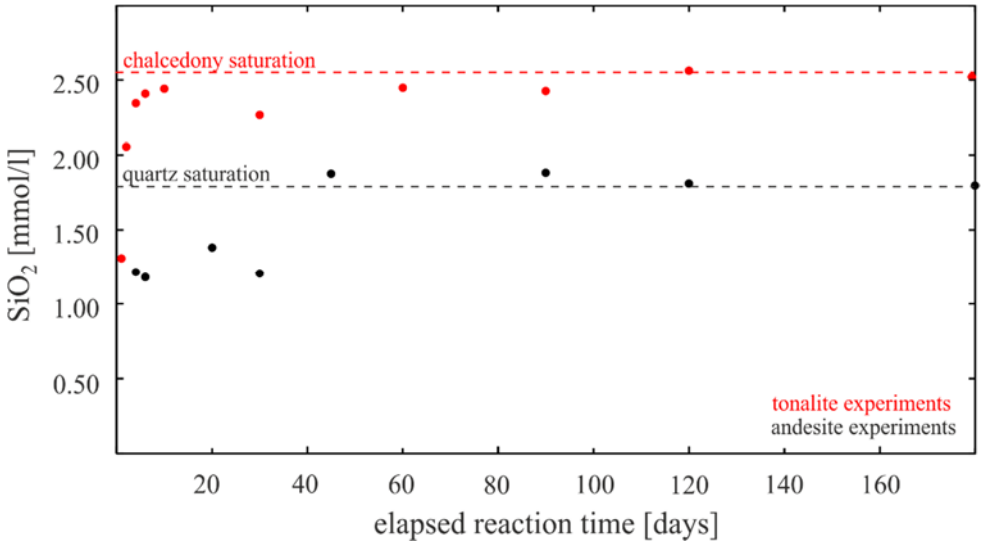

Fig. 7.2: Modeled solubilities of quartz (dotted black lines) and chalcedony (dotted red lines) at an experimental temperature of 140 °C and in-situ pH (corrected pH 6.9 for the tonalite fluids and pH 7.7 for the andesite fluids) reveal that tonalite fluids equilibrated with respect to chalcedony and andesite fluids with respect to quartz.

To transfer these implications from the laboratory experiments to temperature calculations for the natural spring conditions of the study area, a determination of the reservoir rock for each spring is required. Strontium isotope composition has proven to be a useful tool for reservoir rock recognition. From results of determinations of strontium isotopes in fluid and rock samples in the study area in combination with the spatial distribution of the springs considering the regional lithology change from north to south (Held et al., this issue), an interaction with plutonic reservoir rocks is assumed for the springs Car, Liq and Chi. Following the implications from the laboratory experiments, we assume saturation with respect to chalcedony for these springs. For all other springs (Liu, Poz, Men, Pal, Pan, Rin, RinCo, SL and Tra), for which strontium isotope data indicates a volcanic (Liu, Poz,

Pan, SL and Tra) or an intermediate (volcanic to plutonic) signature (Men, RinCo, Rin and Pal), we assume the fluid to originate from volcanic rocks and to be saturated with respect to quartz.

7.2.3 Effects of dilution and boiling

Since SiO_2 geothermometry relies on the solubility of a single mineral phase, this method is particularly prone to interference from changes in the amount of solvent. During fluid ascent from reservoir depth to spring discharge, the amount of solvent potentially changes due to dilution with superficial waters (increase of solvent) or due to boiling (decrease of solvent), both of which alter the SiO_2 concentration to one in dis-equilibrium with reservoir conditions.
A shift of the stable isotopes of water from the local meteoric water line towards heavier compositions would indicate boiling and associated steam-loss (Giggenbach, 1992). However, being aligned along the local meteoric water line (Held et al., 2017), a steam-loss related decrease in solvent can be ruled out. Thus, SiO_2-based temperatures can be considered to yield minimum values. However, dilution occurs pervasively in the study area and was documented for each spring (Held et al., this issue) by using chlorofluorocarbons as an anthropogenic tracer. Since it is only present in very young waters (infiltration before 1960), they are able to determined the proportion of modern waters in a discharged fluid from mixing models. Degrees of dilution range from 5 – 50 % depending on the spring. On that basis, we recalculated the undiluted in-situ SiO_2 concentrations by applying simple binary mixing of the fluids investigated and the water composition of Lake Villarrica, representing a possible surficial end-member. The corrected concentrations are then used to calculate SiO_2 temperatures.

7.2.4 Corrected SiO_2 temperatures

It has been shown that each of the considered interfering factors, the deviation of in-situ pH from measured pH at discharge (*section 7.2.1*), the different equilibrated SiO_2 polymorphs (*section 7.2.2*) and effects of dilution and boiling (*section 7.2.3*), alter the resulting SiO_2 temperatures by several tens of degrees Kelvin.

The adjusted equilibration temperature for the springs in the study area comprising all corrections are displayed in *Fig. 7.3*. The reservoir fluid fraction of each spring is plotted as a measure of dilution versus analysed SiO_2 concentrations. The equilibration temperature is indicated by polymorph- and pH-dependent mixing-isotherms. *Fig. 7.3a* illustrates the temperatures for Car, Chi and Liq for equilibration with chalcedony at pH 9. *Fig. 7.3b* depicts in-situ temperatures calculated based on

equilibration with quartz for the intermediate pH range (pH 8 and pH 8.5). *Fig. 7.3c* shows the adjusted temperatures for the springs with low in-situ pH values (pH 6.5 and 7.5).

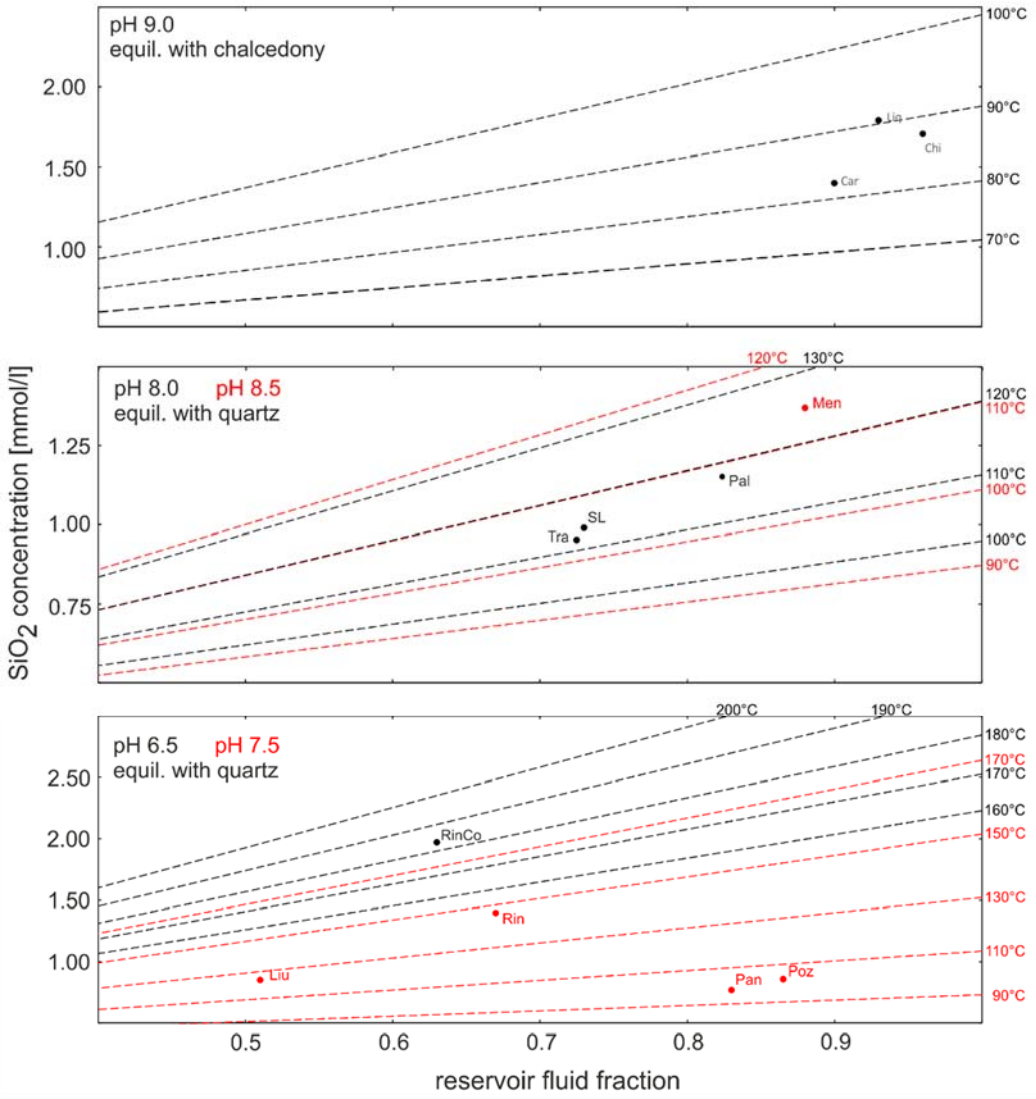

Fig. 7.3: Analysed SiO_2 concentrations plotted versus the reservoir fluid fraction (degree of dilution) for the Villarrica springs. The equilibration isotherms (dashed lines) modeled for in-situ pH and the equilibrated SiO_2 polymorph, display the reconstituted reservoir SiO_2 temperature for Car=84°C, Liq=91°C, Chi=87°C, Liu=125°C, Poz=104°C, Men=108°C, Pal=119°C, Pan=99°C, Rin=147°C, RinCo=184°C, SL=111°C and Tra=110°C.

7.3 Na-K Geothermometry

The in-situ temperature deduction from Na^+ and K^+ concentrations of a fluid is a (semi-) empirical method. In fact, the thermodynamic basis is still subject of discussion. There are studies proclaiming a simultaneous solubility equilibrium of albite and K-feldspar (e.g. Arnórsson, 2000a). Other authors describe a temperature dependent equilibrium of the cation substitution of Na- and K-feldspars (e.g. Can, 2002; Giggenbach, 1988) according to

$$K^+ + Albite \Leftrightarrow Na^+ + Orthoklase \qquad (E7.6)$$

However, geothermometer equations are typically established by correlating the cation ratios and equilibration temperatures of natural systems. Different input data sets, i.e. fluid compositions from geothermal systems from all over the world, representing different geological settings, different lithologies and different temperature niveaus, have led to a large number of different existing equations.

7.3.1 Effects of reservoir lithology on equilibrium

Previous studies already revealed diverging obtained temperatures when applying different Na-K geothermometer formulae (e.g. Arnórsson, 2000a). To evaluate these differences between existing Na-K geothermometers we balance a selection of commonly used equations for Na-K geothermometry (Arnórsson, 1983; Diaz-Gonzalez et al., 2008; Fournier, 1979; Giggenbach, 1988; Truesdell, 1975; Verma and Santoyo, 1997) for 140 °C (the reaction temperature of the experiments). Particularly in view of the logarithmic scale, *Fig. 7.4* perfectly illustrates the largely differing Na^+/K^+ ratios, which are required to satisfy the equations for the given temperature. Additionally to these theoretical ratios, the development of Na^+/K^+ ratios of the fluids derived from laboratory experiments are plotted versus elapsed reaction time.

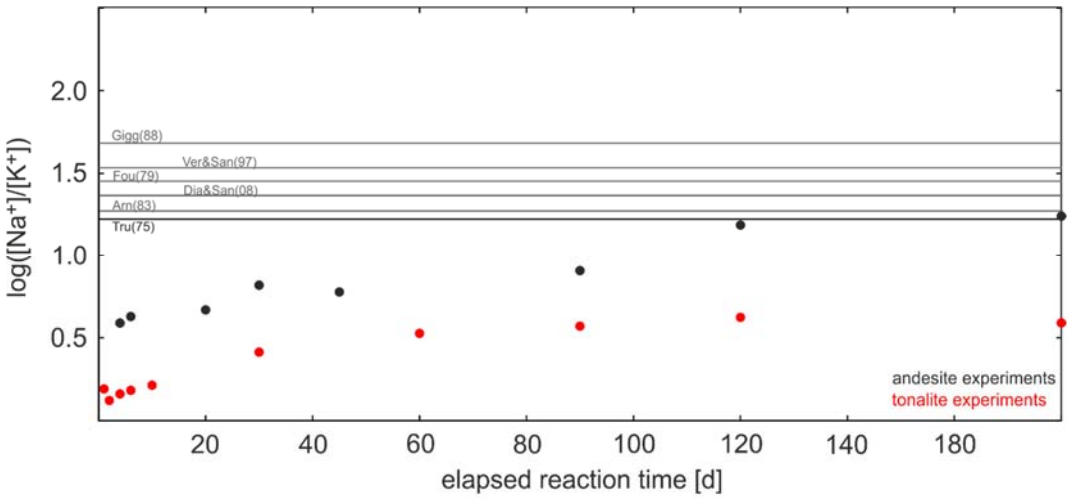

Fig. 7.4: Logarithmic plot of Na^+/K^+ ratios of experimental fluids (red: tonalite, black: andesite) versus elapsed reaction time, together with theoretical Na^+/K^+ ratios representing 140 °C according to Giggenbach (1988), Verma and Santoyo (1997), Fournier (1979), Diaz-Gonzalez et al. (2008), Arnórsson (1983) and Truesdell (1975).

After about 120 days both experimental series reach steady state conditions in terms of their Na^+/K^+ ratio. For the fluids derived from the andesite experiments, the reaction temperature of 140 °C is very well represented by the formulae from Truesdell (1975) and Arnórsson (1983). However, the fluids derived from the tonalite experiments are obviously not suitable for a temperature determination using an existing Na-K geothermometer equation, since the formula of Truesdell (1975) reflects the lowest documented Na^+/K^+ ratio. Most probably this strong deviation in terms of Na^+/K^+ ratio of the tonalite fluid can be explained by the absence of K-feldspar from the rock matrix, which prevents the cation substitution leading to a K^+ enrichment of the fluid.

According to our findings from the laboratory experiments and to the large number of differing Na^+/K^+ ratios reported previously, we conclude that there is not only one unique temperature dependent Na^+/K^+ equilibrium valid for all geothermal fluid, but obviously several, which are apparently strongly dependent upon reservoir lithology. On the other hand, there is a large number of different Na-K geothermometers, obviously accounting for this variety of different fluid types. Thus, the application of an inappropriate geothermometer to a fluid sample would result in incorrect temperature determination (e.g. Na-K temperature of andesite experiment, determined according to Giggenbach (1988) would yield 200 °C (ΔT = 60 K)). From that point of view, the application of the appropriate Na-K geothermometer, which represents the type of fluid genesis, is a crucial task.

7.3.2 Apropriate Na-K temperatures

To investigate the fluid equilibrium in terms of the Na^+/K^+ ratio, we suggest the evaluation of the stability of the feldspars governing the Na-K geothermometer. To illustrate this, measured fluid compositions (*annex*) are plotted versus the modeled phase stability of Na- and K-aluminosilicates (*Fig. 7.5*) using data from Delany and Lundeen (1991). This method facilitates the evaluation of the fluid composition in relation to the thermodynamic stability of albite and K-feldspar for the presumed range of reservoir temperatures. The Na^+/K^+ ratio reflected by their common field boundary is a necessary condition to satisfy the concurrent equilibrium of both feldspars. In doing so, we assume that both feldspars are present in depth, that they show pure end-member compositions and that the applied thermodynamic data reflects their solubility. The figure also contains theoretical Na^+/K^+ ratios, deduced from balancing existing geothermometer equations for the expected reservoir temperature range. It is shown, that the formula of Fournier (1979) exactly matches this necessary Na^+/K^+ ratio. Equations of other authors (e.g. Arnórsson (1983), Diaz-Gonzalez et al. (2008), Giggenbach (1988)) would here represent alternative states of Na^+/K^+ equilibrium. It is shown, that the fluids considered in this study can be divided into three groups in terms of Na^+/K^+ equilibrium. The springs Car, Men, Poz, Tra, Pal and SL obviously show a Na^+/K^+ ratio necessary for a concurrent thermodynamic equilibrium with both feldspars and geothermometer temperatures for them can therefore be calculated using the geothermometer of Fournier (1979).

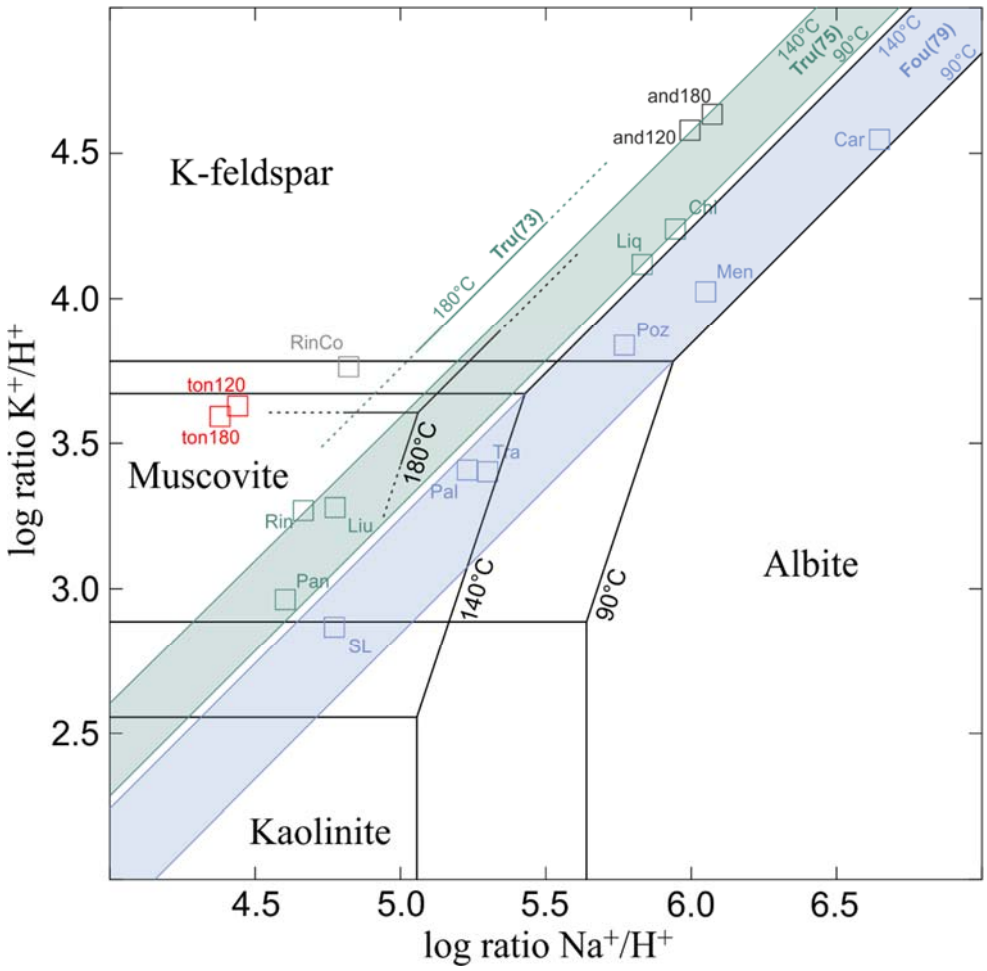

Fig. 7.5: Fluids from Villarrica springs and experimental fluids plotted versus modeled stability of aluminosilicates (at 90 °C, 140 °C and 180 °C), together with theoretical Na^+/K^+ ratios from geothermometer formulae of Fournier (1979) in blue color and from Truesdell (1975) in green color. The ratio deduced from Fournier (1979) exactly matches thermodynamic equilibria of albite and K-feldspar. The ratio from Truesdell (1975), whereas, reflects an equilibrium beeing more enriched in K^+. After allocation of spring fluids to the approriate geothermometer the following temperature are obtained: Car=92 °C, Liq=85 °C, Chi=93 °C, Liu=127 °C, Poz=114 °C, Men=113 °C, Pal=126 °C, Pan=107 °C, Rin=142 °C, SL=111 °C and Tra=111 °C.

For the samples Pan, Rin, Liu, Liq, Chi and the andesite experiment the formulation of Truesdell (1975) is the most applicable Na-K geothermometer. Being significantly enriched in K^+. For the tonalite experiments none of the common Na-K geothermometer reflects experimental reaction temperature, leading to strong temperature overestimation. The same applies to the spring RinCo. Na-K temperatures exceed in-situ temperature estimations of other geothermometers by far.

7.4 Discussion

In this study methods for the improvement of the two most widely used solute geothermometers are proposed. However the basic premises for these two differ.The SiO_2 geothermometer relies on solid, well-quantifiable thermodynamic solubility data, but is very prone to interferences from external influences. In contrast, the thermodynamic basis of Na-K geothermometers, being mostly developed by empirically correlating field data (temperature and contents), is rather poorly understood. Since a cation ratio is considered, the results are rather insensitive to secondary processes. Thus the improvements of the two geothermometers are differently implemented.

It is shown, that initial SiO_2 temperatures for the springs around the volcanoes and to the north of the study area (compare *Fig. 7.7*) are significantly lower than the corresponding Na-K temperatures (*Table 7.2*), whereas quartz based temperature estimations are relatively high for the samples Car, Chi and Liq. These springs (plutonic reservoir) differ from the northern springs in several aspects relating to geothermometry. The smallest dilutions in the study area (4 - 10 %), very high pH values at high discharge temperatures (pH >9.0 at 80 - 85 °C) and chalcedony being the equilibrated polymorph, these parameters can explain the initial overestimated SiO_2 temperatures. On the other hand the choice of quartz as the equilibrated polymorph, the relatively low pH and the large dilution (up to 50 %) explain the relatively low SiO_2 temperature estimates for the northerly springs.

The empirical nature of the Na-K geothermometers makes a comparable quantitative analysis and correction procedure impossible. However, it was shown that a large number of different Na-K geothermometers exist, leading to widely differing temperatures for one measured Na^+/K^+ ratio (*Table 7.1*). Thus, results may vary from significant underestimations to considerable overestimations, depending on which formula was chosen. Based on the evaluation of the stability of Na- and K-aluminosilicate phases, the suggested approach facilitates the determination of the type of Na^+/K^+ equilibrium of the fluid and the allocation of the appropriate application.

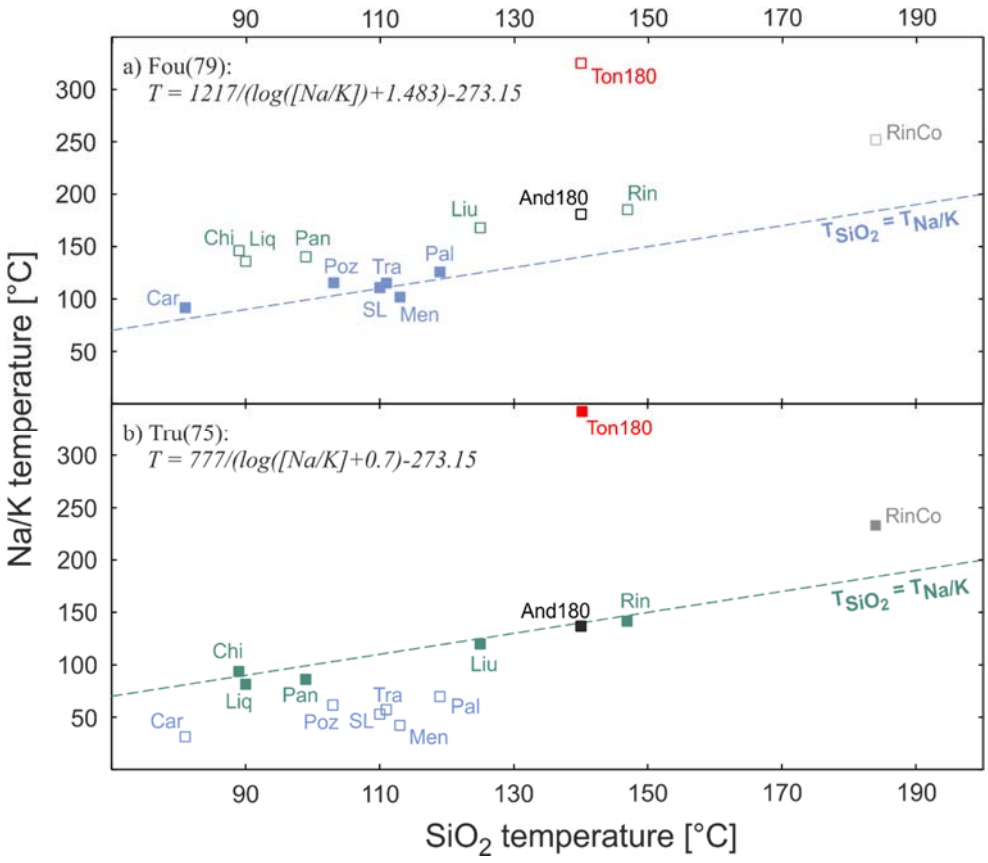

Fig. 7.6: Cross-plots of improved SiO_2 temperatures versus improved Na-K temperatures. a) Na-K temperatures calculated according to Fournier (1979). b) Na-K temperatures calculated according to Truesdell (1975).

The cross-plot of the improved temperature estimates for both geothermometers (*Fig. 7.6*) enables a reliability assessment for the improvement procedure. As expected, no correlation is found for the sample RinCon and for the fluid from the tonalite experiment, due to dis-equilibrium in the sense of Na-K geothermometers. The SiO_2 and Na-K temperatures for all other samples show very good correlations. Compared to initial geothermometer calculations, the temperatures obtained from the selected geothermometers strongly converge to results with very small deviations of $\Delta T \leq 10$ K (*Table 7.2*).

Table 7.2: Improved SiO_2 and Na-K temperatures reveal results of very good accordance compared to the largely varying initial reservoir temperature estimations for the Villarrica springs using formulae from [1](Arnórsson, 1983), [2](Can, 2002), [3](Diaz-Gonzalez et al., 2008), [4](Fournier, 1977), [5](Fournier, 1979), [6](Truesdell, 1975), [7](Giggenbach, 1988), [8](Nieva and Nieva, 1987), [9](Tonani, 1980), [10](Verma and Santoyo, 1997).

	initial			after refinement	
	SiO_2		Na/K	SiO_2	Na/K
[°C]	chalc 1, 4	qtz 1, 4, 10	2, 3, 5, 6, 7, 8, 9, 10		
Car	99/100	124/128	31 - 113	84	92
Chi	110/112	133/139	93 - 165	87	93
Liq	113/115	135/141	84 - 158	91	85
Liu	73/74	102/103	120 - 186	125	127
Poz	72/74	102/103	56 - 135	104	114
Men	98/99	123/127	42 - 123	108	113
Pal	87/88	114/117	70 - 146	119	126
Pan	68/69	98/99	86 - 159	99	107
Rin	99/100	124/128	142 - 202	147	142
RinCo	119/121	140/147	233 - 264	184	-
SL	80/81	108/110	53 - 132	111	111
Tra	79/80	107/109	57 - 135	110	111

To demonstrate the reliability of improvement we compare the findings of this study (*Table 7.2*) to temperatures derived from multicomponent geothermometry (Nitschke et al., 2017b) (*Table 7.1*). Both methods yield consistent results. This is especially the case for the springs in the volcanic part of the study area, for which the improved SiO_2 and Na-K temperatures both fall within the given range of the multicomponent approach. For the plutonic reservoir in the southern part (samples Car, Chi and Liq), results from this study and mean multicomponent temperatures still fit very well (<20 K). These deviations can be explained by the use of slightly differing in-situ pH values for these fluids of high pH (pH ≥9.0 at discharge). At that pH level, even marginal differences of modeled in-situ pH values affect SiO_2 solubility, and alter chalcedony temperatures.

Furthermore, temperatures (*Table 7.1*) deduced from oxygen isotope fractionation (Held et al., this issue) fit well (<25 K) for the springs from volcanic reservoirs, i.e. Liu, Poz, Pal, SL and Tra and in particular for the sparsely diluted springs Car, Chi and Liq (<8 K) in the plutonic domain. However, SiO_2 and Na-K temperature estimations for the springs Pan and in particular for Rin and RinCo differ to a greater extent. Since results from this study and from multicomponent geothermometry are

consistent, we consider the temperatures based on oxygen isotope fractionation to be the outliers. It is striking, that these fluids show higher total sulfate concentrations than the other springs. Therefore, assuming a dis-equilibrium of sulfate oxygen isotope fractionation and temperature due to interference from extraneous sulfate (e.g. dissolution during ascent) seems to be plausible. Furthermore, it is at least remarkable that high discrepancies occur for springs with high degrees of shallow dilution (Rin and RinCo).

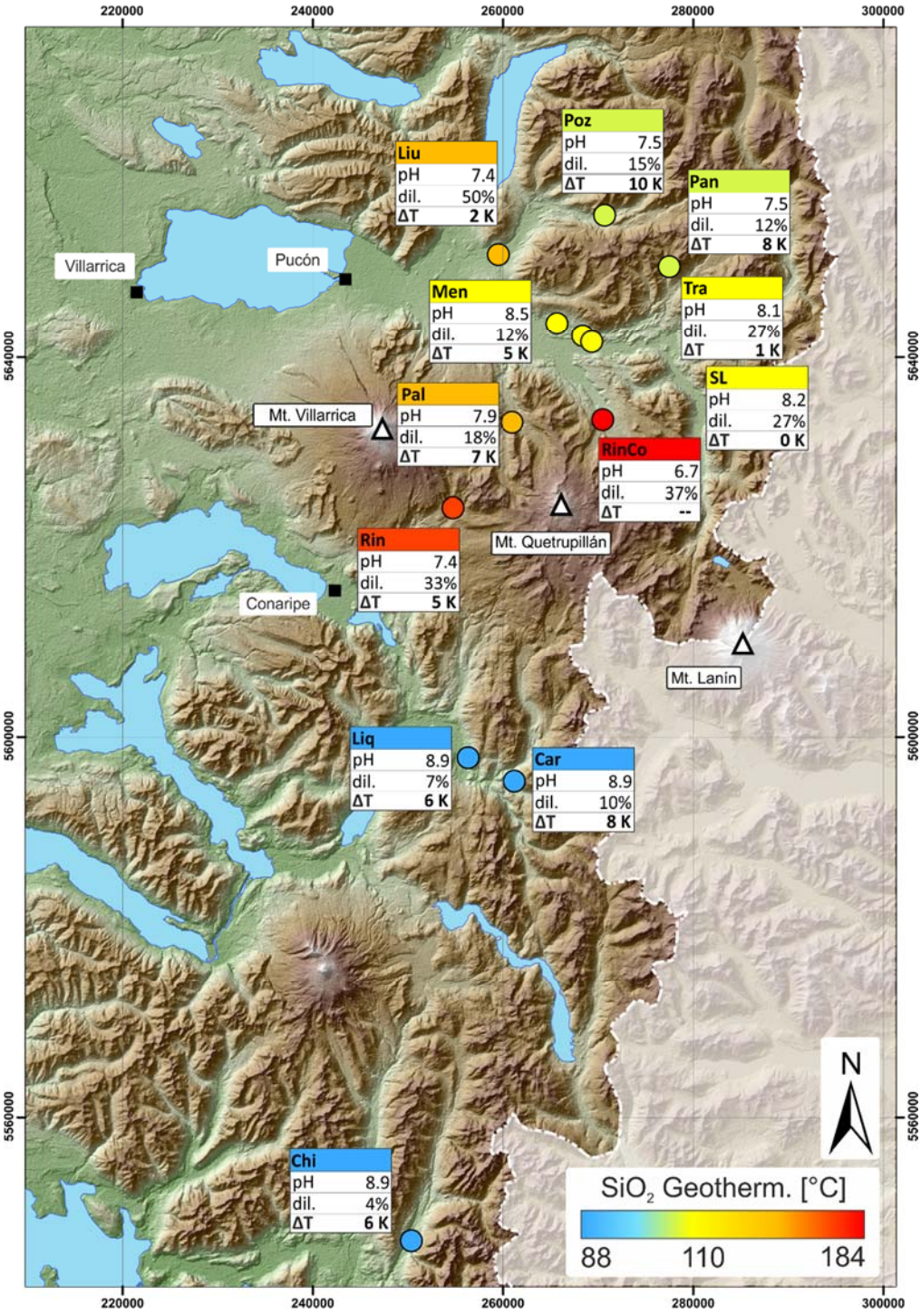

Fig. 7.7: Map of the study area showing calculated temperature distribution (ΔT of improved SiO_2 and Na-K geothermometers), the corrected in-situ pH and the degree of dilution for each spring.

The high reliability of the method presented here and the temperatures obtained is also reflected by the temperature distribution across the study area (*Fig. 7.7*). Supporting the estimations of Held et al. (this issue), the three southern springs within the plutonic reservoirs showing the coolest temperatures. It seems plausible, that the highest temperatures are obtained for the springs close to the volcanoes and decreasing temperatures for the springs with increasing distance to the north.
The high convergence of the results from multiple methods (SiO_2, Na-K, multicomponent geothermometry and oxygen isotope fractionation) also give an information about the meaning of the calculated temperatures. We conclude that the determined values most likely reflect the temperature conditions of a spatially extensive reservoir of near constant temperatures within the geothermal loop, where the residence time of the fluid is long enough to equilibrate with respect to all of the considered processes.

7.5 Conclusions

Highly varying, sometimes unreliable temperature estimations typically obtained by solute geothermometry were the motivation for this study on improving reservoir temperature determination. Previous investigations in the study area applying geothermometers came to inconsistent and partly contradictory results (Held et al., 2016a; Sánchez et al., 2013). Nitschke et al. (2017a) showed an extremely high scattering of results, with differences up to more than 200 K, applying different geothermometers to each fluid sample. Also in the run-up to the suggested methods of improvement, the results of initial calculation of in-situ temperatures using SiO_2 and Na-K geothermometers differ markedly.
In order to obtain consistent and reliable results, a methodology is proposed to improve the two geothermometer applications. For the solubility based SiO_2 geothermometer a quantitative improvement procedure is demonstrated. Numerical methods were used to correct solubility sensitive pH values measured at spring discharge on true in-situ conditions. For the first time, by using chlorofluorocarbon concentration data, effects from dilution with superficial waters, were corrected and thus, original in-situ SiO_2 concentrations were determined. Furthermore, results from laboratory experiments revealing different equilibration behavior depending upon reservoir rock mineralogy, were transferred to the natural system, specifying the equilibrated SiO_2 polymorph for each fluid.
The results of the laboratory experiments together with the evaluation of existing Na-K geothermometers lead to the conclusion that there is obviously a large variety of equilibrium states of fluids with respect to their Na^+/K^+ ratio. This requires the application of the appropriate Na-K geothermometer accounting for that individual

lithology dependent equilibrium. We demonstrate the evaluation of fluid type by modeling the stability of Na-K geothermometer governing feldspars (albite and K-feldspar) under in-situ conditions, facilitating the allocation of the appropriate geothermometer.
It is shown that the application of the suggested method of improvement results in reliable, well-constrained subsurface temperatures with estimations of SiO_2 and Na-K temperatures strongly converge from initially far more than 100 K to deviations of ≤10 K for all springs in the Villarrica area. Also a comparison to previous studies using the multicomponent geothermometer approach and oxygen isotope fractionation reveals very good agreement of temperatures predicted. Despite the high reliability of results demonstrated, the study is still a first step on the way to a systematical quantification and correction of geothermometer uncertanities. Since high sensitivity to site dependent parameters is expected, the findings have to be transferred and adapted to other sites. We plan to apply the methods to geothermal systems with different reservoir characteristics (temperature, reservoir rocks and fluid types) and to benchmark this methodology quantitatively. Therefore, the approach will be applied to a geothermal system, where additionally to natural discharging springs a borehole provides access to the reservoir for direct temperature measurements.

Acknowledgments

The study is part of a collaborative research project of Karlsruhe Institute of Technology (KIT) and the Andean Geothermal Center of Excellence (CEGA, Fondap-Conicyt 15090013). The authors appreciate the support of the BMBF-CONICYT International Scientific Collaborative Research Program (FKZ 01DN14033/ PCCI130025). Additional support from the Helmholtz portfolio project “Geoenergy” and the Helmholtz program “Renewable Energies”, topic “Geothermal Energy Systems”, is gratefully acknowledged. We also thank the EnBW Energie Baden-Württemberg AG for supporting geothermal research at the KIT.

Annex

*Main constituents (mg/L) of natural geothermal spring fluids in the study area and fluids from laboratory experiments equilibrating two reservoir rock analogues from the study area (originally presented in Held et al. (2017) and Nitschke et al. (2017b)). *total alkalinity: calculated from tritration (comprising HCO_3^- and CO_3^{2})*

	Sample	pH	Na	K	Ca	Mg	SiO_2	Al	Cl	SO_4	alkalinity*
Geothermal spring fluids	Carranco (Car)	8.9	180	2.54	4.42	0.02	84.0	0.09	34.1	59.1	40.0
	Chihuio (Chi)	8.9	109	4.17	13.0	0.03	102	0.04	13.9	189.9	72.3
	Liquine (Liq)	9.1	68.9	2.32	4.40	0.04	107	0.14	17.4	80.3	55.9
	Liucura (Liu)	7.9	65.6	3.47	11.0	1.57	51.0	0.05	35.3	76.3	58.0
	Los Pozones (Poz)	9.1	71.7	1.57	11.6	0.14	50.4	0.04	46.2	79.1	31.8
	Menetue (Men)	9.3	73.6	1.27	6.74	0.39	82.1	0.05	46.2	65.9	51.3
	Palguin (Pal)	8.7	67.2	1.82	5.61	0.48	67.9	0.07	21.1	79.4	45.4
	Panqui (Pan)	8.0	63.9	2.20	42.9	0.40	46.1	0.02	25.5	163.9	22.9
	Rincon (Pan)	7.6	68.1	4.57	12.0	1.91	83.9	0.09	20.9	114.5	67.1
	Rinconada (RinCo)	6.1	113	16.5	27.0	22.9	118	0.04	40.6	151.1	294.1
	San Luis (SL)	9.1	50.4	1.05	6.64	0.42	59.4	0.03	7.86	18.3	36.3
	Trancura (Tra)	9.0	50.4	1.12	7.86	0.42	57.1	0.12	8.08	1.5	33.0
Andesite experiments	AND_4	8.2	67.8	17.5	14.2	0.15	73.0	0.37	33.2	21.5	99.7
	AND_6	8.4	71.2	16.8	14.3	0.12	70.8	0.36	34.4	21.4	97.9
	AND_20	8.5	87.3	18.8	11.2	0.08	82.9	0.35	42.9	10.3	75.5
	AND_30	8.5	90.7	13.8	9.35	0.06	72.4	0.47	40.6	8.8	95.2
	AND_60	8.3	99.1	16.2	10.2	0.14	109	0.37	46.8	9.9	110
	AND_90	8.3	111	13.8	14.4	0.19	113	0.21	55.5	14.0	117
	AND_120	8.3	108	7.05	10.5	0.08	109	0.21	41.1	14.6	101
	AND_180	8.4	118	5.96	9.94	0.09	106	0.14	43.4	15.6	104
Tonalite experiments	TON_1	7.2	98.8	63.7	115	2.54	78.5	0.06	15.3	396	73.3
	TON_2	7.0	88.8	67.2	76.5	0.85	124	0.21	13.5	325	58.3
	TON_4	7.0	94.6	65.4	78.7	0.52	141	0.16	12.0	325	60.7
	TON_6	7.1	96.0	63.1	75.8	0.50	145	0.14	12.8	321	64.5
	TON_10	7.1	97.7	59.9	43.2	0.34	147	0.14	22.1	262	59.4
	TON_20	7.0	94.2	43.6	65.0	0.36	152	0.15	13.0	228	68.1
	TON_30	7.2	102	39.6	26.6	0.23	136	0.17	13.8	147	78.1
	TON_45	7.1	99.0	35.0	52.6	0.44	126	0.17	18.2	317	74.3
	TON_60	7.2	105	31.3	33.1	0.37	147	0.14	15.8	179	80.7
	TON_90	7.2	101	27.2	36.1	0.48	146	0.12	15.5	155	85.9
	TON_120	6.7	127	30.5	50.8	0.52	157	0.07	14.9	235	68.6
	TON_180	6.8	139	35.9	50.5	0.99	152	0.06	16.7	308	103

8 Conclusion and Outlook

For reaching the ambitious targets given by the International Energy Agency of a 2000 % growth of the worldwide produced geothermal energy until 2050 and thus, of contributing to 3.5 % of the world electricity production (IEA, 2011), the development of geothermal energy has to be strongly accelerated.
The often harsh chemistry of geothermal fluids is still one of the major obstacles for a fast development of effective geothermal energy utilization. Scaling formation and corrosion as results of highly mineralized fluids, still pose major engineering and operational challenges (Brown, 2011; Gunnarsson and Arnórsson, 2003). Beside this, exploration uncertainties, contributing to high prospecting and financial risks in early project stages, have to be reduced. One major goal exploring a geothermal system is the determination of reservoir temperatures. Therefore, solute geothermometers, which are often afflicted to large uncertainties, are commonly applied.
The study aimed to improve the process understanding and quantification of water-rock interaction and related dissolution and precipitation processes, as being the governing processes of geothermal fluid composition and scaling formation, and being basis for the evaluation of temperatures via geothermometers. The exact knowledge of the prevailing chemical system and the fluid composition in depth is of great importance. However, geothermal fluids, typically sampled at the surface, do not reflect in-situ conditions. Re-equilibration processes induced by changing physical parameters (depressurization, boiling, dilution, dissolution and precipitation) during ascent alter the chemical system. Even when a borehole provides direct access to the reservoir, samples taken at the wellhead may have already significantly changed (*chapter 5*). The goal of this work was to improve the understanding of this complex system and particularly to establish approaches to quantify the involved processes.

8.1 Major Findings and Outlook in the Field of Scaling Formation

The objectives of the first study (*chapter 5*) were to numerically investigate and quantify the thermo-hydraulic-chemical (THC) processes of geothermal single well operations. In a case study of investigating the GeneSys production test of well Gt1 Groß-Buchholz, Hanover, Germany, the successful application of a fully coupled reactive transport model was demonstrated. Due to the high brine salinity, the Pitzer ion interaction model was applied and its capability of adequately quantifying such systems could be displayed. A practical abstraction of the chemical

system together with an appropriate parameterization of ion pairs and triples enables a very good representation of reality.
The parameterization and its verification for the considered chemical system was done by comparison with solubility data from literature as well as by conducting laboratory experiments (*chapter 4.1*).
It was shown, that such models can quantify the complex interaction of temperature, flow, permeability and precipitation/dissolution. Doing so, a quantification of processes leading to changes in composition from reservoir fluid to wellhead samples is possible. In the presented study, the reservoir fluid composition with respect to the major components controlling scaling formation, was numerically determined. Only with this data, a realistic chemical boundary conditions in reservoir depth for further numeric evaluations can be set.
The concept of geothermal single well applications, foreseen for the establishment in existing boreholes, for instance in abandoned oil and gas wells, may be a low-risk concept compared to conventional doublet systems. However, the study reveals rather strong cooling effects on the produced brine by the descending fluid in the counterflow section. The model depicts the immediate increase of the temperature gradient in the production string right at the depth of the ending annulus. For cooling-induced scaling formation, the potential of solid accumulation is largest at this point. The approach has proven to be suitable for modeling the THC conditions causing the salt plug. The location of the salt plug and the total amounts of precipitated salts nearly perfectly match on-site observations.
The model can be used in future works for reliable determination of reservoir brine composition, assessment of scaling potential, for the prediction of solid accumulation rates as a function of produced volume, for the design of operation schemes for avoiding scaling and for the development of inhibition scenarios. The numerical reproduction of the complete clogging of the pipe needs considerations of additional chemico-physical processes (e.g. transport of solids, adhesion laws, etc.) and therefore requires further research and code adaptions. Precipitation of halite in this study was calculated based on its thermodynamic properties. This is usually done for fast precipitating minerals, for instance also for calcite. It reflects reality for these minerals very well, due to their quasi-instantaneous precipitation behavior. Other scaling forming minerals showing a kinetic behavior compared to the time discretization of such models. Thus, for future studies of other systems, investigating e.g. barite or silica scaling, a kinetic precipitation model must be considered.

8.2 Major Findings and Outlook in Geothermometry

Uncertainties of classical solute geothermometers are typically large. The application of different geothermometers to one sample not uncommonly leads to high variation of obtained temperatures, often > 100 K. The goal of the studies

regarding geothermometry (*chapter 6* and *chapter 7*) was to reduce the high uncertainties of reservoir temperature determination from fluid composition. Basic assumption of all existing solute geothermometers is the temperature-only control of chemical equilibrium of reservoir rocks and geothermal fluid. Different equilibria are considered: a) single mineral solubility (SiO_2) and b) equilibria of cation ratios (e.g. Na^+/K^+) or multiple mineral equilibria (multicomponent geothermometry).
Multicomponent geothermometry provides certain advantages compared to classical solute geothermometers. The performance assessment study (*chapter 6*) reveals that already in a first-step calculation without corrections from interfering processes, this method is significantly better constraint. Variations of results are within a range of 50 K. The statistical approach of considering a larger number of mineral equilibria, leads to a distribution of equilibration temperatures. This enables the identification of outliers. Dis-equilibrium of a single phase (e.g. supersaturated quartz due to chalcedony saturation) is less critical for the mean equilibration temperature. Being a solubility controlling parameter for the large majority of reservoir minerals, the pH of the fluid is a crucial and critical parameter to the same extend. The same applies to the aluminum concentration. As measured values for both parameters can differ significantly from in-situ conditions, an approach for the correction on conditions in depth was developed. Based on the equilibria assumption, the equilibration temperature spread was minimized, by variation of pH and aluminum concentration. Doing so, it is shown that well-constraint equilibration temperatures within a range of ≤ 25 K for the geothermal springs of the Villarrica area are obtained, fitting very well to the results from SiO_2 and Na-K temperatures (*chapter 7*).

Solute geothemometers are a standard method in geothermal exploration. They have been developed and applied for nearly six decades. Typically, geothermometer equations were obtained by correlating borehole temperature measurements with fluid compositions. In order to overcome the occurring large uncertainties of the method, numerous revised and improved correlations have been published. Commonly, these studies anticipate the causes for the inaccuracies rather in errors of data correlation and measurement errors of both, temperature and fluid composition. Therefore, method advances has been suggested mostly based on statistical improvements of data and correlations of new datasets, always assuming that interrelations are solely controlled by temperature. As this study (*chapter 7*) shows, this is a strongly simplified first-order model. Fluid equilibria within the reservoir are also highly sensitive to the type of reservoir rock. The SiO_2 concentration (equilibrated polymorph) as well as the Na^+/K^+ equilibrium are effected by the reservoir rock composition.
Secondary interfering factors like dilution and boiling, the role of the in-situ pH, re-equilibration processes and different SiO_2 concentrations controlling polymorphs are actually well known, but they are usually only qualitatively discussed in literature so

far. The aim of this study was the identification of interfering factors of the SiO_2 and Na-K geothermometers, representing the two most commonly used applications. It was demonstrated that SiO_2 geothermometers are very sensitive to dilution (and boiling), pH of the fluid and to the polymorph which controls saturation. Results from laboratory experiments, geochemical models and chlorofluorocarbon concentrations of the spring fluids enable an adaption of the data on in-situ conditions and facilitate a correction of SiO_2 temperatures.

The laboratory experiments together with the evaluation of existing Na-K geothermometers lead to the conclusion that there are obviously a number of fluid types in terms of Na-K geothermometry. However these fluids are apparently in a state of equilibrium, they show variations in their Na^+/K^+ ratio. This requires the application of the appropriate Na-K geothermometer accounting for that individual equilibrium. An approach is suggested, to model the stability of Na-K geothermometer governing feldspars (albite and K-feldspar) under in-situ conditions, which supports the allocation of the appropriate geothermometer equation.

As a results of the site-specific geothermometer evaluation, this study shows the correction of the two most important classical geothermometers for the medium enthalpy volcanic system in the Villarrica area. The obtained SiO_2 and Na-K temperatures fit very well to results from multicomponent geothermometry (*chapter 6*). The variation between both SiO_2 and Na-K temperatures converge from initially >> 100 K to significantly low deviations of ≤ 10 K.

This presented evaluation and correction approach is still very site-specific. In a next step, a site with a different temperature niveau and/or a different reservoir lithology has to be investigated. Beside of SiO_2 and Na-K methods, there are also a number of other geothermometer, which are worth considering for a similar correction procedure. Furthermore, a benchmarking of the method with reliable in-situ temperatures would increase confidence in results. A geothermal system, where a number of hot springs discharge and boreholes provide direct access to the reservoir (direct temperature measurements), would perfectly meet these requirements.

Appendix

A Formation of alternating layered Ba-Sr-sulfate and Pb-sulfide scaling in the geothermal plant of Soultz-sous-Forêts

This study has been published in Journal of Mineralogy and Geochemistry

NITSCHKE, F., SCHEIBER, J., KRAMAR, U. and NEUMANN, T. (2014): Formation of alternating layered Ba-Sr-sulfate and Pb-sulfide scaling in the geothermal plant of Soultz-sous-Forêts. J. Min.Geochem. 191/2, 145-156.

Abstract

Scaling formation in surface installations of geothermal power plants can substantially affect power production by impairing the heat transfer and reducing pipe diameters. In addition, the mineral deposits can incorporate naturally occurring radioactive nuclides into the crystal lattice during precipitation and have to be regarded as a potential hazard to health and environment. A profound understanding of formation mechanisms should facilitate the prevention of scaling in the future. Therefore fluid samples and scalings from the geothermal power plant at Soultz-sous-Forêts were investigated in detail. Fluid shows a total salinity (TDS) of 92 g/l and can be classified as Na-(Ca)-Cl-type. Considerations of the saturation state reveal a slight oversaturation with respect to barite ($BaSO_4$) and celestine ($SrSO_4$).
X-Ray diffraction measurements together with scanning electron microscopic observation reveal that the scalings consist of barite-celestine solid solution ($BaSrSO_4$) interlayered with very fine layers of galena (PbS). The mineralogical composition was confirmed by X-ray fluorescence analysis showing a bulk composition of Ba (31.7 – 34.6 %), Sr (10.8 – 12.1 %), Pb (6.2– 12.4 %) and S (13.1 – 14.5 %) for the sulfates, and Pb (66.6 %) and S (11.7 %) for the sulfidic part of the scalings. Other metals/metalloids like Sb (5.6 %), Cu (4.2 %), As (2.3 %) and Fe (2.0 %) were found to be present in minor amounts in the sulfides. Sulfur isotope studies show strong fractionation between the sulfate ($\delta^{34}S$ = +15‰) and sulfide ($\delta^{34}S$ = -12‰) phases. This indicates that bacterial sulfate reduction occurs, initiating sulfide precipitation from sulfate-rich fluids. The layered structure of the scalings can be correlated well with the operation state of the plant. Accordingly, sulfate layers precipitate under regular operation conditions, whereas sulfides formed during start and shut-off phases of the plant.

A 1 Introduction

The use of geothermal energy for power production is going to be a key technology within the energy mix of the future. Geothermal energy is able to supply baseload demands and features greatly flexible controllability. This is a decisive advantage compared to other renewable energy sources. Being on its way to an economic energy source, geothermal power production is still facing a number of challenges. One of these is the formation of scalings, where minerals precipitate from produced fluid and accumulate on the surfaces of the installations perfused by the fluid.

Depending on numerous factors like the type of reservoir rock, fluid origin and age as well as p-T conditions of the reservoir, geothermal fluids often show strongly elevated contents of dissolved minerals and an associated high potential of scaling (Eggeling et al., 2013; Huenges et al., 2004; Pauwels et al., 1993, 1993; Sanjuan et al., 2011). Values of Total Dissolved Solids (TDS) for the fluid of Soultz-sous-Forêts reach 100 g/l (Sanjuan et al., 2010). In consequence of decreasing p-T conditions of the ascending fluids, the dissolution properties of the fluid change. When the formation of a mineral phase is kinetically not inhibited, the fluid tends to produce scalings. After the initial formation of a nucleus, a crystal grows to a critical size and adheres to surfaces exposed to the fluid. With an ongoing feed of oversaturated fluid, crystal growth will continue (Bjornstad and Stamatakis, 2006).

In addition to the change of pressure and temperature, Testa et al. (1993) consider other factors provoking scaling. Therefore the change of solubility could be induced by the mixture of the fluid with incompatible water, especially in offshore oil projects, where sulfate-rich seawater is injected. Together with the usually high contents of alkaline earth elements of the formation water, this can cause corresponding sulfate scaling (Bjornstad and Stamatakis, 2006; Testa et al., 1993).

A common phenomenon is the microbially induced formation of scalings. Microbial sulfate reduction and the resulting H_2S production can provoke the formation of heavy metal sulfides (Schröder et al., 2007; Wolfgramm et al., 2009). Inagaki et al. (2002) consider extreme thermophilic bacteria to contribute to fast precipitation of siliceous scalings in Japanese geothermal projects. Wolfgramm et al. (2009) discuss further reasons for scaling formation. Especially for carbonate scaling, they considered CO_2 degasification of the fluid to be the main factor. Furthermore they also name variations of Eh-pH conditions of the fluid as well as electrochemical reactions.

In literature from both, geothermal projects and oil industry, five different classes of scalings are distinguished. Numerous examples describe carbonate scalings consisting of calcite, more or less dolomitic, but also of aragonite (Bjornstad and Stamatakis, 2006; Stahl et al., 2000; Wolfgramm et al., 2009). Subordinated to those, the occurrence of witherite, siderite (Bjornstad and Stamatakis, 2006) and malachite (Holl et al., 2003) has been observed. Furthermore, sulfates are common scalings. At this barite represents the most abundant mineral (Corsi, 1987; Holl et al., 2003;

Lebedev, 1972; Schmidt et al., 2000; Wolfgramm et al., 2009). Together with barite, celestine coprecipitates frequently (Bjornstad and Stamatakis, 2006; Schröder et al., 2007). Both minerals form a complete solid solution series. At some sites also gypsum was observed and at more elevated temperatures also anhydrite (Bjornstad and Stamatakis, 2006; Corsi, 1987). Sulfides represent another common scaling class, which shows great diversity. So galena was observed quite often, but also copper-, zinc-, iron- and antimony sulfides (Bjornstad and Stamatakis, 2006; Corsi, 1987; Holl et al., 2003; Schmidt et al., 2000). In addition, zero-valent metals were often found in association with sulfides. Beside of frequently appearing lead, also zinc, copper, iron and vanadium could be observed (Lebedev, 1972; Wolfgramm et al., 2009). Silicate scalings represent the last group. Here amorphous SiO_2, like opal, is the most abundant phase (Corsi, 1987).
Continuous precipitation of scaling will lead to a decline of the pipe diameters of the installation and could end up in obstruction of pipes. Impairing the contact of fluid and pipe walls in the heat exchanger, scalings act as insulators and decrease plants efficiency considerably. Furthermore, radionuclides incorporation in the crystal lattice of the precipitates is frequently observed in geothermal projects and in the oil industry as well (Schröder et al., 2007; Testa et al., 1993; Worden et al., 2000). In the geothermal plant of Soultz-sous-Forêts the radionuclides ^{226}Ra, ^{228}Ra and ^{210}Pb occur as coprecipitated components (Sanjuan et al., 2011).

A 2 The geothermal project Soultz-sous-Forêts

Soultz-sous-Forêts is located in north eastern France in the western part of the Upper Rhine Graben (URG). The regional stratigraphy of the URG can be roughly divided into three parts. A carboniferous fractured granitic basement is covered by Permian to Jurassic sediments, which are followed by the Tertiary graben filling (Schumacher, 2002).
The operation site was chosen due to a local high surface heat flow anomaly of close to 150 W/m^2 (Kohl et al., 2000) and the associated high thermal gradient, explained by free circulation cells reaching in the basement and convection of hot fluid within major faults (Pribnow and Schellschmidt, 2000). Since the geothermal project at Soultz-sous-Foret started in 1987, one exploration well (EPS1) and four geothermal wells (GPK1, GPK2, GPK3 and GPK4) were drilled. Having a depth of about 3600 m (GPK1) and over 5000 m (GPK2, GPK3 and GPK4), they reach into the fractured crystalline basement of the Rhine Graben. In 2008, the power plant unit with a net capacity of 1.5 MW_e was put into operation. At Soultz-sous-Forêts electricity is generated from an Enhanced Geothermal System (EGS). A natural geothermal fluid with a temperature of close to 200 ° C (Sanjuan et al., 2010) is produced from a fractured granitic reservoir. Heat of the produced fluid is withdrawn

in heat exchanger systems and transferred to the power generation unit by an organic fluid. The cooled fluid (around 70 ° C) is reinjected into the reservoir.
The reservoir rocks are well characterized by means of drilling and geophysical studies. From the top of the basement at around 1400 m (Hooijkaas et al., 2006) to the borehole bottom-most depth, three different granite types occur (Dezayes et al., 2005; Hooijkaas et al., 2006). Until a depth of roughly 3200 m, the reservoir rock consists of a porphyritic monzogranite. Although the top and the bottom of the monzogranite was exposed to hydrothermal alteration, the major part from 1570 to 2700 m depth is largely unaltered. Beneath 3200 m depth, Dezayes et al. (2005) describes a biotite- and amphibole-rich granite and below 4800 m a fine-grained two-mica granite is found. As Permian sediments are missing in the area of Soultz, the top of the granitic reservoir is directly overlain by the Buntsandstein, which contains baritic veins as a result of hydrothermal activity (Aquilina et al., 1997).
The geothermal fluid in the granitic reservoir is highly mineralized with TDS values of 90 g/l to 100 g/l and show a pH value of about 4.6 to 5.0, depending on degassing of CO_2 during sampling (Sanjuan et al., 2011; Vaute et al., 1998). The content of dissolved minerals is strongly dominated by Na and Cl. Also Ca, K, Mg, Sr, Li, Fe and SO_4 and Br show relevant concentrations for TDS. Recent measurements reveal a gas-liquid-ratio of 75 to 107 vol.-% (Sanjuan et al., 2011) with a gas phase consisting of around 85 vol.-% CO_2, 10.5 vol.-% N_2, and trace amounts of CH_4, H_2 and He (Sanjuan et al., 2011). Estimations based on geothermometer deliver fluid temperatures in the range of 220 °C to 240 °C, which is higher than measured bottom-hole temperature nearly 200 °C. These authors suggest that the Buntsandstein has an important influence on the fluid composition and propose the fluid to migrate from the graben center, where the Buntsandstein reaches greatest depth, towards the Soultz horst.
During production, scalings continuously precipitate in the surface installations particularly in the heat exchanger system and at the cold side of the power plant (Scheiber et al., 2012). These deposits were analyzed several times in previous studies. Different precipitation conditions (location of sampling within the installations, length of production periods before sampling) lead to a great variety of evaluated chemical and mineralogical compositions of scalings. Sanjuan et al. (2011) analyzed solid samples from the heat exchanger systems or preceded filters. In most of the samples solid solutions of barite and celestine (up to 60 mass-%) were found. Few samples show a presence of barite-celestine only in trace amounts. Likewise depending on sample, galena occurs as trace but also as major phase, whereas calcite, maghemite, chalcopyrite show trace to minor contents. Another study carried out by (Sanjuan et al., 2013), where scalings were sampled on the hot side of the plant, shows occurrence of abundant drilling grease and magnetite. Here, fragments of reservoir rock were represented by silicates like quartz, feldspars, illite, chlorite, muscovite and biotite. Contents of barite and celestine vary between trace and dominating amounts. Sulfides like galena, pyrite and sphalerite occur only in small

amounts (< 1 mass-%). In scalings, sampled from the separator, where fluid is depressurized, calcite is present in concentrations of up to around 15 mass-%.

A 3 Materials and Methods

A 3.1 Fluids

During the sampling for this study, borehole GPK2 was used for production, GPK1 and GPK3 for injection. GPK4 was not in operation**.** During production fluid temperature at the wellhead was around 160 ° C and between 70 ° to 75 ° C at the cold site of the plant.

Fluid was sampled five times over a period of two weeks at the warm site of the plant, where it enters the surface installations. The sampling started right after activation of the well for starting production in August 2011. For sampling the fluid was cooled to 25 ° C and pressure was relieved. Physico-chemical parameters were measured on site using a Mettler Toledo MP120 with an InLab®Expert Pro electrode for determination of pH value and temperature. The electrical conductivity was measured with a Jenway Conductivity Meter 4200. Aliquots of fluid samples were filtered (0.45 µm) and for the determination of the cations the pH was adjusted to a value between 1 and 2 by adding suprapure HNO_3 (65%).

The main cations (Na, K, Ca Mg, Si, Mn, Fe, Li and Al) were determined by the mean of inductively coupled plasma optical emission spectrometry (ICP-OES) using a Varian 715 ES. Due to the wide range of concentrations, it was necessary to measure the fluid differently diluted. For the quantification of Na and K, the fluid was diluted to 1:100. For all other elements mentioned above, the dilution was 1:20. Relative uncertainty of the measurements, derived from reproducibility of concentrations of standard solutions, is in the range of 5 %.

The determination of anions was conducted by ion chromatography (IC). Therefore a Dionex ICS 1000 was used. Due to high concentrations Cl was measured in a dilution of 1:2000. For the measurements of F, Br, NO_3, PO_4 and SO_4 the samples were diluted 1:200. Repeated analyses of reference solutions allow quantifications of measurement uncertainties, which vary from anion to anion (2.5 % for Cl, lower for other anions).

Trace elements were quantified by inductively coupled plasma mass spectrometry (ICP-MS) on a Thermo Fisher Scientific XSERIES II. Therefore the samples were diluted to 1:100. Elements in the range between Ti and As were measured in the collision cell mode to avoid impacts of argon interferences on these masses. Reference samples were reproduced with a relative deviation of 1 %.

To evaluate the saturation state of the fluid, average measured concentrations of Ba and Sr were compared to the solubility of barite and celestine. Therefore the values

were plotted together with published maximum solubility of barite (Templeton, 1960) and celestine (Davies and Collins, 1971; Reardon and Armstrong, 1987; Strübel, 1966) over the salinity of the fluid (equivalent NaCl fluid) and for relevant temperatures.

A 3.2 Scalings

During a shut-down period of the plant for revision, the heat exchanger system was opened and scalings were sampled on the 14th of September 2011. They were formed since the 22th of March 2011 when the heat exchanger system was cleaned for the last time. In this time the sytem was in operation with considerable volume of perfusing fluid from the 22th of March to the 2th of April and from the 6th of September to the 14th of September.
Most of the scalings show the habit of small platelets with only a few millimeter of thickness. The samples were washed in deionized water and subsequently dried at 40° C. For our study only minerals, which precipitated in the surface installations, were considered. Other components, such as reservoir rock fragments, were disregarded. Detailed description of samples and location of sampling can be found in *Table A1*.

Table A1: Description of scaling samples and location of sampling

Sample	Position of sampling
FORC	Filter prior to the heat exchanger
EVAPback	Entry of evaporator
EVAPfront	Exit of evaporator
PRE2back	Middle part of preheater 2
PRE2front	Exit of preheater 2
PRE1back	Middle part of preheater 1
PRE1front	Exit of preheater 1

The determination of scaling bulk chemical composition was carried out by energy-dispersive X-ray fluorescence (EDXRF). Therefore scaling platelets were grinded by hand in an agate mortar. 1 g of sample powder was measured with a TracorSpectrace 5000 in Spectrocups closed with 6 µm polypropylene as supporting film. Different kind of filters were applied in order to carry out accurate analytics for the elements of interest. For the light elements (S, Cl, K and Ca) an aluminum filter (0.100 mm of thickness) was used. Elements with X-ray energies in the intermediate range (K-Lines of Ti, Mn, Fe, Cu, Zn, Ga, As, Br, Rb, Sr and L-Lines of Pb) were

quantified by using a palladium filter (0.125 mm of thickness). For K□ energies of the heavy elements (Mo, Ag, Sb and Ba), a copper filter (0.600 mm of thickness) was used. Regarding the rhodium X-ray tube, measurement parameters were 17.5 W, 50 kV and 0.035 mA. Detection Unit was a Si(Li) semiconductor detector. Element concentrations were quantified with the software PyMca applying fundamental parameters. Due to the heavy element dominated matrix, measurement errors are dominated by matrix effects and are estimated to be ~10 % after matrix correction for the light elements and ~5 % for the heavier elements.

To obtain the mineralogical phases a powder X-ray diffraction (XRD) was carried out. As for the EDXRF, sample preparation was conducted analogously. The samples show a significant activity due to the incorporated radionuclides. Especially ground sample powder poses a threat when inhaling. Sample preparation (grinding, preparation of sample holder) was carried out with the utmost caution under the premise of reducing health hazards. Therefore a sample preparation of optimal quality was difficult to achieve. The samples were analyzed with a Bruker AXS D8 Advanced. A Cu-tube ($Cu_{K\alpha}$=1.5405 Å) was used operating at 30 kV and 35 mA. The measurements were carried out in an angular range of 5° to 70° with a step width of 0.01°. Measurement time was 0.5 s per step. For the identification reference data from the open source data base MinCryst (for galena and jordanite) and from the JCPDS-PDF-2, 2002 (for the solid solution of barite and celestine) were used.

Furthermore scalings were analyzed with a scanning electron microscope (SEM) with coupled energy-dispersive X-ray spectroscopy (EDX). This method yields information about the morphological structure of the samples as well as semi-quantitative information of phase composition and single grain composition. For studying the structure, cross sections of scalings were analyzed visually and by EDX spot analyses. Samples were coated with carbon and fixed on sample holder using conductive silver. For the measurements a FEI Quanta 650 FEG ESEM was used in high vacuum mode at 15 kV.

A 3.3 Sulfur Isotope Determination

To approach the mechanisms of precipitation, the sulfur isotopic composition of the scalings was determined. For considering the isotopic composition of possible sulfur sources of the scalings, also reservoir rock samples of the three different granite types occurring in the Soultz reservoir, and hydrothermal baritic veins of the Buntsandstein were analyzed. Sample description is documented in *Table A2*. For determination of $\delta^{34}S$ values, the isotopes ^{32}S and ^{34}S were measured by mass spectrometry using a coupled device arrangement of elemental analyzer (HEKAtech Euro EA) and mass spectrometer (GV Instruments IsoPrime).

Table A2: Description of reservoir rock samples

Sample	Depth [m]	Rock type
FRACFILL a	1204	Baritic vein (Buntsandstein)
FRACFILL b	1270	Baritic vein (Buntsandstein)
FRACFILL c	1270	Baritic vein (Buntsandstein)
GRNT 1775	1775	Monzogranite (Fazies I)
GRNT 2065	2065	Monzogranite (Fazies I)
GRNT 2680	2680	Monzogranite (Fazies II)
GRNT 3730	3730	Bt- and Am-rich granite
GRNT 4678	4678	Bt- and Am-rich granite
GRNT 4979	4979	Two-mica granite

For avoiding a mixed signal of sulfatic and sulfidic sulfur, these fractions were separated before measurements.

A.3.3.1 Separation of sulfur fractions of scaling

The scalings mainly consist of barite-celestine and galena. As galena is an acid volatile sulfide (AVS), it can be dissolved by using concentrated HCl (Zaback and Pratt, 1991). Whereas (Ba,Sr)SO_4 is virtually insoluble in HCl, it remained as residue in the separating agent representing the sulfatic sulfur fraction of the sample. For analysis it was recovered by centrifuging and filtering (0.45 µm) the solution.
Therefore powdered scalings were treated at 85 °C for two hours in a solution of 10 g of $SnCl_2$ dissolved in 100 ml of HCl (6 molar) under nitrogen atmosphere. During this treatment AVS were decomposed to H_2S according to equation (*EA.1*). Here $SnCl_2$ avoids a possible oxidation of the arising gas.

$$PbS + 2HCl \rightarrow H_2S + Pb^{2+} + 2Cl^- \qquad (EA.1)$$

H_2S is captured and led through a precipitating agent, which consists of 1500 ml of deionized water, 12.3 g $Cd(CH_3COO)_2$ (cadmium acetate) and 150 ml CH_3COOH (acetic acid). According to equation (2) the reduced sulfur precipitates as CdS.

$$H_2S + Cd(CH_3COO)_2 \rightarrow CdS + 2CH_3COOH \qquad (EA.2)$$

For recovery of reduced sulfur fraction, CdS was filtered off (0.45 µm). Both, the sulfidic as well as the sulfatic fraction were dried at 105 °C prior to measurements.

A.3.3.2 Separation of sulfur fractions from the reservoir rock and baritic veins

Samples of the granitic reservoir rock and hydrothermal baritic veins of the Buntsandstein formation were ground by using an agate disc mill. In order to extract beside of AVS also pyrite, which are both possible sulfidic components in the granite as well as in the baritic veins, suitable extraction procedure according to Canfield et al. (1986) was chosen. The principle is very similar to the above described procedure for the scaling samples. Sulfidic compounds were decomposed to H_2S and precipitated as CdS. As separating agent a $CrCl_2$ solution and concentrated HCl was used. The $CrCl_2$ solution was prepared by dissolution of 265 g of $CrCl_3$ x $6H_2O$ in 1000 ml deionized water. After adding 50 ml of concentrated HCl, the solution was led through a Jones reductor column filled with amalgamated Sn granulate (grain size 0.3 – 1.5 mm). During flow through Cr^{3+} is reduced to Cr^{2+}, as it is indicated by color change from dark green to light blue. 65 ml of the prepared solution were added to 35 ml of concentrated HCl. Separation and precipitation processes were carried out analogously to the separation of sulfur fractions of the scalings. As no measureable amount of sulfatic sulfur is contained in the granitic reservoir samples, only the extracted reduced sulfur was further processed. Due to the fact that barite and sulfides occur in the vein sample of the Buntsandstein (FRACFILL_a), both, a sulfatic and a sulfidic fraction were obtained. As sample FRACFILL_b and FRACFILL_c contain no sulfides, they were measured directly without any separation.

A 4 Results

A 4.1 Fluid Chemistry

The fluid composition is strongly dominated by Cl and Na (*Table A3*). Taking also the substantial amounts of Ca into account, the fluid can be classified to a Na-(Ca)-Cl-type. With a total salinity (TDS) of 92 g/l, the concentration of Na, Cl and Ca together covers more than 90 % of the dissolved load. With pH values shifting between 5.1 and 5.3, the system conditions are slightly acidic. As the pH value was measured on depressurized samples, effects of degassing (mainly CO_2) have to be taken into account. Therefore in-situ values of 4.6 to 4.8 are slightly lower (Sanjuan et al., 2011).

Beside of the above named ions, Br and SO_4 respectively K, Sr, L and Mg occur in substantial amounts. The concentrations of Si, B, Rb, Fe, Mn, Cs, and Ba are one order of magnitude lower. Further metal cations, including Pb, Sb and Cu, though participating in scaling formation, show concentrations only in the ppm range.

To evaluate the saturation state of the fluid published solubility data for barite and celestine were plotted and compared to measured Ba and Sr concentrations.

Table A3: Composition of geothermal fluids from Soultz-sous-Forets (nm = not measured; bdl = below detection limit)

Sample	Temperature [°C]	pH	Conductivity [mS]	Alkalinity [meq/l]	Cl [mg/l]	Br [mg/l]	SO_4 [mg/l]	F [mg/l]	NO_3 [mg/l]
Fluid 9.8.11	22.2	5.2	109.3	3.31	57900	238	201	3.30	bdl
Fluid 11.8.11	nm	5.3	134.5	3.15	58100	239	188	3.75	bdl
Fluid 13.8.11	nm	5.3	nm	2.89	58600	240	186	3.50	bdl
Fluid 19.8.11	26.6	5.1	129.6	2.85	59200	237	189	3.61	bdl
Fluid 24.8.11	31.1	5.1	116.7	2.85	59400	249	202	4.06	bdl

Sample	Na [mg/l]	Ca [mg/l]	K [mg/l]	Sr [mg/l]	Li [mg/l]	Mg [mg/l]	Si [mg/l]	B [mg/l]	Rb [mg/l]
Fluid 9.8.11	20600	7210	3270	472	148	116	95.0	37.1	25.9
Fluid 11.8.11	21300	7590	3460	479	149	120	98.0	37.6	26.4
Fluid 13.8.11	22200	7830	3590	478	152	122	100	37.9	26.4
Fluid 19.8.11	21100	7480	3430	475	157	127	102	37.4	26.2
Fluid 24.8.11	20200	7300	3350	474	153	127	100	37.8	26.3

Sample	Fe [mg/l]	Mn [mg/l]	Cs [mg/l]	Ba [mg/l]	As [mg/l]	Zn [mg/l]	Pb [µg/l]	Ni [µg/l]	Sb [µg/l]
Fluid 9.8.11	25.6	14.3	14.8	9.38	7.92	2.29	2610	364	167
Fluid 11.8.11	22.6	14.4	14.8	9.58	8.66	2.59	417	37.3	75.7
Fluid 13.8.11	22.3	14.7	15.0	11.9	8.51	2.30	324	19.2	65.1
Fluid 19.8.11	23.4	15.1	15.1	9.73	9.12	2.31	159	bdl	48.5
Fluid 24.8.11	23.9	15.2	15.2	10.6	9.25	2.32	102	bdl	56.2

Sample	Be [µg/l]	Ti [µg/l]	Cr [µg/l]	Mo [µg/l]	Cu [µg/l]	Cd [µg/Ll	Co [µg/l]	V [µg/l]	Ag [µg/l]
Fluid 9.8.11	35.3	23.9	16.2	14.6	bdl	10.1	8.90	7.70	0.60
Fluid 11.8.11	36.4	25.9	2.00	10.1	12.1	9.30	2.80	7.00	1.10
Fluid 13.8.11	35.7	26.0	1.30	9.20	11.6	8.50	2.70	6.40	1.00
Fluid 19.8.11	36.5	22.5	1.10	7.80	bdl	9.00	2.60	5.70	0.60
Fluid 24.8.11	35.6	24.7	1.10	7.10	bdl	8.60	2.60	5.70	0.60

Therefore the salinity of the Soultz fluid was converted to a NaCl-solution with equivalent concentration (1.55 mol/l). Results are displayed in *Fig. A1*. According to this, by applying the concentrations of Sr and Ba measured in this study, the fluid is slightly oversaturated with respect to celestine, but below saturation for barite.

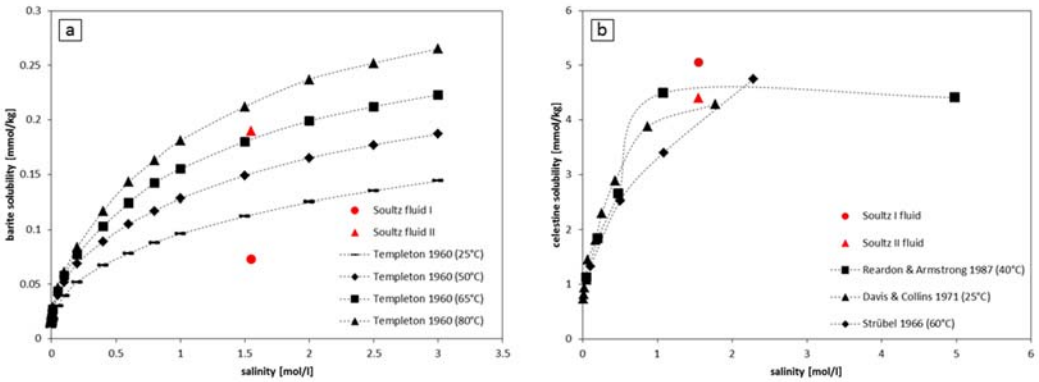

Figure A1: Saturation state of the Soultz fluid. Ba2+ (a) and Sr2+ (b) concentrations of Soultz fluid plotted in comparison to published solubility data of celestine and barite versus total salinity (NaCl). Soultz fluid I represents data measured in this study. Soultz fluid II represents data of Scheiber et al. (2013).

A 4.2 Mineralogy and Geochemistry of Scalings

Based on the results of X-ray diffraction measurements two types of scalings can be distinguished (*Fig. A2*). Sample PRE2front consists exclusively of sulfides. Galena is the dominating phase. Beside of galena, other sulfides, with peak positions close to galena, seem to be present. As a possible additional phase, jordanite may be contained.

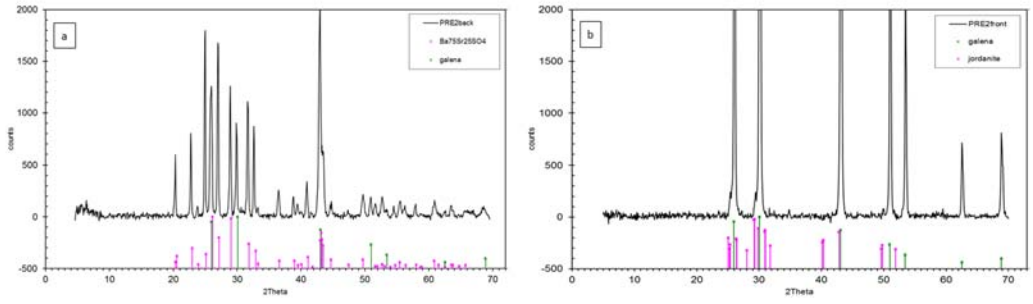

Figure A2: Diffraction patterns of samples PRE2back (a) and PRE2front (b) show two scaling types. PRE2back represents scalings consisting of barite-celestine solid solution and of galena, PRE2front shows dominating galena, stibnite and jordanite.

All other samples investigated (displayed by the example of PRE2back) contain only minor amounts of galena. A solid solution of barite and celestine could be investigated as the predominant phase. The peak shift suggests a strontium rich barite

with an approximated stoichiometry of $Ba_{75}Sr_{25}SO_4$. Neither pure barite nor pure celestine has been detected.

Results of EDXRF analyses support this assumption (*Table A4*). According to them all samples, except of PRE2front, show high concentrations of Ba (31.7 – 34.7 % mass fraction), Sr (10.8 – 12.1 % mass fraction) and S (11.7 – 13.8 % mass fraction). Lead is also present in substantial amounts (6.2 – 12.4 % mass fraction). Sample PRE2front mainly consists of Pb (66.6 % mass fraction) and S (14.5 % mass fraction). Also Sb, Fe, As and Cu are present in greater amounts. Together, these elements account for more than 10 % mass fraction in sample PRE2front, but are also present in trace amounts in all other samples. Furthermore a number of trace elements with widely varying concentrations were identified quantitatively (*Table A4*).

Table A4: Scaling bulk chemical composition

Sample	S [%]	Sr [%]	Ba [%]	Pb [%]	Sb [%]	As [%]	Cu [%]	Fe [%]	Ti [%]	Ca [%]	Cl [%]
FORC	13.4	11.9	34.6	6.2	1.2	0.8	0.1	4.9	0.1	1.2	0.4
EVAPfront	13.1	10.8	31.7	11.2	1.7	0.3	1.2	4.7	0.3	1.1	0.9
PRE2back	11.7	12.1	34.7	10.7	2.1	0.2	0.8	1.1	0.1	0.9	0.5
PRE2front	14.5	0.2	0.5	66.6	5.6	2.3	4.2	2.0	0.1	0.6	2.2
PRE1back	13.8	11.0	32.6	12.4	3.7	0.7	0.2	0.5	0.1	1.3	0.1
PRE1front	13.8	11.0	32.8	11.0	3.2	0.7	0.2	1.7	0.5	1.4	0.2

Sample	K [ppm]	Mn [ppm]	Zn [ppm]	Ga [ppm]	Mo [ppm]	Ag [ppm]	Br [ppm]	Rb [ppm]
FORC	1900	1430	483	361	489	87	88	63
EVAPfront	865	1730	1120	451	77	247	63	121
PRE2back	201	1400	350	383	144	195	54	141
PRE2front	2160	453	1720	1700	330	2310	756	331
PRE1back	700	1390	262	400	38	55	0	147
PRE1front	1740	1390	140	367	233	124	55	108

Coupled SEM/EDX analysis reveals, that apart from the main phases identified by XRD, also other phases are present in all samples. EDX spot analyses indicate that, beside of galena, numerous metals and metaloids (Sb, As, Fe, Cu, Zn and Al) are also bound in sulfidic compounds (polymetal sulfides).

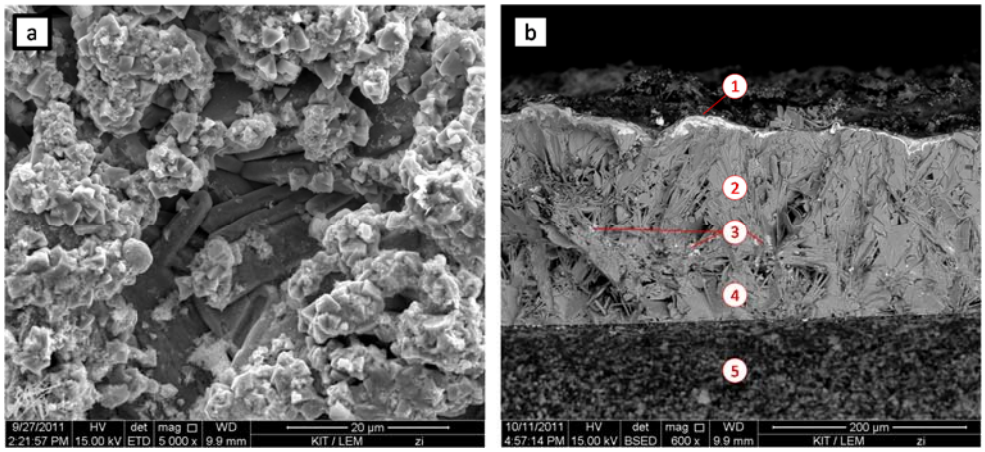

Figure A3: SEM image of sample EVAPback. a) Light grey, fine-grain tetrahedral and octahedral sulfides forms the upper layer which was originally oriented to the pipes wall. Below a layer of tabular dark grey sulfates occur (ETD mode). b) Cross section of sample EVAPback (from Scheiber et al. (2012)) (BSED mode) with a sulfidic layer as interface to the fluid (1). One rudimentary sulfidic layer (3) is embedded between two thicker sulfatic layers (2 and 4). Sulfidic interface to the pipes wall (described in a) is not visible, as it is covered by the sample holder (5).

Cross section analyses of the scalings performed by SEM/EDX show a layered structure parallel to the pipe surface, suggesting an alternating precipitation of two mineral phases. The first precipitate, which has originally faced the pipe wall, obviously consists of sulfides (*Fig. A3a*). Subsequently, two thicker (up to 100 µm) sulfatic layers were formed. In between those, a rudimentary sulfidic layer is embedded. Another layer of sulfides (~ 5 – 10 µm thick) represents the actual interface to the fluid (*Fig. A3b*).

A 4.3 Sulfur Isotopes

Results of the isotopic analysis of sulfur species of scaling and reservoir rocks are presented in *Table A5*. The values are displayed as the deviation from standard isotopic composition of the Canyon Diablo Troilit (CDT) in per mill [‰], which is used as reference material by convention.

It is found, that the isotopic composition of the scalings are highly variable. The $\delta^{34}S$ values for sulfatic sulfur range from 15.1 to 15.9 ‰. Whereas sulfidic sulfur is depleted in ^{34}S, showing values between -9.5 to -13.3 ‰. Consequently, relative isotopic fractionation within the two sulfur fractions of the scalings is in the range of -25.4 to -27.2 ‰. Sulfur species of rock vein mineralization show similar results. $\delta^{34}S$ values of barite vary between 15.9 and 18.8 ‰, whereas the associated sulfide shows a value of -12.3 ‰. Thus fractionation of sulfur species in the secondary mineralization of the Buntsandstein to those in the pipes of the plant with a value of

-28.2 ‰ is very similar. Unfortunately no measureable amount of sulfate could be extracted from the granitic reservoir rock. $\delta^{34}S$ values of the sulfidic components of the granites vary from 0.9 to -6.0 ‰.

Table A5: Table 5: Results of sulfur isotope analysis for scalings, baritic veins of the Buntsandstein and for the granitic reservoir

Svsteme	Sulfur fraction	Sample	$\delta^{34}S$ [‰]
scales	S(-II)	FORC	-9.5
		EVAPfront	-12.0
		PRE2back	-11.7
		PRE2front	-13.3
		PRE1back	-11.1
		PRE1front	-10.7
	S(VI)	FORC	15.9
		EVAPfront	15.2
		PRE2back	15.1
		PRE1back	15.4
		PRE1front	15.4
rock veins	S(-II)	FRACFILL a	-12.3
	S(VI)	FRACFILL a	15.9
		FRACFILL b	18.7
		FRACFILL c	18.8
granite	S(-II)	GRNT 1775	-0.3
		GRNT 2065	-6.0
		GRNT 2680	-2.1
		GRNT 3730	-0.7
		GRNT 4678	-1.9
		GRNT 4979	0.9

A 5 Discussion and Conclusion

Scalings at the Soultz geothermal plant consist mainly of Ba-Sr-sulfate solid solution and galena (and polymetal-sulfides respectively). Applying the measured concentrations of this study the fluid is oversaturated with respect to celestine but being below saturation for barite. For concentrations given by Scheiber et al. (2013) saturation seems to be exceeded for both phases at relevant temperatures of around 70 °C (*Fig. A1*). By converting the Soultz fluid to an equivalent NaCl-concentration, this method disregards the impact of the valence of dissolved cations on the solubility. Therefore the evaluated saturation state is a simplified estimation and yields rather high uncertainties. Furthermore solubility of barite decreases with

decreasing temperature, whereas the solubility of celestine increases. Consequently a solubility estimation concerning the solid solution $[Ba,Sr]SO_4$ is difficult, even more as thermodynamic equilibrium relations were not sufficiently understood (Felmy et al., 1993). Since the solid solution precipitates within the heat exchanger system, saturation must be exceeded in consequence of the heat withdrawal. But the sulfide phases were obviously formed due to other mechanisms. In accordance to our results, literature data shows an occurrence of sulfate-rich fluids being completely depleted in sulfidic anions (Sanjuan et al., 2011). Shifting redox conditions are a prerequisite for precipitating sulfides. However, as a reduced sulfur species in the fluid was never measured so far, an overall redox change in the fluids may be excluded. Thus being not component of the initially produced fluid, sulfidic species have to be formed within the surface installation. A possible mechanism is sulfate reduction. In general two reduction processes are conceivable: on one side, the thermochemical sulfate reduction (TSR), on the other side, the bacterial sulfate reduction (BSR).

By considering the isotope fractionation between precipitated sulfate and sulfide, the sulfur isotopic composition of the system is a useful indicator for identifying these mechanisms (Bechtel et al., 1998; Habicht and Canfield, 2001; Rees, 1973; Thode et al., 1961). TSR is well known from deep oil reservoirs. Sulfate is reduced in a reaction with reactive organic matter. The accompanied sulfur isotope fractionation results in isotopic lighter sulfides compared to the original isotopic composition of the sulfate. $\delta^{34}S$ fractionation for naturally occurring TSR processes results usually in very low values of -3 ‰ to -7 ‰ or even below (Krouse, 1977; Machel et al., 1995). In laboratory experiments fractionations of up to 20 ‰ were found (Machel et al., 1995). Although sulfides resulting from TSR display highest fractionation at lower temperature limit between 80 °C to 180 °C (Cross et al., 2004), which would correspond to temperatures in the surface installations of Soultz, reaction kinetics of up to geological timeframes of several 100 000 of years (Cross et al., 2004; Machel et al., 1995) are too slow for scaling formation.

Sulfides, which result from BSR, typically show a sulfur isotopic composition that is 15 ‰ to 30 ‰ lighter than the original sulfate (Coleman et al., 1985; Machel et al., 1995): If intermediate products like thiosulfates and polysulfides are involved, fractionations of up to 65 ‰ can occur (Machel et al., 1995).

$\delta^{34}S$ values of sulfates and sulfides of the scalings investigated differ significantly with an average fractionation of 26 ‰ (*Table A5*). The high fractionation values strongly indicate a microbial reduction of the sulfate and therefore a biogenic formation of sulfides in the scalings. A prerequisite for this process is the presence of an electron donor (Bechtel et al., 1998; Kemp and Thode, 1968). Scheiber et al. (2012) found indication for this by detecting (SEM-analysis) organic matter on scaling samples of Soultz-sous-Forêts.

The very similar isotopic composition of the sulfate of the produced fluid (Sanjuan et al. (2010) give $\delta^{34}S$ values of 12.6 to 17.4 ‰ for the dissolved sulfate) and of the

scalings (15.1 to 15.9 ‰), but also the complete depletion of dissolved sulfidic sulfur, leads to the conclusion, that the dissolved sulfate of the fluid is the predominant source of sulfate for the scalings.

Since virtually no fractionation effects are expected for the sulfate precipitation process (Tuttle et al., 2009), isotopic compositions of sulfate dissolved in the fluid and sulfate of the scalings reflect a direct sulfate phase precipitation from oversaturated fluid. Whereas reduced sulfur is formed by microbial sulfate reduction. High metal concentrations in the fluid initiate immediate precipitation of the reduced sulfur species as metal sulfides in consequence of a local exceeding of solubility. This direct local removal of sulfide anions from the fluid by instant precipitation could explain the fact that reduced sulfur was never detected in the geothermal fluid of Soultz.

SEM/EDX-analysis of scaling cross section show a fine laminated structure. Both surfaces of the sample, the original interface to the pipe wall and the one oriented to the fluid, consist of sulfide layers (*Fig. A3a* and *Fig. A3b*). A third, more rudimentary sulfidic layer is embedded in between two comparative thick internal sulfate layers. This layering suggests that sulfate and sulfide were not formed at the same time, but rather separately, driven by a cyclic activity of bacteria. Activity fluctuation can be caused by oxygen entry in the system, since sulfate reducers are active in anaerobic environments only (Bottrel H.S. et al., 2000; Rudnicki et al., 2001; Stetter et al., 1990), but also by the absence of organic matter as electron donor. In the case of Soultz it is more likely the temperature, which limits the microbial activity. During regular production temperatures in most parts of the plant exceed the upper temperature limit of sulfate reducers by far. Even for the activity of hyperthermophilic bacteria, temperatures are too high (Burggraf et al., 1990; Elsgaard et al., 1994; Machel, 2001; Stetter et al., 1990)**.** As the scalings were formed during two production periods, the sequence, quantity and thickness of scaling layers correlate well with the operation state of the plant. Accordingly, the two thicker sulfate layers should have been precipitated under regular operation conditions. On the other hand, sulfides are rather formed during the start and shut-off phases of production, when temperatures are not too high for microbial activity.

Conclusively, a plausible formation mechanism for the scaling can be described as follows: The precipitation of barite-celestine solid solution from an oversaturated fluid occurs during regular production conditions due to the heat withdrawal. The sulfides rather precipitate during start and shut-off phases of the plant, when temperatures for the activity of sulfate reducers are suitable.

Acknowledgements

This work has been carried out with financial support of EnBW. GEIE enables the access to fluid and solid samples and all necessary data. The authors are kindly thankful for the enlightening discussions with Dr. Albert Genter (GEIE), Dr. Thomas Kölbel (EnBW), and Prof. Thomas Kohl (KIT). Many thanks are owed to Dr. Jörg-Detlef Eckhardt and Dipl.-Min. Jens Glowacky from MPA Karlsruhe for facilitating the XRD measurements and their support. Equally, many thanks to Dipl.-Ing. Volker Zibat from Laboratory for Electron Microscopy (LEM) for carrying out the SEM analyses.

B References

Aquilina, L., Ladouche, B., Doerflinger, N., Seidel, J.L., Bakalowicz, M., Dupuy, C., Le Strat, P., 2002. Origin, evolution and residence time of saline thermal fluids (Balaruc springs, southern France): implications for fluid transfer across the continental shelf. Chemical Geology (192), 1–21.

Aquilina, L., Pauwels, H., Genter, A., Fouillac, C., 1997. Water-rock interaction processes in the Triassic sandstone and the granitic basement of the Rhine Graben: Geochemical investigation of a geothermal reservoir. Geochimica et Cosmochimica Acta (61), 4281–4295.

Arnórsson, S., 1983. Chemical Equilibria in Icelandic Geothermal Systems-Implications for Chemical Geothermometry Investigations. Geothermics 12, 119–128.

Arnórsson, S., 2000a. Isotopic and Chemical Techniques in Geothermal Exploration, Development and Use. International Atomic Energy Agency, Vienna.

Arnórsson, S., 2000b. The Quartz- and Na/K Geothermometers. I. New Thermodynamic Calibration, Proceedings World Geothermal Congress 2000, Kyushu - Tohoku, Japan. May 28 - June 10.

Arnórsson, S., Sigurdsson, S., Svavarsson, H., 1982. The chemistry of geothermal waters in Iceland. I. Calculation of aqueous speciation from 0° to 370°C. Geochimica et Cosmochimica Acta 46 (9), 1513–1532.

Bächler, D., Kohl, T., 2005. Coupled thermal-hydraulic-chemical modelling of enhanced geothermal systems. Geophysical Journal International 161 (2), 533–548.

Bear, J., 1972. Dynamics of Fluids in Porous Media. Dover Publications Inc., New York.

Bechtel, A., Pervaz, M., Püttmann, W., 1998. Role of organic matter and sulphate-reducing bacteria for metal sulphide precipitation in the Bahloul Formation at the Bou Grine Zn/Pb deposit (Tunisia). Chemical Geology 144 (1-2), 1–21.

Beerepoot, M., 2011. Technology Roadmap: Geothermal Heat and Power. International Energy Agency, 52 pp. Accessed 30 March 2016.

Bertani, R., 2015. Geothermal Power Generation in the World 2010-2014 Update Report. Proceeding: World Geothermal Congress, Melbourne, Australia.

Bethke, C.M., 2008. Geochemical and Biogeochemical Reaction Modeling Second Edition, 565 pp.

Bjornstad, T., Stamatakis, B., 2006. Mechanisms of mineral scaling in oil and geothermal wells studied in laboratory experiments by nuclear techniques. Czechoslovak Journal of Physics, 405–415.

BMUB, 2016. Klimaschutzplan 2050 - Klimaschutzpolitische Grundsätze und Ziele der Bundesregierung, 91 pp.

Bödvarsson, G., 1960. Exploration and Exploitation of natural heat in Iceland. Bulletin of Volcanology 23, 241–250.

Bottrel H.S., Monster, J., Tellam J.H., Lloyd J.W., Fisher Q.J., Newton R.J., 2000. Controls on bacterial sulphate reduction in a dual porosity aquifer system: the Lincolnshire Limestone aquifer, England. Chemical Geology (169), 461–470.

Bretherton, F.P., Bryan, K., Woodes, J.D., 1990. Climate Change: The IPCC Scientific Assessment, New York, USA.

Brown, K., 2011. Thermodynamics and kinetics of silica scaling. International Workshop on Mineral Scaling, Manila, Philippines.

Brown, K., 2013. Mineral Scaling in Geothermal Power Production: Geothermal Training Programm. United Nations University, Reykjavik, Island.

Burggraf, S., Jannasch H.W., Nicolaus, B., Stetter, K.O., 1990. Archaeoglobus profundus sp. nov., Represents a New Species within the Sulfate-reducing Archaebacteria. Systematic and Applied Microbiology 13 (1), 24–28.

Can, I., 2002. A new improved Na/K geothermometer by artificial neural networks. Geothermics 31 (6), 751–760.

Canfield, D.E., Raiswell, R., Westrich, J.T., Reaves, C.M., Berner, R.A., 1986. The use of chromium reduction in the analysis of reduced inorganic sulfur in sediments and shales. Chemical Geology 54 (1-2), 149–155.

Coleman, M.L., Berner, R.A., Durand, B., Meadows, P.S., Eglington, G., 1985. Geochemistry of Diagenetic Non-Silicate Minerals Kinetic Considerations. Mathematical and Physical Sciences 315 (1531), 39–56.

Corsi, R., 1987. Scaling and corrosion in geothermal equipment: Problems and preventive measures. Geothermics 15, 839–856.

Crabtree, M., Eslinger, D., Fletcher, P., Miller, M., Johnson, A., King, G., 1999. Fighting Scale-Removal and Prevention. Oilfield Review 11 (2), 30–45.

Cross, M.M., Manning, D.A., Bottrell, S.H., Worden, R.H., 2004. Thermochemical sulphate reduction (TSR): Experimental determination of reaction kinetics and implications of the observed reaction rates for petroleum reservoirs. Organic Geochemistry 35 (4), 393–404.

Crubash, U., Meehl, G.A., 2001. Projections of Future Climate Change: Climate Change 2001: The Scientific Basis. Contribution of Working Group I to the Third Assessment Report of the Intergovernmental Panel on Climate Change, New York, USA., 58 pp. Accessed 8 June 2017.

D'Amore, F., Gianelli, G., Corazza, E., 1994. The geothermal area of El Pilar-Casanay, state of Sucre, Venezuela. Geochemical exploration and model. Geothermics (23), 283–304.

Davies, C.W., 1962. Ion association. Butterworths, Washington.

Davies, J.P., Davies, D.K., 1999. Stress-Dependent Permeability: Characterization and Modeling, SPE Annual Technical Conference and Exhibition, Houston, Texas, USA. 1999.

Davies, J.W., Collins, A.G., 1971. Solubility of Barium and Strontium Sulfates in Strong Electrolyte Solutions. Environmental Science & Technology 5 (10).

Debye, P., Hückel, E., 1923. Zur Theorie der Elektrolyte: Gefrierpunktserniedrigung und verwandte Erscheinungen. Physikalische Zeitschrift 24 (11), 185–206.

Delany, J.M., Lundeen, S.R., 1991. The LLNL thermochemical data base -- revised data and file format for the EQ3/6 package.

Dezayes, C., Genter, A., Hooijkaas, G.R., 2005. Deep-Seated Geology and Fracture System of the EGS Soultz Reservoir (France) based on Recent 5km Depth Boreholes, World Geothermal Congress, Antalya, Turkey. 24-29 April.

Diaz-Gonzalez, L., Santoyo, E., Reyes-Reyes, J., 2008. Tres nuevos geotermómetros mejorados de Na/K usando herramientas computacionales y geoquimiométricas: aplicación a la predicción de temperaturas de sistemas geotérmicos. Revista Mexicana de Ciencias Geológicas 25 (3), 465–482.

Eggeling, L., Genter, A., Kölbel, T., Münch, W., 2013. Impact of natural radionuclides on geothermal exploitation in the Upper Rhine Graben. Geothermics 47, 80–88.

Ellis, A.J., 1970. Quantitative interpretation of chemical characteristics of hydrothermal systems. Geothermics 2, 516–528.

Elsgaard, L., Isaksen, F., Jørgensen B.B., Alayse, A.-M., Jannasch H.W., 1994. Microbial sulfate reduction in deep-sea sediments at the Guaymas Basin hydrothermal vent area: Influence of temperature and substrates. Geochimica et Cosmochimica Acta 58, 3335–3343.

Felmy, A.R., Raj, D., Moore, D.A., 1993. The solubility of (Ba,Sr)SO4 precipitates: Thermodynamic equilibrium and reaction path analysis. Geochimica et Cosmochimica Acta 57 (4345-4363).

Field, C.B., Barros, V.R., Dokken, D.J., Mach, K.J., Mastrandrea, M.D., Bilir, T.E., Chatterjee, M., Ebi, K.L., Estrada, Y.O., Genova, R.C., Girma, B., Kissel, E.S., Levy, A.N., MacCracken, S., Mastrandrea, P.R., White, L.L., 2014. Climate Change 2014: Impacts, Adaptation, and Vulnerability. Part A: Global and Sectoral Aspects. Contribution of Working Group II to the Fifth Assessment Report of the Intergovernmental Panel on Climate Change, New York, USA.

Filiz, S., Tarcan, G., Gemici, U., 2000. Geochemistry of the Germencik Ggeothermal Fields, Turkey. Worls Geothermal Congress, Kyushu-Tohoku, Japan.

Fouillac, C., Michard, G., 1981. Sodium/lithium ratio in water applied to geothermometry of geothermal reservoirs. Geothermics 10 (1), 55–70.

Fournier, R.O., 1977. Chemical geothermometers and mixing models for geothermal systems. Geothermics 5, 41–50.

Fournier, R.O., 1979. A Revised Equation for the Na/K Geothermometer. Geothermal Resources Council Transactions 3, 221–224.

Fournier, R.O., 1991. Water geothermometers applied to geothermal energy, in: D'Amore, F. (Ed.), Applications of Geochemistry in Geothermal Reservoir Development. UNITAR, Rome, Italy.

Fournier, R.O., Potter, R.W., 1979. Magnesium Correction to the Na-K-Ca Chemical Geothermometer. Geochimica et Cosmochimica Acta 43, 1543–1550.

Fournier, R.O., Potter, R.W., 1982. Revised and expanded silica (quartz) geothermometer. Geothermal Resource Council Bulletin (11), 3–12.

Fournier, R.O., Rowe, J.J., 1966. Estimation of underground temperatuires from the silica content of water from hot springs and wet-steam wells. American Journal of Science (264), 685–697.

Fournier, R.O., Truesdell, A.H., 1973. An empirical Na-K-Ca geothermometer for natural waters. Geochimica et Cosmochimica Acta 37 (5), 1255–1275.

Francke, H., Kraume, M., Saadat, A., 2013. Thermal–Hydraulic Measurements and Modelling of the Brine Circuit in a Geothermal Well. Environmental Earth Sciences 70 (8), 3481–3495.

Franco, A., Vaccaro, M., 2013. On the Use of Heat Pipe Principle for the Exploitation of Medium–Low Temperature Geothermal Resources. Applied Thermal Engineering 59 (1-2), 189–199.

Frigo, D.M., Jackson, L.A., Doran, S.M., Trompert, R.A., 2000. Chemical Inhibition of Halite Scaling in Topsides Equipment, International Symposium on Oilfield Scale, Aberdeen, United Kingdom. 2000.

Galoppi, G., Biliotti, D., Ferrara, G., Carnevale, E.A., Ferrari, L., 2015. Feasibility Study of a Geothermal Power Plant with a Double-Pipe Heat Exchanger. Energy Procedia 81, 193–204.

Giggenbach, W.F., 1988. Geothermal solute equilibria. Derivation of Na-K-Mg-Ca geoindicators. Geochimica et Cosmochimica Acta 52, 2749–2765.

Giggenbach, W.F., 1992. Isotopic shifts in waters from geothermal and volcanic systems along convergent plate boundaries and their origin. Earth and Planetary Science Letters 113, 495–510.

Giggenbach, W.F., Goguel, R.L., 1989. Collection and analysis of geothermal and volcanic water and gas discharges, 4th Edition ed. Petone, New Zealand.

Gislason, S.R., Heaney, P.J., Veblen, D.R., Livi, K., 1993. The difference between the solubilitiy of quartz and chalcedony: the cause? Chemical Geology 107, 363–366.

GISTEMP, 2017. GISS Surface Temperature Analysis (GISTEMP). NASA Goddard Institute for Space Studies.

Greenberg, J.P., Møller, N., 1989. The Prediction of Mineral Solubilities in Natural Waters: A Chemical Equilibrium Model for the Na-K-Ca-Cl-SO_4-H_2O System to High Concentration from 0 to 250°C. Geochimica et Cosmochimica Acta 53 (10), 2503–2518.

Guan, H., Keatch, R., Benson, C., Grainger, N., Morris, L., 2008. Mechanistic Study of Chemicals Providing Improved Halite Inhibition, SPE International Oilfield Scale Conference, Aberdeen, United Kingdom. 2008.

Gunnarsson, I., Arnórsson, S., 2003. Silica scaling: The main obstacle in efficient use of high-temperature geothermal fluids. International Geothermal Conference, Reykjavik, Iceland.

Gunnarsson, I., Arnórsson, S., 2005. Impact of silica scaling on the efficiency of heat extraction from high-temperature geothermal fluids. Geothermics 34 (3), 320–329.

Habicht, K.S., Canfield, D.E., 2001. Isotope fractionation by sulfate-reducing natural populations and the isotopic composition of sulfide in marine sediments. Geol 29 (6), 555.

Hansen, J., Ruedy, R., Sato, M., Lo, K., 2010. Global Surface Temperature Change. Rev. Geophys. 48 (4), 644.

Harvey, C., Beardsmore, G., Moeck, I., Rüter, H., 2016. Geothermal Exploration: Global Strategies and Applications. IGA Academy Books, Bochum, Germany.

Harvie, C.E., Møller, N., Weare, J.H., 1984. The prediction of mineral solubilities in natural waters: The Na-K-Mg-Ca-H-Cl-SO4-OH-HCO3-CO3-CO2-H2O system to high ionic strengths at 25°C. Geochimica et Cosmochimica Acta 48 (4), 723–751.

Hasan, A.R., Kabir, C.S., 2012. Wellbore Heat-Transfer Modeling and Applications. Journal of Petroleum Science and Engineering 86-87, 127–136.

Hedenquist, J.W., 1991. Boiling and dilution in the shallow portion of the Waiotapu geothermal system, New Zealand. Geochim. Cosmochim. Acta (55), 2753–2765.

Held, S., Nitschke, F., Schill, E., Morata, D., Eiche, E., Kohl, T., 2017. Hydrochemistry of the hot spring fluids of the Villarrica geothermal system in the Andes of Southern Chile. Geothermal Research Council Transactions 41.

Held, S., Nitschke, F. Schill, E., Schneider, J., Morata, D., Neumann, T., Kohl, T., this issue. Geochemical characterization of the geothermal system at the Villarrica Volcano, Southern Chile; Part 1: Impacts of Lithology on the geothermal reservoir. Geothermics.

Held, S., Schill, E., Pavez, M., Diaz, D., Morata, D., Kohl, T., 2015. Tectonic control of the geothermal system at Mt. Villarrica - Insights from geophysical and geochemical surveys, in: , Chilean Geological Conference 2015, La Serena, Chile.

Held, S., Schill, E., Pavez, M., Diaz, D., Morata, D., Kohl, T., 2016a. Effects of major fault zones on geothermal reservoirs – a case study at Villarrica Volcano, Southern Chile, in: , Proceeding European Geothermal Congress 2016, Strasbourg.

Held, S., Schill, E., Pavez, M., Díaz, D., Muñoz, G., Morata, D., Kohl, T., 2016b. Resistivity distribution from mid-crustal conductor to near-surface across the 1200 km long Liquiñe-Ofqui Fault System, southern Chile. Geophys. J. Int. 207 (3), 1387–1400.

Helgeson, H.C., Garrels R.M., Mackenzie, F. T., 1969. Evaluation of irreversible reactions in geochemical processes involving minerals and aqueous solutions: II. Applications. Geochim. Cosmochim. Acta 33, 455–481.

Hesshaus, A., Houben, G., Kringel, R., 2013. Halite Clogging in a Deep Geothermal Well – Geochemical and Isotopic Characterization of Salt Origin. Physics and Chemistry of the Earth, Parts A/B/C 64, 127–139.

Holl, H.G., Hurter, S., Saadat, A., Köhler, S., Wolfgramm, M., Zimmermann, G., Trautwein, U., Winter, H., Legarth, B., Huenges, E., 2003. First hand experience in a second hand borehole: Hydraulic experiments and scaling in the geothermal well Groß Schönebeck after reopening. International Geothermal Conference, Reykjavik, Iceland.

Hooijkaas, G.R., Genter, A., Dezayes, C., 2006. Deep-seated geology of the granite intrusions at the Soultz EGS site based on data from 5km-deep boreholes. Geothermics 35 (5-6), 484–506.

Hückel, E., 1925. Zur Theorie konzentrierter wässriger Lösungen starker Elektrolyte. Physikalische Zeitschrift 26.

Huenges, E., Holl, H.G., Legarth, B., Zimmermann, G., Saadat, A., 2004. The Stimulation of a Sedimantary Geothermal Reservoir in the Northern German Basin: Case Study Groß Schönebeck. Twenty-Ninth Workshop on Geothermal Reservoir Engineering, Stanford, California. January 26-28.

IEA, 2011. Technology Roadmap: Geothermal Heat and Power. IEA, International Energy Agency, Paris, France, 52 pp.

Inagaki, F., Sakihama, Y., Inoue, A., Kato, C., Horikoshi, K., 2002. Molecular phylogenetic analyses of reverse-transcribed bacterial rRNA obtained from deep-sea cold seep sediments. Environmental Microbiology 4 (5), 177–286.

Jung, R., Orzol, J., Jatho, R., Kehrer, P., Tischner, T., 2005. The Genesys-Project: Extraction of Geothermal Heat from Tight Sediments, Thirthies Workshop on Geothernal Reservoir Engineering, Stanford University, California, USA. 2005.

Kan, A., Tomson, M., 2012. Scale Prediction for oil and gas production. SPE Journal 17 (2), 362–378.

Karakuş, H., Şimşek, Ş., 2013. Tracing deep thermal water circulation systems in the E–W trending Büyük Menderes Graben, western Turkey. Journal of Volcanology and Geothermal Research 252, 38–52.

Karingithi, C.W., Arnórsson, S., Grönvold, K., 2010. Processes controlling aquifer fluid compositions in the Olkaria geothermal system, Kenya. Journal of Volcanology and Geothermal Research 196 (1-2), 57–76.

Kemp, A., Thode, H., 1968. The mechanism of the bacterial reduction of sulphate and of sulphite from isotope fractionation studies. Geochimica et Cosmochimica Acta 32 (71-91).

Kharaka, Y.K., Mariner, R.H., 1989. Chemical Geothermometers and Their Application to Formation Waters from Sedimentary Basins, in: Naeser, N., McCulloh, T.H. (Eds.), Thermal History of Sedimentary Basins. Methods and Case Histories. Springer Verlag, New York.

Kleinitz, W., Dietzsch, G., Köhler, M., 2003. Halite Scale Formation in Gas-Producing Wells. Chemical Engineering Research and Design 81 (3), 352–358.

Kohl, T., Bächler, D., Rybach, L., 2000. Steps towards a comprehensive thermo-hydraulic analysis of the HDR test site Soultz-sous-Forêts. World Geothermal Congress, Kyushu-Tohoku, Japann.

Kohl, T., Brenni, R., Eugster, W., 2002. System Performance of a Deep Borehole Heat Exchanger. Geothermics 31 (6), 687–708.

Krouse, H., 1977. Sulfur isotope studies and their role in petroleum exploration. Journal of Geochemical Exploration 7, 189–211.

Lebedev, L.M., 1972. Minerals of contemporary hydrotherms of Cheleken. Geochemistry International 9, 485–504.

Li, J., Lin, Y., Gmehling, J., 2005. gE Model for Single- and Mixed-Solvent Electrolyte Systems. 3. Prediction of Salt Solubilities in Aqueous Electrolyte Systems. Industrial & Engineering Chemistry Research 44 (5), 1602–1609.

Machel, H.G., 2001. Bacterial and thermochemical sulfate reduction in diagenetic settings – old and new insights. Sedimentary Geology 140, 143–175.

Machel, H.G., Krouse, H., Sassen, R., 1995. Products and distinguishing criteria of bacterial and thermochemical sulfate reduction. Applied Geochemistry 10, 373–389.

MacQuarrie, K.T., Mayer, K.U., 2005. Reactive transport modeling in fractured rock: A state-of-the-science review. Earth-Science Reviews 72 (3-4), 189–227.

Mahon, W., 1966. Silica in hot water discharged from drillholes at Wairakei, New Zealand. New Zealand Journal of Science (9), 135–144.

McGuinness, M.J., 2014. Correct Energy Conservation in Geothermal Wellbore Simulation. Geothermics 51, 429–433.

Meller, C., Bremer, J., Ankit, K., Baur, S., Bergfeldt, T., Blum, P., Canic, T., Eiche, E., Gaucher, E., Hagenmeyer, V., Heberling, F., Held, S., Herfurth, S., Isele, J., Kling, T., Kuhn, D., Mayer, D., Müller, B., Nestler, B., Neumann, T., Nitschke, F., Nothstein, A., Nusiaputra, Y., Orywall, P., Peters, M., Sahara, D., Schäfer, T., Schill, E., Schilling, F., Schröder, E., Selzer, M., Stoll, M., Wiemer, H.-J., Wolf, S., Zimmermann, M., Kohl, T., 2016. Integrated research as key to the development of a sustainable geothermal energy technology. Energy Technology (5), 1–44.

Merkel, B., Planer-Friedrich, B., 2009. Grundwasserchemie: Praxisorientierter Leitfaden zur numerischen Modellierung von Beschaffenheit, Kontamination und Sanierung. Springer, New York.

Michard, G., 1990. Behaviour of major elements and some trace elements (Li, Rb, Cs, Sr, Fe, Mn, W, F) in deep hot waters from granitic areas. Chemical Geology 89 (1-2), 117–134.

Morey, G.W., Fournier, R.O., Rowe, J.J., 1962. The solubility of quartz in water in the temperature interval from 29°C to 300°C. Geochimica et Cosmochimica Acta 26 (10), 1029–1043.

Mroczek, E.K., Stewart, M.K., Scott, B.J., 2003. Chemistry of the Rotorua Geothermal Field Part 2: Discharging Wells - update of chemical and isotopic composition and comparison with historic data. Institute of Geological & Nuclear Science, 49 pp.

Mundhenk, N., Huttenloch, P., Sanjuan, B., Kohl, T., Steger, H., Zorn, R., 2013. Corrosion and scaling as interrelated phenomena in an operating geothermal power plant. Corrosion Science 70, 17–28.

Mutlu, H., 1998. Chemical geothermometry and fluid–mineral equilibria for the Ömer–Gecek thermal waters, Afyon area, Turkey. Journal of Volcanology and Geothermal Research (80), 303–321.

Nieva, D., Nieva, R., 1987. Developments in geothermal energy in Mexico—part twelve. A cationic geothermometer for prospecting of geothermal resources. Heat Recovery Systems and CHP 7 (3), 243–258.

Nitschke, F., Held, S., Himmelsbach, T., Kohl, T., 2017. THC simulation of halite scaling in deep geothermal single well production. Geothermics 65, 234–243.

Nitschke, F., Held, S., Mundhenk, N., Villalon, I., Kohl, T., Neumann T., 2015. Reactivity of Chilean Reservoir Rocks and the Use of Geochemical Tools for Reservoir Characterization. Proceedings: European Geothermal Workshop, Straßbourg, France.

Nitschke, F., Held, S., Villalon, I., Mundhenk, N., Kohl, T., Neumann T., 2016. Geochemical Reservoir Exploration and Temperature Determination at the Mt. Villarrica Geothermal System, Chile. Proceedings: European Geothermal Congress, Straßbourg, France.

Nitschke, F., Held, S., Villalon, I., Neumann, T., Kohl, T., 2017a. In-situ Temperature Determination at the Villarrica Geothermal System, Southern Chile: Implications from Laboratory Experiments for Geothermometry, in: , 42nd Workshop on Geothermal Reservoir Engineering, Stanford, California.

Nitschke, F., Held, S., Villalon, I., Neumann, T., Kohl, T., 2017b. Assessment of Performance and Parameter Sensitivity of Multicomponent Geothermometry applied to a Medium Enthalpy Geothermal System. Geothermal Energy 5 (12).

Nitschke, F., Scheiber, J., Kramar, U., Neumann, T., 2014. Formation of alternating layered Ba-Sr-sulfate and Pb-sulfide scaling in the geothermal plant of Soultz-sous-Forêts. Journal of Mineralogy and Geochemistry 191 (2), 145–156.

Orzol, J., Jung, R., Jatho, R., Tischner, T., Kehrer P., 2005. The GeneSys-Project: Extraction of Geothermal Heat from Tight Sediments, World Geothermal Congress, Antalya, Turkey. 2005.

Palmer, C.D., Ohly, S.R., Smith, R.W., Neupane, G., McLing, T., Manson, E., 2014. Mineral Selection for Multicomponent Equilibrium Geothermometry. Geothermal Research Council Transactions 38.

Pang, Z.-H., Reed, M.H., 1998. Theoretical chemical thermometry on geothermal waters: Problems and methods. Geochim. Cosmochim. Acta 62 (6).

Parkhurst, D.L., Appelo, C., 2013. Description of Input for PHREEQC Version 3—A Computer Program for Speciation, Batch-Reaction, One-Dimensional Transport, and Inverse Geochemical Calculations, 519 pp.

Parkhurst, D.L., Thorstenson, D.C., Plummer, L.N., 1980. PHREEQE : a computer program for geochemical calculations: Water-Resources Investigations Report 80-96. U.S. Geological Survey, Water Resources Division,

Pauwels, H., Fouillac, C., Fouillac, A.-M., 1993. Chemistry and isotopes of deep geothermal saline fluids in the Upper Rhine Graben: Origin of compounds and water-rock interaction. Geochimica et Cosmochimica Acta 57, 2737–2749.

Peiffer, L., Wanner, C., Spycher, N., Sonnenthal, E.L., Kennedy, B.M., Iovenitti, J., 2014. Optimized multicomponent vs. classical geothermometry: Insights from modeling studies at the Dixie Valley geothermal area. Geothermics 51, 154–169.

Pepin, J., Person, M., Phillips, F., Kelley, S., Timmons, S., Owens, L., Witcher, J., Gable, C., 2015. Deep fluid circulation within crystalline basement rocks and the role of hydrologic windows in the formation of the Truth or Consequences, New Mexico low-temperature geothermal system. Geofluids 15 (1-2), 139–160.

Pérez-Zárate, D., Santoyo, E., Guevara, M., Torres-Alvarado, I.S., Peiffer, L., Martínez-Frías, J., 2015. Geochemometric modeling and geothermal experiments of Water/Rock Interaction for the study of alkali-feldspars dissolution. Applied Thermal Engineering 75, 1244–1261.

Pitzer, K.S., 1973. Thermodynamics of Electrolytes. I. Theoretical Basis and General Equations. Journal of Physical Chemistry 77 (2), 268–277.

Pitzer, K.S., 1991. Ion Interaction Approach: Theory and Data Correlation: Chapter 3 of Activity Coefficients in Electrolyte Solutions. CRC Press, Boca Raton, Florida.

Pitzer, K.S., Mayorga, G., 1973. Thermodynamics of Electrolytes. II. Activity and Osmotic Coefficients for Strong Electrolytes with one or both Ions Univalent. Journal of Physical Chemistry 77 (19), 2300–2308.

Powell, T., Cumming, W., 2010. Spreadsheets for Geothermal Water and Gas Geochemistry, in: , Thirty-Fifth Workshop on Geothermal Reservoir Engineering, Stanford, California.

Pribnow, D., Schellschmidt, R., 2000. Thermal tracking of upper crustal fluid flow in the Rhine graben. Geophysical Research Letters 27 (13), 1957–1960.

Pruess, K., Oldenburg C., Moridis G., 2012. TOUGH2 User's Guide, Version 2.1.

Raymond, J., Williams-Jones, A.E., Clark, J.R., 2005. Mineralization associated with scale and altered rock and pipe fragments from the Berlín geothermal field, El Salvador; implications for metal transport in natural systems. Journal of Volcanology and Geothermal Research 145 (1-2), 81–96.

Reardon, E.J., Armstrong, D.K., 1987. Celestine (SrSO4) solubility in water, seawater and NaCl solution. Geochimica et Cosmochimica Acta 51, 63–72.

Reed, M., Spycher, N., 1984. Calculation of pH and mineral equilibria in hydrothermal waters with application to geothermometry and studies of boiling and dilution. Geochimica et Cosmochimica Acta 48 (7), 1479–1492.

Rees, C.E., 1973. A steady-state model for sulphur isotope fractionation in bacterial reduction processes. Geochimica et Cosmochimica Acta 37 (5), 1141–1162.

Rudnicki, M.D., Elderfield, H., Spiro, B., 2001. Fractionation of sulfur isotopes during bacterial sulfate reduction in deep ocean sediments at elevated temperatures. Geochimica et Cosmochimica Acta 65 (5), 777–789.

Sánchez, P., Pérez-Flores, P., Arancibia, G., Cembrano, J., Reich, M., 2013. Crustal deformation effects on the chemical evolution of geothermal systems: The intra-arc Liquiñe–Ofqui fault system, Southern Andes. International Geology Review 55 (11), 1384–1400.

Sánchez-Rivera, E., Vallejos-Ruiz, O., Badilla, A., Guido-Sequeira H., 2005. Chemical Treatments of Fluids on the Miravalles Geothermal Field: Investigation, Application and its Relationship with Reservoir Management, World Geothermal Congress, Antalya, Turkey. 24-29 April.

Sandengen, K., 2006. Prediction of mineral scale formation in wet gas condensate pipelines and in MEG (mono ethylene glycol) regeneration plants. Doctoral thesis, Trondheim, 209 pp.

Sanjuan, B., Brach, M., Béchu, E., Touzelet, S., Crouzet, C., Jean-Prost, V., 2011. Soultz EGS pilot plant exploitation: Phase III: Scintific program about on-site operations of geochemical monitoring and tracing (2010-2013). BRGM, Orléans, France.

Sanjuan, B., Millot, R., Ásmundsson, R., Brach, M., Giroud, N., 2014. Use of two new Na/Li geothermometric relationships for geothermal fluids in volcanic environments. Chemical Geology 389, 60–81.

Sanjuan, B., Millot, R., Dezayes, C., Brach, M., 2010. Main characteristics of the deep geothermal brine (5km) at Soultz-sous-Forêts (France) determined using geochemical and tracer test data. Comptes Rendus Geoscience 342 (7-8), 546–559.

Sanjuan, B., Millot, R., Innocent, C., Dezayes, C., Scheiber, J., Brach, M., 2016. Major geochemical characteristics of geothermal brines from the Upper Rhine Graben granitic basement with constraints on temperature and circulation. Chemical Geology 428, 27–47.

Sanjuan, B., Rose, P., Gerard, A., Crouzet, C., Touzelet, S., Gautier, A., Charlot, A., 2013. Geochemical monitoring at Soultz-sous-Forêts (France) between October 2006 and March 2007, after the chemical stimulations (RMA, NTA and OCA) carried out in the wells GPK-4 and GPK-3. BRGM, Orléans, France, 18 pp. Accessed 13 June 2017.

Santoyo, E., Díaz-González, L., 2010. A New Improved Proposal of the Na/K Geothermometer to Estimate Deep Equilibrium Temperatures and Their Uncertainties in Geothermal Systems, Proceedings World Geothermal Congress 2010, Bali, Indonesia. 25-29 April.

Sawin, J.L., 2012. Renewables 2013: Global Status Report, Paris, 178 pp. Accessed 30 March 2016.

Scheiber, J., Nitschke, F., Genter, A., 2012. Geochemical and Mineralogical Monitoring of the Geothermal Power Plant in Soultz sous Forêts (France). Proceedings: Thirty-Seventh Workshop on Geothermal Reservoir Engineering, Stanford, California.

Scheiber, J., Seibt, A., Birner, J., Genter, A., Moeckes, W., 2013. Application of a Scaling Inhibitor System at the Geothermal Power Plant in Soultz-sous-Forêts: Laboratory and On-site Studies. Proceedings: European Geothermal Congress, Pisa, Italy.

Schmidt, A.P., Hartog, F.A., van Os, B., Schuiling, R.D., 2000. Production of 210Pb from a Slochteren Sandstone gas reservoir. Applied Geochemistry 15 (9), 1317–1329.

Schröder, H., Teschner, M., Köhler, M., Seibt, A., Krüger, M., Friedrich, H.-J., Wolfgramm, M., 2007. Long term reliability of geothermal plants – Examples from Germany. Proceedings: European Geothermal Congress Unterhaching, Germany.

Schumacher, M.E., 2002. Upper Rhine Graben: Role of preexisting structures during rift evolution. Tectonics 21 (1), 6-1-6-17.

Simsek, S., 2003. Hydrogeological and isotopic survey of geothermal fields in the Buyuk Menderes graben, Turkey. Geothermics 32 (4-6), 669–678.

Spycher, N., Peiffer, L., Sonnenthal, E.L., Saldi, G., Reed, M.H., Kennedy, B.M., 2014. Integrated multicomponent solute geothermometry. Geothermics 51, 113–123.

Stahl, G., Patzay, G., Weiser, L., Kalman, E., 2000. Study of calcite scaling and corrosion processes in geothermal systems. Geothermics 29, 105–119.

Steefel, C.I., Lasaga, A.C., 1994. A Coupled Model for Transport of Multiple Chemical Species and Kinetic Precipitation/Dissolution Reactions with Application to Reactive

Flow in Single Phase Hydrothermal Systems. American Journal of Science 294 (5), 529–592.

Sterner, S.M., Felmy, A.R., Oakes, C.S., Pitzer, K.S., 1998. Correlation of Thermodynamic Data for Aqueous Electrolyte Solutions to Very High Ionic Strength Using INSIGHT: Vapor Saturated Water Activity in the System $CaCl_2$-H_2O To 250°C and Solid Saturation. International Journal of Thermophysics 19 (3), 761–770.

Stetter, K.O., Fiala, G., Huber, G., Huber, R., Segerer, A., 1990. Hyperthermophilic microorganisms. Microbiology Reviews 6 (2), 117–124.

Stocker, T.F., Qin, D., Plattner, G.K., Tignor, M. Allen, S.K., Boschung, J. Nauels, A., Xia, Y. Bex, V., Midgley, P.M., 2013. IPCC-Intergovernmental Panel on Climate Change-Physical Science Basis, New York, USA.

Strübel, G., 1966. Die hydrothermale Löslichkeit von Cölestin im System SrSO4-NaCl-H2O. Neues Jahrbuch für Mineralogie, 99–107.

Tassi, F., Aguilera, F., Darrah, T., Vaselli, O., Capaccioni, B., Poreda, R.J., Delgado Huertas, A., 2010. Fluid geochemistry of hydrothermal systems in the Arica-Parinacota, Tarapacá and Antofagasta regions (northern Chile). Journal of Volcanology and Geothermal Research 192 (1-2), 1–15.

Templeton, C.C., 1960. Solubility of Barium Sulfate in Sodium Chloride Solutions from 25°C-95°C. Journal of Chemical & Engineering Data 5 (4), 514–516.

Testa, C., Desideri, D., Meli, M.A., Roselli, C., Bassignani, A., Finazzi, P.B., 1993. Radium, uranium and thorium concentrations in low specific activity scales and in waters of some oil and gas production plants. Journal of Radioanalytical and Nuclear Chemistry 170 (1), 117–124.

Thode, H., Monster, J., Dunford, H., 1961. Sulphur isotope geochemistry. Geochimica et Cosmochimica Acta 25 (3), 159–174.

Tischner, T., Evers, H., Hauswirth, H., Jatho, R., Kosinowski, M., 2010. New Concepts for Extracting Geothermal Energy from One Well: the GeneSys-Project, World Geothermal Congress, Bali, Indonesia. 2010.

Tonani, F., 1980. Some Remarks on the Application of Geochemical Techniques in geothermal exploration, in: Strub, A.S., Ungemach, P. (Eds.), Advances in European Geothermal Research. Proceedings of the Second International Seminar on the Results of EC Geothermal Energy Research, Strasbourg.

Truesdell, A.H., 1975. Summary of Section 3 - Geochemical Techniques in Exploration, Proceedings: Second United Nations Symposium on the Development and Use of Geothermal Resources, San Francisco, California. May 20-29, 1975.

Tuttle, M., Breit, G.N., Cozzarelli, I.M., 2009. Processes affecting Δ34S and Δ18O values of dissolved sulfate in alluvium along the Canadian River, central Oklahoma, USA. Chemical Geology 265 (3-4), 455–467.

Vaute, L., Aquilina, L., Gentier, S., Pinault, J.-L., Rose, P., 1998. Tests de traçage réalisé sur le site géothermique de Soultz-sous-Forêts. BRGM, Orléans, France, 134 pp. Accessed 13 June 2017.

Verma, A., Pruess, K., 1988. Thermohydrological Conditions and Silica Redistribution Near High-Level Nuclear Wastes Emplaced in Saturated Geological Formations. Journal of Geophysical Research 93 (B2), 1159–1173.

Verma, M.P., 2000. Revised Quartz Solubility Temperature Dependence Equation along the Water-Vapor Saturation Curve, Proceedings World Geothermal Congress 2000, Kyushu - Tohoku, Japan. May 28 - June 10.

Verma, S.P., 2015. Chemical and Isotope Geothermometers to Estimate Geothermal Reservoir Temperature and Vapor Fraction, Proceedings World Geothermal Congress 2015. World Geothermal Congress, Melbourne, Australia.

Verma, S.P., Santoyo, E., 1997. New improved equations for Na/K, Na/Li and SiO_2 geothermometers by outlier detection and rejection. Journal of Volcanology and Geothermal Research 79 (1-2), 9–23.

Wang, Z., McClure, M.W., Horne, R., 2009. A Single-Well EGS Configuration Using a Thermosiphon, Thirthy-Fourth Workshop on Geothermal Reservoir Engineering, Stanford University, California, USA. 2009.

Wolery, T., Jove-Colon, C., Rard, J., Wijesinghe, A., 2004. Pitzer Database Development: Description of the Pitzer Geochemical Thermodynamic Database data0.ypf. Appendix I in In-Drift Precipitates/Salts Model (P. Mariner). U.S. Department of Energy.

Wolfgramm, M., Rauppach, K., Sibt, A., 2009. Langfristige Betriebsführung und Monitoring geothermischer Anlagen in Deutschland, Der Geothermiekongress 2009. Der Geothermiekongress 2009, Bochum, Germany. 17-19 November.

Worden, R., Manning, D., Lythgoe, P., 2000. The origin and production geochemistry of radioactive lead (210 Pb) in NORM-contaminated formation waters. Journal of Geochemical Exploration 69-70, 695–699.

Wylde, J.J., Slayer, J.L., 2010. Halite Scale Formation Mechanisms, Removal and Control: A Global Overview of Mechanical, Process, and Chemical Strategies, World Geothermal Congress, Bali, Indonesia. 2010.

Xu, T., Spycher, N., Sonnenthal, E., Zheng, L., Pruess, K., 2012. TOUGHREACT User's Guide: A Simulation Program for Non-isothermal Multiphase Reactive Transport in Variably Saturated Geologic Media, Version 2.0.

Yang, J.-m., Hou, G.-Y., Ding, T.-R., Kou, P., 2010. Measurement of Solubilities in the Ternary System NaCl+$CaCl_2$+H_2O and KCl+$CaCl_2$+H_2O at 50°C. Journal of the Korean Chemical Society 54 (3), 269–274.

Yang, J.-m., Liu, X.-l., Liang, P.-P., 2011. Solubilities of Salts in the Ternary Systems NaCl+$CaCl_2$+H_2O and KCl+$CaCl_2$+H_2O at 75°C. Russian Journal of Physical Chemistry A 85 (7), 1149–1154.

Zaback, D.A., Pratt, L.M., 1991. Isotopic composition and speciation of sulfur in the Miocene Monterey Formation: Reevaluation of sulfur reactions during early diagenesis in marine environments. Geochimica et Cosmochimica Acta 56, 763–774.

Zhang, G., Spycher, N., Xu, T., Sonnenthal, E., Steefel, C., 2006. Reactive Geochemical Transport Modeling of Concentrated AqueousSolutions: Supplement to TOUGHREACT User's Guide for the Pitzer Ion-Interaction Model. LBNL Earth Science Division, 48 pp.

C Declaration of Authorship

THC Simulation of Halite Scaling in Deep Geothermal Single Well Production

Nitschke, F.; Held, S.; Himmelsbach, T.; Kohl, T. (2017): THC simulation of halite scaling in deep geothermal single well production. *Geothermics 65*, 234-243. doi: 10.1016/j.geothermics.2016.09.009

This study was carried out in collaboration with the BGR (Federal Institute for Geoscience and Natural Resources) that provided me with production test data and the EnBW Energie Baden-Württemberg supporting geothermal research at the KIT. For this study, I performed the computations, I interpreted the results and finally I wrote the manuscript.

Assessment of Performance and Parameter Sensitivity of Multicomponent Geothermometry applied to a Medium Enthalpy Geothermal System

Nitschke, F.; Held, S.; Villalon, I.; Neumann, T.; Kohl, T. (rev. subm. to *Geothermal Energy*)

The study was part of a collaborative research project of Karlsruhe Institute of Technology (KIT) and the Andean Geothermal Center of Excellence (CEGA, Fondap-Conicyt 15090013). The BMBF- CONICYT International Scientific Collaborative Research Program (FKZ 01DN14033/ PCCI130025) provided further funding. Additional support was given under the topic “Geothermal Energy Systems” of the Helmholtz portfolio project “Geoenergy” and by EnBW Energie Baden-Württemberg AG.
In this study I identified the research demand. I carried out the laboratory work and developed the numeric approach to compute reservoir temperatures. Finally, I wrote the manuscript.

Geochmical Characterization of the Villarrica Geothermal System, Southern Chile, Part II: Site-specific Re-evaluation of SiO_2 and Na-K Solute Geothermometers

Nitschke, F.; Held, S.; Neumann, T.; Kohl, T. (to be subm. to *Geothermics*)

The study is part of a collaborative research project of Karlsruhe Institute of Technology (KIT) and the Andean Geothermal Center of Excellence (CEGA, Fondap-Conicyt 15090013). The BMBF- CONICYT International Scientific Collaborative Research Program (FKZ 01DN14033/ PCCI130025) provided further funding. Additional support was given under the topic "Geothermal Energy Systems" of the Helmholtz portfolio project "Geoenergy" and by EnBW Energie Baden-Württemberg AG.

For this study, I created the concept of this investigation, developed a multi-step approach to refine the geothermometers and wrote the manuscript.

D Publications

Journals and Proceedings

Nitschke, F.; Held, S.; Villalon, I.; Neumann, T.; Kohl, T. (submitted after revision): Site-specific Re-evaluation of Classical SiO_2 and Na-K Solute Geothermometers – A Case Study of the Villarrica Geothermal System, Southern Chile. Submitted to Geothermics. **(peer-reviewed)**

Held, S.; Nitschke, F.; Schill, E.; Morata, D.; Eiche, E.; Kohl, T. (accepted): Hydrochemistry of the hot spring fluids of the Villarrica geothermal system in the Andes of Southern Chile. GRC Transactions, 41. **(peer-reviewed)**

Nitschke, F.; Held, S.; Villalon, I.; Neumann, T.; Kohl, T. (2017): Assessment of Performance and Parameter Sensitivity of Multicomponent Geothermometry applied to a Medium Enthalpy Geothermal System. Submitted to Geothermal Energy. **(peer-reviewed)**

Nitschke, F.; Held, S.; Villalon, I.; Neumann, T.; Kohl, T. (2017): In-situ Temperature Determination at the Villarrica Geothermal System, Southern Chile: Implications from Laboratory Experiments for Geothermometry. In: Proceedings, 42st Workshop on Geothermal Reservoir Engineering. Stanford University, Stanford, California, February 13-15.

Nitschke, F.; Held, S.; Himmelsbach, T.; Kohl, T. (2017): THC simulation of halite scaling in deep geothermal single well production. Geothermics 65, 234-243. **(peer-reviewed)**

Meller, C.; Bremer, J.; Ankit, K.; Baur, S.; Bergfeldt, T.; Blum, P.; Canic, T.; Eiche, E.; Gaucher, E.; Hagenmeyer, V.; Heberling, F.; Held, S.; Herfurth, S.; Isele, J.; Kling, T.; Kuhn, D.; Mayer, D.; Müller, B.; Nestler, B.; Neumann, T.; Nitschke, F.; Nothstein, A.; Nusiaputra, Y.; Orywall, P.; Peters, M.; Sahara, D.; Schäfer, T.; Schill, E.; Schilling, F.; Schröder, E.; Selzer, M.; Stoll, M.; Wiemer, H.-J.; Wolf, S.; Zimmermann, M.; Kohl, T. (2016): Integrated research as key to the development of a sustainable geothermal energy technology. Energy Technology, 5, 1 – 44. **(peer-reviewed)**

Nitschke, F.; Held, S.; Villalon, I.; Mundhenk, N.; Kohl, T.; Neumann, T. (2016): Geochemical Reservoir Exploration and Temperature Determination at the Mt. Villarrica Geothermal System, Chile. In: Proceedings, European Geothermal Congress, Strasbourg, France, September19-24.

Nitschke, F.; Held, S.; Himmelsbach, T.; Kohl, T. (2015): The Application of THC Code TOUGHREACT-Pitzer on Failure Conditions of Geothermal Project GeneSys. In: Proceedings, European Geothermal Workshop, Strasbourg, France, October 19-20.

Nitschke, F.; Held, S.; Mundhenk, N.; Villalon, I.; Kohl, T.; Neumann, T. (2015): Reactivity of Chilean Reservoir Rocks and the Use of Geochemical Tools for Reservoir Characterization. In: Proceedings, European Geothermal Workshop, Strasbourg, France, October 19-20.

Villalon, I.; Nitschke, F.; Held, S.; Morata, D. (2015): Lithological controls influencing the geochemistry of geothermal systems in the vicinity of Villarrica volcano: an experimental approach. In: Proceedings, XIV. Chilean Geological Conference, La Serena, Chile, October 4-8.

Nitschke, F.; Scheiber, J.; Kramar, U.; Neumann, T. (2014): Formation of alternating layered Ba-Sr-sulfate and Pb-sulfide scaling in the geothermal plant Soultz-sous-Forêts. Journal of Mineralogy and Geochemistry 191/2, 145-156. **(peer-reviewed)**

Nitschke, F.; Scheiber, J.; Neumann, T. (2013): Geochemisch-mineralogische Charakterisierung der Scalings in der Geothermieanlage Soultz-sous-Forêts. In: Chancen der Energiewende: wissenschaftliche Beiträge des KIT zur 1. Jahrestagung des KIT-Zentrums Energie. KIT Scientific Reports; 7640.

Scheiber, J.; Nitschke, F.; Seibt, A; Genter, A. (2012): Geochemical and mineralogical monitoring of the geothermal power plant in Soultz-sous-Forêts (France). In: Proceedings, 37th Workshop on Geothermal Reservoir Engineering, Stanford University, Stanford, California, USA.

Presentations with Abstracts

Nitschke, F.; Held, S.; Villalon, I.; Kohl, T.; Neumann, T. (2016): Villarrica Geothermal System, Chile: Case Study on Refining of Classical Solute-Geothermometers. Workshop ‘Geothermische Fluide in salinaren Systemen, Karlsruhe, November 24-25.

Nitschke, F.; Held, S.; Himmelsbach, T.; Kohl, T. (2016): THC-Modeling of Gt1 Borehole Conditions during the 2011 Failed Circulation Test of the Deep Geothermal Project GeneSys in Hanover. 25. Tagung der Fachsektion Hydrogeologie in der DGGV, Karlsruhe, April 13-17.

Nitschke, F.; Scheiber, J.; Kramar, U.; Neumann, T. (2013): Formation Mechanisms of Sulfate and Sulfide Scalings in the Geothermal Power Plant of Soultz-sous-Forêts: Insights from Sulfur Isotope Analyses. Joint annual Meeting DMG&GV, Tübingen.

Nitschke, F.; Scheiber, J.; Neumann, T. (2012): Bildungsmechanismen der Sulfat-Sulfid-Scales in der Geothermieanlage Soultz-sous-Forêts. Der Geothermiekongress, Karlsruhe, November, 13-16.

E Acknowledgements

I have to say thank you to many people who have accompanied me throughout the time of my PhD and supported me writing this thesis.

First, I have to say thank you to my supervisor Prof. Dr. Thomas Kohl for giving me the opportunity to work in the my fields of interest and for allowing so much “chemistry” in his working group.

Thank you to Prof. Dr. Thomas Neumann for taking the responsibility of being co-supervisor and for fruitful discussions on chemical issues.

Thank you Basti, for days full of scientific discussions and for the many private lessons in numerics.

Thank you Nico, for lots of discussions on geochemistry and everything else.

Many thanks to Claudia Mößner for her uncomplicated support in laboratory issues.

I would like to thank Ignacio Villalon, Julian Maaz and Dorothee Siefert for helping to increase my understanding in water-rock interaction processes with their studies in the framework of their thesis and “Projektstudien”.

Many thanks to Silke, for keeping that administrative stuff away from me.

Thank you Andi, for being there all the time and for encouraging me in hard times.

Finally, I like to thank my parents for their unconditional support all along my way.